

dienst informatieverwerking



KALMAN FILTERS FOR THE DESCRIPTION
AND PREDICTION OF TIDAL MOTION

An evaluation of the 1-D approach
in the Dutch coastal area

P.G.J. ten Brummelhuis

B. de Jong

A.W. Heemink

TWENTE UNIVERSITY OF TECHNOLOGY

DEPARTMENT OF APPLIED MATHEMATICS

CONTENTS

PREFACE

NOTATIONS

Chapter 1	INTRODUCTION	1
Chapter 2	THE DETERMINISTIC MODEL OF THE TIDAL MOTION IN THE DUTCH COASTAL AREA	
§ 1	Introduction	6
§ 2	The tidal motion in the southern part of the North Sea	7
§ 3	Meteorological effects	10
§ 4	The dynamical equations and boundary conditions	11
§ 5	The model along the coast	16
§ 6	The Eastern Scheldt model	18
§ 7	Discretization	21
Chapter 3	DISCRETE FILTER THEORY	
§ 1	Introduction	23
§ 2	Linear filtering theory	23
§ 3	Stability of the filter	29
§ 4	Nonlinear filtering	31
§ 5	Specification of the filter	36
Chapter 4	APPLICATION TO TIDAL MOTION PROBLEMS	
§ 1	Introduction	41
§ 2	The filter as a descriptive model	43
§ 3	Parameter Estimation	65
§ 4	Optimization of sampling networks	75
§ 5	Short term predictions	79
Chapter 5	CONCLUSIONS	121
	REFERENCES	124

PREFACE

This report is a result of the cooperation between the Data Processing Division of Rijkswaterstaat and the Mathematical Physics Group of the Twente University of Technology. This cooperation exists already for many years on an informal basis and has been formalized occasionally by a contract between our institutes.

The first contract -"Contract MARTHA"- was carried out during a 2 years period in 1979-1981 and its main object was to investigate the usefulness of Kalman filters for tidal motion problems in instationary situations using shallow water equations to describe the dynamics. Although good results were obtained in predicting the water levels in the mouth of the Eastern Scheldt, on the basis of on-line measurements of water levels in the North Sea along the Dutch and Belgian coast, it turned out that more reliable predictions for the water levels could be obtained by including in the existing open sea model for the water movements along the coast also a model describing the water movements in the Eastern Scheldt estuary. This point of view has been formulated as a new research project -"Contract MARTHA II"- which has been carried from november 1983 until september 1984.

As in the first project it was our intention to use simple mathematical models containing stochastic parameters which, by using Kalman filters, are continuously adapted to changing external conditions, e.g. the meteorological situation, the bottom condition, etc.

The design and testing of the Kalman filter for the Eastern Scheldt model as well as the design of the procedure to link it to the existing filter for the open sea tidal model has been performed at the Twente University of Technology by the first two authors. Further refinement and tuning of the filter has been accomplished by the first and the third author at the Data Processing Division of Rijkswaterstaat

The authors wish to express their gratitude to the Data Processing Division for their financial support, and in particular to ir. W.F. Volker for his helpful suggestions and the fruitful discussions during the period of this research project.

Paul G.J. ten Brummelhuis
Bartele de Jong
Arnold W. Heemink

NOTATIONS

x, y	space coordinates
t, τ	time coordinate
u	velocity
h	water levels above some reference level (here: N.A.P.)
h_0	undisturbed water level
D	depth of the bottom below the reference level
A	cross-sectional area
$b = \frac{\partial A}{\partial n}$	width of a channel branch
P	wetted perimeter
g	acceleration of gravity
f	Coriolis coefficient
$\underline{V}, V = \underline{V}$	wind velocity
s	"set-up" against the coast
C_d	wind stress coefficient
$\omega = 2\pi\nu$	angular frequency
λ	wavelength of a tidal constituent
ϕ	phase angle
ψ	angle between \underline{V} and the positive x-axis
$\tilde{\psi}$	angle between \underline{V} and the positive y-axis
μ, η	friction coefficients
ρ	reflection coefficient in boundary condition
$\Delta x, \Delta t, \Delta t_k$	distances in the computational grid
θ	$\Omega_{\Delta x, \Delta t}, \Delta t = \Delta t_k = t_{k+1} - t_k$ weighting parameter in the Preissmann scheme
$\underline{x}(t_k)$	deterministic state vector, $t = t_k$
$\tilde{\underline{x}}(t_k), \hat{\underline{x}}(t_k)$	realisations of $\underline{x}(t_k)$
$\underline{u}(t_k)$	input vector, $t = t_k$
$\Phi(t_{k+1}, t_k), \tilde{\Phi}(t_{k+1}, t_k)$	state transition matrices $t_k \rightarrow t_{k+1}$ (deterministic)
$\underline{z}(t_k)$	measurement vector, $t = t_k$
$\underline{X}(t_k), \hat{\underline{X}}(t_k)$	stochastic state vector, $t = t_k$
$\mathcal{A}(t_{k+1}, t_k)$	state transition matrix of the stochastic systems
$\mathcal{W}(t_{k+1}, t_k)$	state transition matrix of the filter
$\underline{Z}(t_k)$	stochastic measurement vector, $t = t_k$
$\underline{W}(t_k)$	system noise, $t = t_k$
$\underline{V}(t_k)$	measurement noise, $t = t_k$

M	measurement matrix
$\underline{m}(\underline{X}(t_k))$	nonlinear measurement vector, $t = t_k$
$\underline{z}(t_k)$	actual measurement realisation
E	(linear) mean operator
$\hat{\underline{X}}(k+i/k)$	mean (expectation) of $\underline{X}(t_{k+i})$, $i > 0$
P(k+i/k)	covariance matrix of $\underline{X}(t_{k+i})$, $i > 0$
Q(k)	covariance matrix of $\underline{W}(t_k)$
R(k)	covariance matrix of $\underline{V}(t_k)$
K(k+1)	Kalman gain matrix
$\sigma, \sigma_p, \sigma_m$	r.m.s. error

CHAPTER 1

INTRODUCTION.

This report gives an exposition of the applications Kalman filters and the related nonlinear filters offer when used in models describing tidal motion in seas and estuaries. In addition to methods that are generally used in this field, for example deterministic and black-box models, Kalman filters can provide significant contributions in particular situations. Although it is not our intention to claim that the use of Kalman filters is the most fruitful method for all problems, it will be shown that these filters exhibit some specific useful properties, not present in the above mentioned conventional methods. Before explaining the fundamental ideas of the Kalman filter and its advantages and disadvantages a short review will be given of other known methods.

The class of deterministic models is based on hydrodynamical equations, both one- and two dimensional, and a well-chosen schematization of the geometry of the area involved. Once such a qualitative model is established certain elements in it can be adjusted to represent an observed proces under different circumstances as closely as possible. Referring to certain elements one may think of parameters in empirical relations such as bottem friction- and wind stress coefficients or, more drastically, the path-length of some stream-section in a complicated geometry. This tuning of the model is necessary since no model is perfect. The incompleteness is caused by the lack of knowledge to describe certain effects in mathematically correct formulae, e.g. by using empirical relations, or the inability to incorporate in the model non dominant features that lie beyond the restrictions of the model, for example a two dimensional effect can not be dealt with in a one dimensional model. However in many cases these deterministic models can be tuned to give good reconstructions of observed phenomena. When the required adaptations during the tuning of the model prove to be relatively small compared to some reference in a basic model, many aspects in the area of model research can be pursued and qualitative and/or quantitative conclusions may be drawn. In this case the reliability of quantitative conclusions depends on the degree to which the effects that can be tuned act as a compensation for physical influences which are not incorporated in the model. For example, the interpretation of a bottom

friction coefficient depends on the correctness of the prescribed geometry of the stream sections. Another conclusion of the discussion above is that these models are not very suited to represent physical behaviour in periods when the external meteorological conditions are changing because these changes require adaptations in the input parameters of the model. In the area of tidal predictions these problems are known in situations a storm develops. Examples of deterministic mathematical models are the IMPLIC and WAQUA models, like GENO, describing the tidal motion in the entire North Sea [Voogt, 1984].

A different approach is found in black-box modelling. By analyzing observation series over very long periods of time a number of parameters is estimated which indicate the correlations between the various physical components of a state. When observations are available "on line" these models make it possible to process these new data in a simple and rapid way. The use of these black box models is however limited by the assumption of stationarity of the observed process resulting in less reliable predictions during instationary situations. Another disadvantage of these models is that they are not based on physical laws, so the interpretation of the parameters is not very clear, although certain physical characteristics are hidden in its structure. The black box models have been applied to numerous problems in the field of water movements, particularly when predictions over certain periods of time are required, such as predictions of swell energy [Poullisse, 1984].

A characteristic property of the first approach is the mathematical formulation of the physical phenomena on which the model is based, an essential point in the second approach is the choice of the model on the basis of huge observation series. These premises are combined in a (stochastic) Kalman filter.

The basis of such a filter is a deterministic model description in which the state vector is conceived as a random variable. This implies that the state of the model at time τ is not only represented by a real valued vector (as in deterministic modelling) but also by means of

- a measure for the uncertainty of this vector, and
- a measure of the correlation between the various components of the state vector at time τ .

The Kalman filter algorithm now defines a way to compute the evolution in time, from τ to $\tau + \Delta\tau$, of the optimal estimate of the state in a least square sense, based on physical laws and information from measurements. Two ways which lead to an estimate of the state at time $\tau + \Delta\tau$ are:

- (i) - by computing an estimate, based on the optimal estimate of the state at time τ (dependent on previous observations) which serves as an initial condition for the deterministic model which describes the evolution of the state, (locally) in time. The uncertainty of this computed estimate depends on the uncertainty of the optimal estimate at time τ and the model errors, since the description of the evolution in time is only an approximation.
- (ii)- by measuring a number of quantities which are related to the state vector and are affected by measurement errors.

Essential is that both results contain information about the state at time $\tau + \Delta\tau$. The last step to complete the evolution in time is to derive an optimal estimate where all available information is weighted according to its reliability. The final result is that optimal estimates are found, not only for the observed quantities (which are in many cases the water levels) but for all components of the state vector because of the correlations between them. In particular, certain parameters can be estimated. Strictly spoken, parameters are assumed to be constant and independent of other physical quantities which induces the absence of correlations with other components of the state vector. However, since in many models empirical relations are used the appearing parameters do not fulfil this statement, e.g. recount the dependence of the friction coefficient in tidal motion on the phase of the tide. The filter algorithm prescribed above enables us to adapt the various parameters to varying circumstances, the so-called adaptive filtering.

Besides this application in the field of model research one can put the emphasize on the construction of an optimal initial condition for a model in order to give predictions of the behaviour of a physical process in time. The calculation indicated in point (i) is in fact a prediction over a time interval $\Delta\tau$, the length of which is determined by the sampling frequency. The prediction interval can of course be extended and this is pursued in the subsequent chapters of this report to compute short term predictions of the tidal motion in the Dutch coastal area.

A third application of the stochastic filter is the use in the optimization of the distribution of sampling points. In that case we focus our attention to the uncertainties of the optimal estimates and the variation of these uncertainties when sampling points are added or removed. The positions of a limited number of sampling points and the nature of the sampled quantities are chosen as to provide as much information as possible.

This exposition shows the wide range of applicability of Kalman filters which does not imply however that it is always the best suited method, this should be assured in every particular situation. One of the major advantages of the filter is its recursive character: once a measurement is processed its influence is totally stored in the new optimal estimate of the state vector, including the associated uncertainty and the correlations. It is therefore very suited to be used on-line. Although the filter is based on a number of assumptions concerning the nature of the model - and measurement errors, it does not suffer from stationarity assumptions and is able to reconstruct also instationary behaviour. The importance of this feature is expressed by the fact that predictions of the water levels in the mouth of the Eastern Scheldt are more important during stormy periods than in situations when the tide follows the astronomical pattern. Besides these positive features the Kalman filter has also some negative properties. Without simplifications in the filter algorithm it is merely impossible to implement a two dimensional model in a filter on a conventional computer because of the rather huge computation time and memory access that is required. The recent emerge of parallel processors however can provide a qualitative step ahead in this field. So, for tidal motions in which a two-dimensional effect is obvious, for example the Coriolis effect, Kalman filters will not be able to generate predictions with a great reliability if a strictly one dimensional physical model is used: the optimal estimates must always be found within the limits of the underlying model. The following approaches can be distinguished:

- Retain a simple, possibly linear, two dimensional deterministic model and approximate the computations of the algorithm. This may lead to the "steady-state" filter where the weighting of every measurement is constant and the time consuming part of the computation can be performed once, off-line. In literature several variations on this principle are available [Lainiotis, 1978, Morf, 1974].

- Use a nonlinear one dimensional model and perform the standard algorithm. The required computation time and memory access is highly dependent on the dimension of the state vector and necessitates the use of a crude grid.

The results which are achieved with this last approach are reflected in this evaluation.

In chapter 2 the deterministic model is given to describe the tidal motion in the southern part of the North Sea and the Eastern Scheldt estuary. Special attention is paid to empirical relations that are used to correct for some two dimensional effects.

Chapter 3 contains the theoretical aspects, brought in a tutorial way, of the Kalman filter and the related nonlinear filters. Also the specification of the nonlinear filters is given which are based on the model described in chapter 2. The main results of all the applications can be found in chapter 4 where as in chapter 5 the conclusions are drawn and some recommendations are formulated.

CHAPTER 2

THE DETERMINISTIC 1-D MODEL OF THE TIDAL MOTION IN THE DUTCH COASTAL AREA.

§ 1 Introduction

In this chapter a simple mathematical model will be developed to describe the tidal motion in the Dutch coastal area. The water motions along the coast and in the Eastern Scheldt estuary will be modelled in a different way. This is done for two reasons. First the geometries in the mentioned areas require different functions to express the dependence of the geometry from the coordinates and the waterlevel and second the description of the two-dimensional effects in the tidal motion along the coast needs additional care. However, both descriptions of the tidal motion are based on the 1-D shallow water equations supplemented with empirical relations.

The characteristics of the tidal motion in the southern part in the southern of the North Sea will be discussed in a quantitative way in §§ 2,3 including the influence of the meteorological phenomena on it. Moreover, the validity of the 1-D approach will become clear.

In §4 the 1-D shallow water equations are given where the analogy between the two subsystems is shown. The model should be completed by boundary conditions. By writing the dynamical equations in the so-called canonical form appropriate boundary conditions can be found in a straightforward way and this form also suggests a physical interpretation we will refer to in the chapters 3 and 4.

The §§ 5 and 6 consist of a complete mathematical model and a discussion of the specific modelling aspects for the considered area along the Dutch coast. This model, stated in a differential form, is discretized into sets of difference equations by using finite difference methods. Again, it appears to be necessary to use different procedures to discretize the equations describing the flow in the estuary. This is pursued in § 7.

§ 2 The tidal motion in the southern part of the North Sea

The Coriolis force, generated by the earth's rotation, strongly influences the tidal motion in the southern part of the North Sea. This section deals with the theory of Kelvin waves, i.e. waves influenced by the Coriolis effect to characterize the specific character of the considered tidal motion.

The Kelvin wave is the analytical solution of the linear 2-D shallow water equations along a straight (coast) line,

$$(2.1.) \quad \frac{\partial u}{\partial t} + g \frac{\partial h}{\partial x} = 0$$

$$(2.2) \quad fu + g \frac{\partial h}{\partial y} = 0$$

$$(2.3) \quad \frac{\partial h}{\partial t} + D \frac{\partial u}{\partial x} = 0$$

where $u(x,y,t)$ and $h(x,y,t)$ are respectively the velocity in the direction of the coast line and the water level above some reference, f the Coriolis coefficient, D the constant depth and g is the acceleration of gravity.

Furthermore it is assumed that the velocities perpendicular to the coast and the convection can be neglected. The absence of bottom friction does not influence the essential properties of the solution, it only simplifies the formulae. A detailed treatment can be found in Dronkers [1964].

If the x -coordinate axis coincides with the coast line, the solution of eq.s (2.1) - (2.3) can be found by separation of variables. For waves of frequency ω it is

$$(2.4) \quad h(x,y,t) = A \exp\left(-f \frac{(y+b)}{\sqrt{gD}}\right) \cos\left(\omega t - \frac{\omega x}{\sqrt{gD}} + \phi\right) + h_0$$

$$(2.5) \quad u(x,y,t) = h(x,y,t) \sqrt{\frac{g}{D}},$$

the amplitude of the wave is decreasing in the positive y direction in case the x and y axes are orientated as indicated in fig. 2.1 and $f > 0$

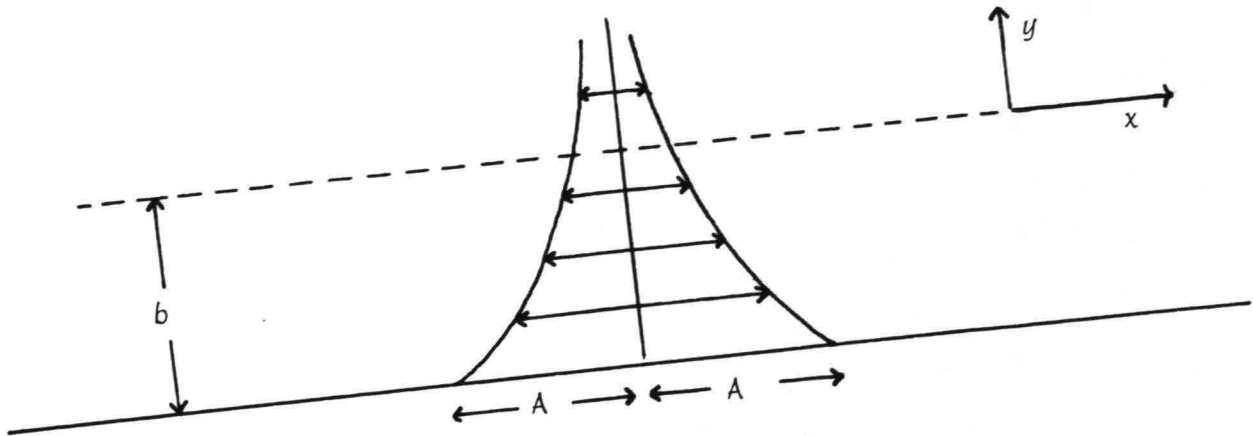


Fig. 2.1 The propagation of a Kelvin wave along a straight coast line

Pay attention to the fact that the Coriolis force induces a purely two dimensional effect but that the propagation of the wave is following a straight line along the coast and is in essence one dimensional.

The occurrence of amphidromic points (latin: flowing in all directions) where the vertical tide is constant while the velocities can not be neglected in general, is now related to the interaction of two Kelvin waves with the same frequency ω , moving in opposite direction between two straight coast lines, see fig. 2.2

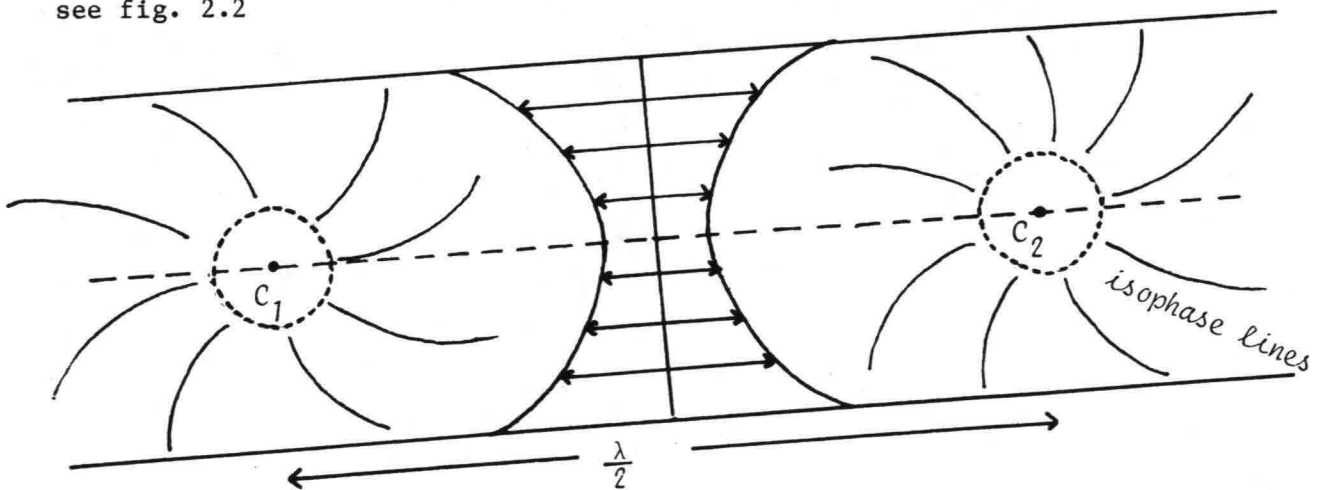


Fig. 2.2 Two Kelvin waves, propagating along a straight line in opposite direction

The position of the amphidromic points c_1 and c_2 can be computed easily. The distance between c_1 and c_2 proves to be $\frac{\lambda}{2}$ with λ the wavelength of the tidal wave.

Because the semi diurnal M_2 tidal component is highly dominant, the theory of Kelvin waves mentioned above can be applied to give a qualitative description of the tidal motion in the southern part of the North Sea. Although the North Sea has a large width, the condition of negligible velocities perpendicular to the coasts of England, Belgium and the Netherlands if compared to the velocities parallel to the coasts is fulfilled [Dronkers, 1964].

The tidal wave, being a Kelvin wave, enters the southern part of the North Sea along the English coast where it has a maximum amplitude. This wave is almost completely reflected at the Street of Dover due to the small size of the trespass and propagates therefore along the coasts of Belgium and the Netherlands again in northern direction together with the tidal wave entering from the Street of Dover. So the tidal motion in this part of the North Sea is mainly generated by the interaction of two Kelvin waves, moving in opposite direction and is, in essence, a one-dimensional phenomenon, see fig. 2.3.

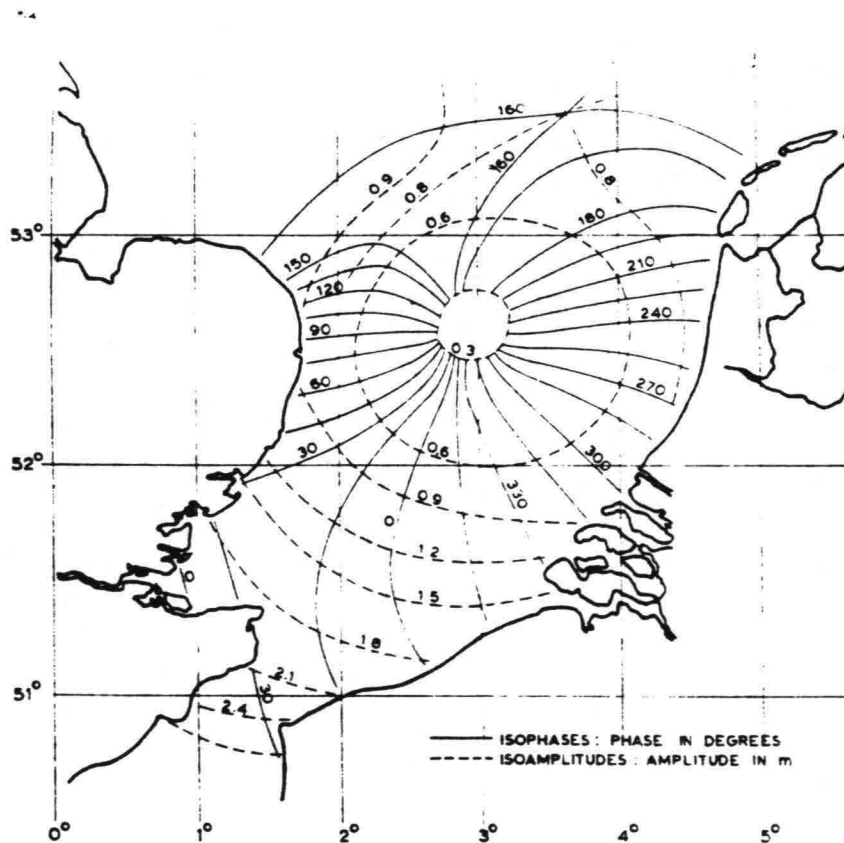


Fig. 2.3 The M_2 tide in the southern part of the North Sea

§ 3 Meteorological effects

The meteorological circumstances affect the water movement in three different ways. The first to be mentioned here is the influence of the atmospheric pressure on the water level through the gradient of the pressure.

Secondly, the wind exerts a force on the water surface till a steady state is reached in which the force due to the wind field is compensated by the gradient of surface tension. In literature empirical relations can be found to describe this steady state [Bretschneider, 1966, 1967].

$$(2.6) \quad \begin{aligned} \underline{F}_w &= C_d \frac{V \underline{V}}{D+h} \\ \frac{ds}{dy} &= \frac{\|\underline{F}_w\|}{g} = C_d \frac{V^2}{g(D+h)} \end{aligned}$$

with \underline{F}_w = force of the wind field
 s = "set-up" of the water
 \underline{V} = wind velocity vector, $V = \|\underline{V}\|$
 C_d = wind stress coefficient

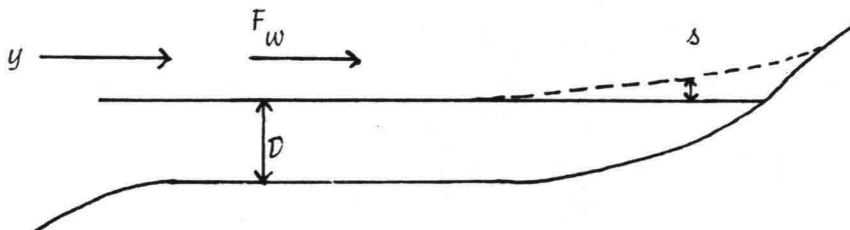


Fig. 2.4 "Set-up" against the coast

Comparison of the two effects leads to the conclusion that the influence of the atmospheric pressure is very small in the southern part of the North Sea, where the depth is less than 50 m [Timmerman, 1975].

The third meteorological effect on the tidal motion is the external surge, defined as the effect on the water level due to meteorological influences occurring outside the North Sea. These may include considerable atmospheric pressure gradients above the very deep Atlantic Ocean or strong wind fields over the shallow waters, north of Scotland. These external surges, entering the North Sea, propagate approximately along the same lines the M_2 tide does.

§ 4 The dynamical equations and boundary conditions

From the previous sections the arguments can be derived to justify the approach to describe the propagation of the tidal wave in the southern part of the North Sea within a 1-D model, because the dominant features can be formulated properly using only one spatial coordinate.

The other part of the geometry we are concerned with is an estuary where the width of the branches is very small compared to the wave lengths of the tidal constituents. Therefore, a 1-D assumption has been made with respect to the propagation of the tidal wave in the estuary. Consequently, there is much correspondence between the dynamical equations governing the flow in the area along the coast and in the estuary itself.

The dynamical equations express the conservation of mass and momentum for a flow in a horizontal plane of infinite dimensions where x is the longitudinal and y the transverse direction. By neglecting the velocities in the transverse ($=y$) direction, which implicates $D(x,y) \cong D(x)$, the 2-D shallow water equations can be transferred to

$$(2.7) \quad \frac{\partial u}{\partial t} + u \frac{\partial u}{\partial x} + g \frac{\partial h}{\partial x} + \mu \frac{u|u|}{D+h} - C_d \frac{V^2 \cos \psi}{D+h} = 0$$

$$(2.8) \quad g \frac{\partial h}{\partial y} + fu - C_d \frac{V^2 \sin \psi}{D+h} = 0$$

$$(2.9) \quad \frac{\partial h}{\partial t} + \frac{\partial}{\partial x} (u(D+h)) = 0$$

with

$h(x,y,t)$ = water level

$u(x,t)$ = velocity

$D(x)$ = depth

μ = friction coefficient

C_d = wind stress coefficient

V = wind velocity

ψ = angle between the direction of the wind and the positive x -axis

f = coriolis coefficient

The eq.s (2.7) and (2.9) define the tidal motion along the x -axis while eq.s (2.8) gives the dependence of $h(x,y,t)$ on y . The set (2.7) - (2.9) is a generalization of (2.1) - (2.3) and incorporates the Kelvin waves.

From eq. (2.8) we can derive the linear expression :

$$(2.10) \quad h(x,y,t) = h(x,y_0,t) + \frac{1}{g} \left\{ -fu(x,y_0,t) - C_d \frac{V^2 \sin\phi}{D+h(x,y_0,t)} \right\} \cdot \{y-y_0\}$$

to approximate the variation of the water level with y . In these equations $u(x,y,t)$ denotes the velocity, averaged over the depth $D(x)$, which may depend on the transverse coordinate y due to the Coriolis force and wind effects. If eq. (2.8) is replaced by eq. (2.10) this dependence is neglected and $u(x,y,t) = u(x,t)$ can be interpreted as a velocity, averaged over a cross-sectional area $A(x,h)$ of arbitrary width $b = b(x,h)$, see fig. 2.5a

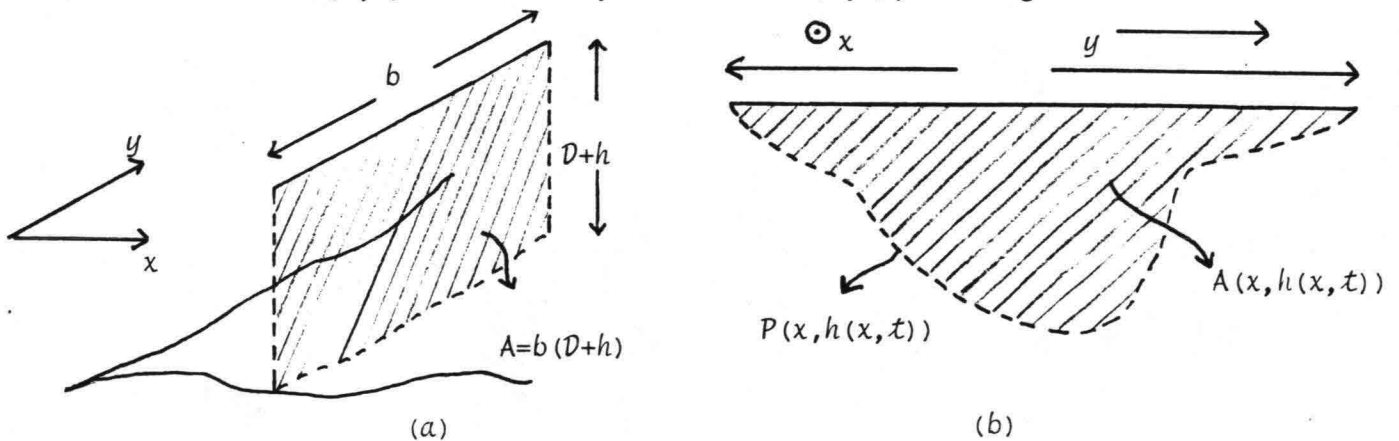


Fig. 2.5

This approach with $u(x,t)$ being the velocity, averaged over $A(x,h)$ is one of the assumptions used to derive a formulation which expresses the conservation of mass and momentum in case of a small dimension (width $b(x,h)$) in the transverse direction, see fig. 2.5b.

Now with $h(x,t) = h(x,y,t)$ averaged over y , and after integration over $A(x,h)$ one finds [Cunge, Holly & Verwey, 1978]

$$(2.11) \quad \frac{\partial u}{\partial t} + u \frac{\partial u}{\partial x} + g \frac{\partial h}{\partial x} + \mu \frac{u|u|P}{A} - C_d V^2 \frac{b}{A} \cos \phi = 0$$

$$(2.12) \quad \frac{\partial h}{\partial t} + \frac{1}{b} \cdot \frac{\partial uA}{\partial x} = 0$$

with P the wetted perimeter, instead of eq.s (2.7) - (2.9).

The eq.s (2.7), (2.9) and (2.10) describing the tidal motion along the coast and eq.s (2.11) and (2.12) used in the estuary have the same structure. This correspondence is noticed, even more obvious, by putting them in the so-called canonical form. This canonical form offers the opportunity to interpret the tidal motion (or more general: water motion) in terms of two interacting travelling waves, propagating in opposite direction. Moreover it leads in a straightforward way to a prescription of appropriate boundary conditions.

Starting from a general set of partial differential equations in conservation form

$$\frac{\partial \underline{u}}{\partial t} + C(\underline{u}) \frac{\partial \underline{u}}{\partial x} + \underline{N}(\underline{u}) = \underline{0}, \text{ where } \underline{u} = \begin{pmatrix} h \\ u \end{pmatrix},$$

eq.s (2.13) and (2.14) can be derived from eq.s (2.7) and (2.9) by using the eigenvalues and corresponding eigenrows of the matrix $C(\underline{u})$ [Abbot, 1970].

$$(2.13) \quad \left[\frac{\partial}{\partial t} + (u + \sqrt{g(D+h)}) \frac{\partial}{\partial x} \right] (u + 2\sqrt{g(D+h)}) = -\mu \frac{u|u|}{D+h} + C_d \frac{V^2 \cos \psi}{D+h}$$

$$(2.14) \quad \left[\frac{\partial}{\partial t} + (u - \sqrt{g(D+h)}) \frac{\partial}{\partial x} \right] (u - 2\sqrt{g(D+h)}) = -\mu \frac{u|u|}{D+h} + C_d \frac{V^2 \cos \psi}{D+h}$$

The transformed eq.s (2.11) and (2.12) are similar to eq.s (2.13) and (2.14)

if $D + h$ is replaced by $\frac{A}{b}$ and a term $-\frac{u}{b} \sqrt{\frac{gb'}{A}} \frac{\partial A}{\partial x}$ is added to the right hand sides of eq.s (2.13) and (2.14).

The dynamical equations can now be interpreted as equations describing the propagation (left hand side terms of eq.s (2.13) and (2.14)) and the deformation (right hand side terms) of quantities

$$u \pm 2\sqrt{g(D+h)}.$$

Along the characteristic directions $\frac{dx}{dt} = u \pm \sqrt{g(D+h)}$ in the (x,t) -plane

$$\left(\frac{\partial}{\partial t} + \frac{\partial}{\partial x} \cdot \frac{dx}{dt} \right) (u \pm 2\sqrt{g(D+h)}) = \frac{D}{Dt} (u \pm 2\sqrt{g(D+h)}) = -\mu \frac{u|u|}{D+h} + C_d \frac{V^2 \cos \psi}{D+h}$$

with $\frac{D}{Dt}$ the total or material derivative.

Consequence

The Quasi Riemann Invariants (Q.R.I.) $u \pm 2\sqrt{g(D+h)}$ propagate in the direction $\frac{dx}{dt} = u \pm \sqrt{g(D+h)}$ and while propagating are deformed by friction forces, meteorological effects and (possibly) geometrical variations. Since the flows associated with tidal motions are sub-critical : $u < \sqrt{g(D+h)}$ the Q.R.I. move in opposite direction, see fig. 2.6.

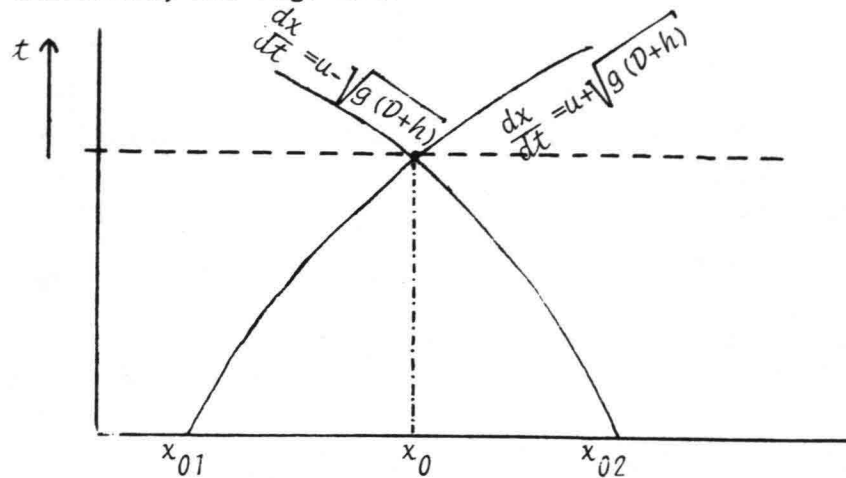


Fig. 2.6 The course of the characteristics in the (x,t)-plane for subcritical flow

On the basis of the earlier mentioned physical interpretation of eq.s (2.13) and (2.14) it is easy to formulate boundary conditions corresponding with the physical configuration of the boundary. We consider the following cases:

1. Total reflection at closed boundaries

$$u = 0 \text{ or}$$

$$(2.15) \quad u - 2\sqrt{g(D+h)} = - [u + 2\sqrt{g(D+h)}]$$

2. A formulation of partial reflection at a boundary can be achieved by introducing a reflection coefficient ρ which is the quotient of the fluctuating parts of $u - 2\sqrt{g(D+h)}$ and $u + 2\sqrt{g(D+h)}$

$$(2.16) \quad \{u - 2\sqrt{g(D+h)} + 2\sqrt{g(D+h_0)}\} = - \rho \{u + 2\sqrt{g(D+h)} - 2\sqrt{g(D+h_0)}\}, \quad 0 \leq \rho \leq 1,$$

h_0 is the undisturbed water level

3. A free outflow boundary implies that reflection is only generated by friction. Since the amplitude of $u - 2\sqrt{g(D+h)} + 2\sqrt{g(D+h_0)}$ will be small, a zero order approximation of a non reflective boundary condition can be obtained by assuming $\mu = 0$ and neglecting the wind influences ($C_d=0$):

$$u - 2\sqrt{g(D+h)} + 2\sqrt{g(D+h_0)} = 0 \quad (\text{compare eq. (2.16) with } \rho = 0)$$

A first order approximation is found using the solution of the linearized system:

$$\frac{\partial h}{\partial t} + H \frac{\partial u}{\partial x} + U \frac{\partial y}{\partial x} = 0$$

$$\frac{\partial u}{\partial t} + U \frac{\partial u}{\partial x} + g \frac{\partial y}{\partial x} + \eta u = 0$$

which is

$$\begin{bmatrix} u(x,t) \\ h(x,t) \end{bmatrix} = C_1 \exp(\alpha x) \begin{bmatrix} 1 \\ \frac{\alpha H}{i\omega} \end{bmatrix} + C_2 \exp(-\alpha x) \begin{bmatrix} 1 \\ \frac{\alpha H}{i\omega} \end{bmatrix} + \begin{bmatrix} U_0 \\ \eta u_0 x \\ -g \end{bmatrix}$$

$$\text{where } \alpha = \frac{i\omega}{\sqrt{1 - \frac{i\eta}{\omega}}}$$

A non reflective boundary condition implies $C_1 = 0$ (the amplitude of the reflected wave equals zero).

The linear relation $\alpha u(x,t) + \beta h(x,t) = c_0$ represents in first order a non-reflective boundary condition if $\alpha + \beta \sqrt{\frac{H}{g}} \sqrt{1 - \frac{i\eta}{\omega}} = 0$.

Using the series Taylor expansion $\sqrt{1 - \frac{i\eta}{\omega}} \approx 1 - \frac{i\eta}{\omega} + \dots$ a first order approximation for $\frac{\eta}{\omega} \ll 1$ is found

$$(2.17) \quad \frac{\partial}{\partial t} (u - 2\sqrt{g \frac{A}{b}}) + \frac{\eta}{2} = 0 \quad [\text{Verboom, 1982}]$$

Note that the non-reflectiveness depends on the frequency ω .

§ 5 The model along the coast.

The previous sections dealt with several aspects related to the tidal motion in the southern part of the North Sea. Now they will be put together to form a comprehensive model of the propagation of the tidal wave along the coast.

The basis of our mathematical model consists of eq.s (2.7) and (2.9). Eq. (2.10) will be used later on when the stochastic model is specified. As the tidal wave and the external surges propagate approximately in the northern direction a measured water level may be used as a boundary condition in point 1 (which coincides with a sampling point) to drive the deterministic model, when in B.G.2 a weakly-reflective boundary condition is imposed, see fig. 2.7. The absence of a wave propagating in the southern direction causes the water level in point 1 to be completely determined by the ingoing Q.R.I. Consequently, in point 1, both formulations of a boundary condition initiate equivalent input signals.

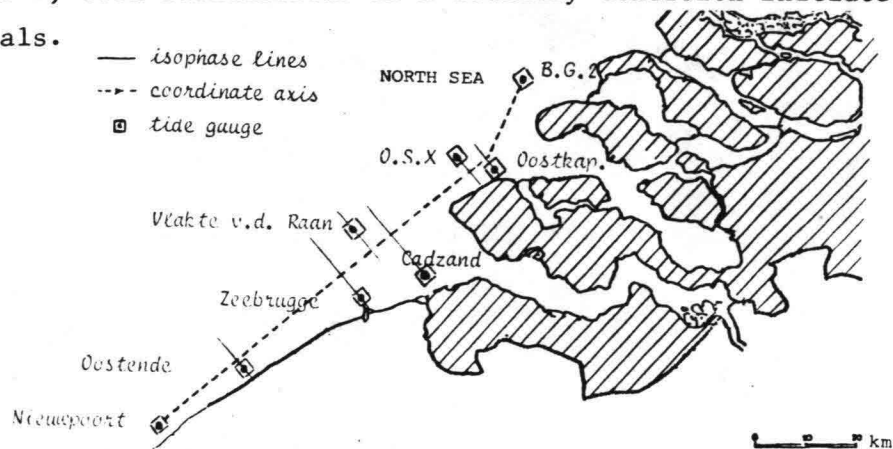


Fig. 2.7 The 1-D model along the coast.

The 1-D model mentioned above proves to be inadequate to represent the internal wind effect perpendicular to the coast properly. Therefore the model will be expanded by an empirical relation (2.18) between wind and set-up against the coast. Let $s(t)$ be the set-up for $y = 0$ the empirical law, derived from eq. (2.6) by Schalkwijk [1947], may be used to express this relationship

$$(2.18) \quad s(t) = \gamma^2(t-\tau) \sin(\omega(t-\tau)) \text{ where } \gamma \text{ a constant and } \tau \text{ the time delay}$$

Another shortcoming of the model is the inability of incorporating influences in the area between the tide gauge station O.S.10 and B.G.2 due to reflected waves generated in the Eastern Scheldt. These influences are not found in

O.S.10 itself because any reflected wave is damped in all directions, like a cylindrical wave. This spheric damping cannot be dealt with in a 1-D model. So, in order to preserve the essence of a tidal wave propagating in northern direction, we are bound by the above formulation with a weakly reflective boundary condition in B.G.2 and the empirical treatment of the internal wind effect.

Summarized

- The model is appropriate to describe the propagation of the tidal wave up to O.S.10 with reasonable accuracy, also accomplished by the fact that unwanted effects of imposed weakly-reflective boundary condition in B.G.2 are totally dissipated between B.G.2 and O.S.10.
- The computed tidal motion in the area north of O.S.10 can show deviations from the sampled data for reasons mentioned above and a possible influence in B.G.2 of a tidal wave propagating south.
- Since it is rather essential to know the tidal motion in the mouth of the Eastern Scheldt, where the tide gauge station O.S.4 is situated the model just presented should be expanded with a schematization of the Eastern Scheldt which will be done in the next section.

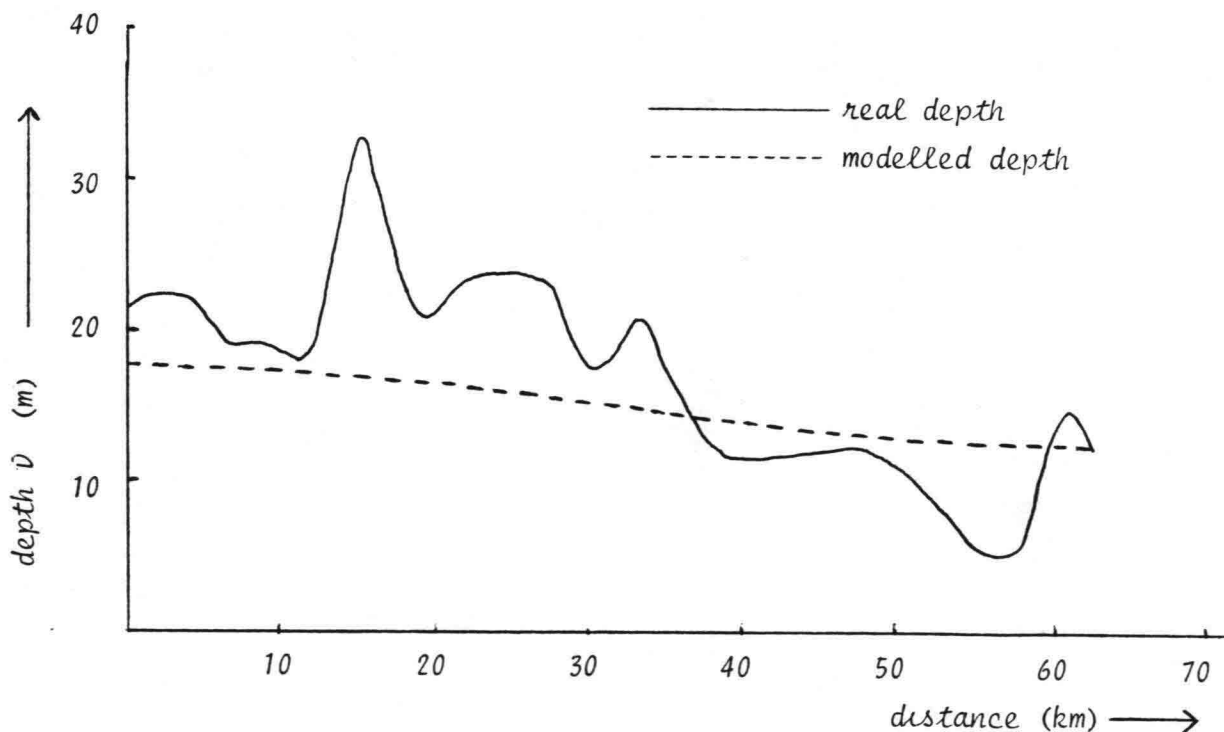


Fig. 2.8 Geometry of the area along the coast.

§ 6 The Eastern Scheldt model

In § 4 the analogy between the eq.s (2.7), (2.9) and eq.s (2.11), (2.12) was shown. For the Eastern Scheldt model the latter set of equations will be used which governs the flow in a channel with a specific geometrical configuration expressed by the quantities P , A and b which are functions of the spatial coordinate and the water level.

Fig. 2.9 gives an overview of the chosen stream sections in the Eastern Scheldt. The basic idea for this choice is rather simple : in the mouth of the Eastern Scheldt there are three major flood gates whereas downstream two branches can be distinguished leading to Rak Zuid and Bergen op Zoom. The proposed schematization is therefore a maximal tolerable simplification.

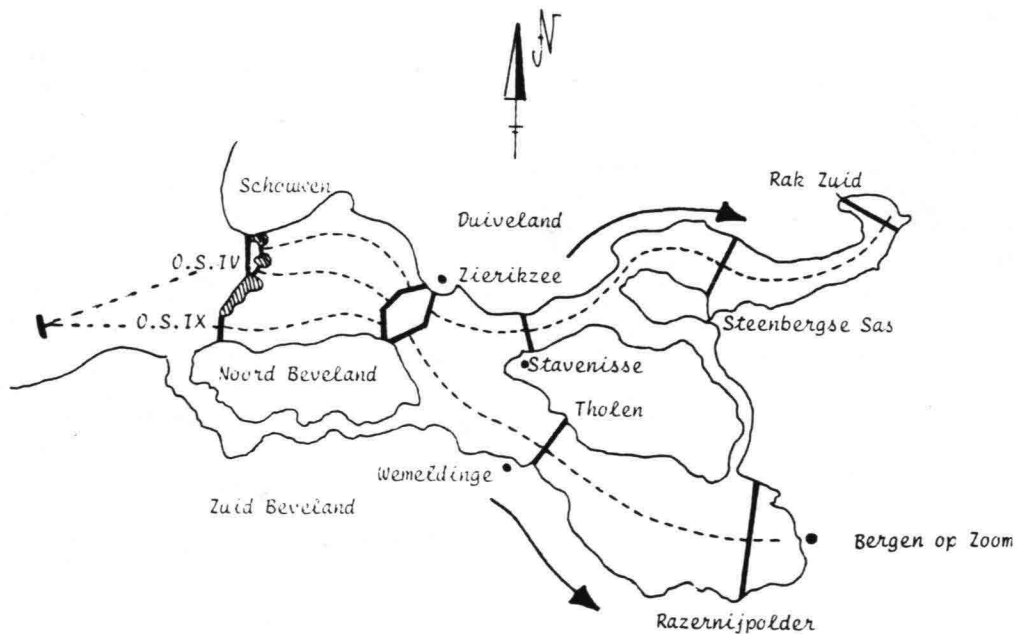


Fig. 2.9 Schematization of the Eastern Scheldt geometry.

In the schematization above a number of points can be found where more than one coordinate-direction is apparent as for example Zierikzee. Locally the one-dimensional dynamical equations are not applicable. We should therefore impose in these points additional continuity conditions to connect the branches. A local distortion of the one-dimensional approach is assumed since the dimension of the area is very small compared to the wavelength of the tidal wave. The continuity demands involve obviously a netto-mass flow equal to zero, see fig. 2.10.

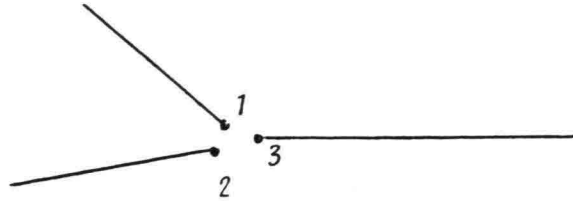


Fig. 2.10

$$(2.19) \quad u(1,t) \cdot A(1,h(1,t)) + u(2,t) \cdot A(2,h(2,t)) = u(3,t) \cdot A(3,h(3,t))$$

Besides (2.18), we state continuity of the quantity $h + \alpha \frac{u^2}{2g}$, see figure 2.11.

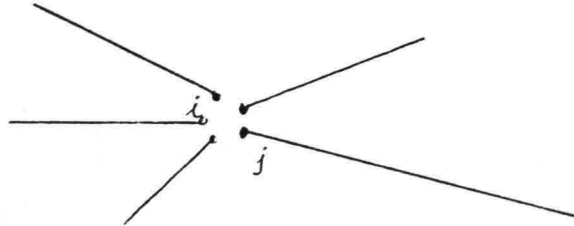


Fig. 2.11.

$$(2.20) \quad h(i,t) + \alpha_{ij} \frac{u^2(i,t)}{2g} = h(j,t) + \alpha_{ij} \frac{u^2(j,t)}{2g}$$

The value of the constant α_{ij} , $0 < \alpha_{ij} < 1$ depends on the mutual ratio of the velocities in the points i and j. For $|u(j,t)| > |u(i,t)|$ we take $\alpha_{ij} = 1$ resulting in continuity of energy-heads whereas for $|u(j,t)| < |u(i,t)|$ $\alpha_{ij} \ll 1$ is suitable [Dronkers, 1964].

This constant α_{ij} can also be found in the convective term in the conservation law of momentum: $\frac{\partial \alpha u^2 A}{\partial x}$, α is a correction factor with respect to the velocity profiles over a cross-sectional area since momentum is transported by the local velocities and not with the average velocities u which occur in our mathematical model.

Connection with the model along the coast

According to the conclusions at the end of § 5 the connection between the two models must consist of the transfer of some quantity at O.S.10 for which we take the water level h (this can be done because a reflection wave is absent in O.S.10).

But again in the stream sections O.S.10 - O.S.9 and O.S.10 - O.S.4 no reflected wave other than due to friction may occur see fig. 2.9. However in O.S.4 and O.S.9 reflection waves will be apparent. Our approach will now be the following. Near O.S.4 and O.S.9 we introduce artificial (internal) boundaries, see figure 2.12.

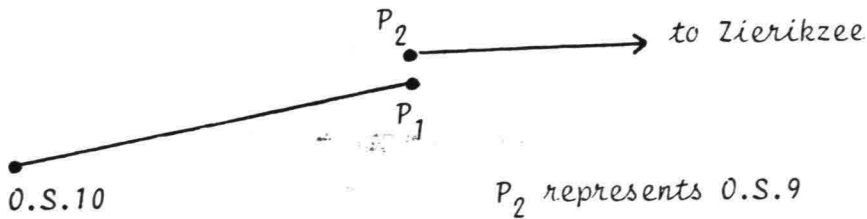


Fig. 2.12 Internal boundary near O.S.9

Now we are bound to prescribe for P_1 a weakly reflecting boundary condition of the form

$$(2.17) \quad \frac{\partial}{\partial x} \left(u - 2\sqrt{g \frac{A}{b}} \right) + \frac{\eta}{2} u = 0$$

The connection between the two models will be completed when we specify the transfer of some quantity between P_1 and P_2 . A logical choice would be to state

$$(2.18) \quad u + 2\sqrt{g \frac{A}{b}} \Big|_{P_1} = u + 2\sqrt{g \frac{A}{b}} \Big|_{P_2}$$

since the tidal wave is assumed to propagate from O.S.10 to O.S.4/O.S.9. Numerical results with the Kalman filter however showed that the phase of this driving signal (2.18) was not consistent with reality: although the amplitude of $u + 2\sqrt{g \frac{A}{b}} \Big|_{P_1}$ was correct the signal arrived too late. In other words the tidal wave which enters the Eastern Scheldt at O.S.4/O.S.9 is not totally determined by the wave propagating from O.S.10 the way it was proposed in our model.

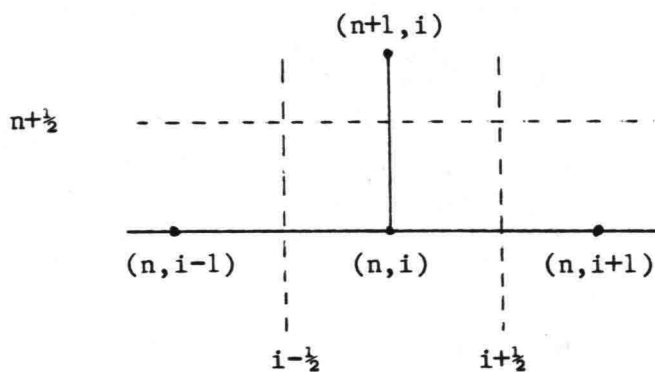
At this point the conclusion must be that the rather linear modelling is too simple and that, for instance, the influences of the geometrical variations are greater than can be represented by specifying only two single channel branches in the area.

The occurrence of a reflection wave in P_2 causes a phase shift of the water level in P_2 if compared to the waterlevel in P_1 . By enlarging artificially the length of the stream sections between O.S.10 and O.S.4/O.S.9 this phase shift in the waterlevels can be compensated. But the transfer of water levels between P_1 , P_2 would mean that the reflection wave in P_2 was ignored in the sense that it would have no effect on the amplitude or mean of the water level at P_2 .

Another possibility is to treat the transfer between P_1 and P_2 (the interior boundary) in the same way compatibility relations are motivated to connect various branches, for example around Zierikzee. The advantages of this approach are that no longer is assumed that the tidal wave propagating from O.S.10 totally determines the arriving wave in the mouth of the estuary and some flexibility is achieved in describing the phase of the waterlevel in P_2 . It would be correct to remark here that in fact we are dealing with some aspects of a black-box approach to represent the flow in this particular area which seems necessary if a one dimensional model is used on a crude grid.

§ 7 Discretization

In order to find a solution (either deterministic or stochastic) the partial differential equations are discretized on a grid $\Omega_{\Delta x, \Delta t}$. Two discretization schemes are used to meet the specific demands of the different geometries and the conditions which are imposed by the use in a Kalman filter algorithm. The well known Lax Wendroff scheme, fig. 2.13, is used to discretize the model along the coast, eq.s (2.7) - (2.9).



The numerical solution of $\frac{\partial U}{\partial t} + \frac{\partial F(U)}{\partial x} + G(U) = 0$ is found according to

$$\begin{aligned}
 \underline{U}_{i+\frac{1}{2}}^{n+\frac{1}{2}} &= \frac{1}{2} \{ \underline{U}_{i-1}^n + \underline{U}_{i+1}^n \} - \frac{\Delta t}{2\Delta x} \{ F(\underline{U}_{i+1}^n) - F(\underline{U}_i^n) \} - \\
 &- \frac{\Delta t}{2} \{ G(\underline{U}_i^n) + G(\underline{U}_{i+1}^n) \} \\
 \underline{U}_i^{n+1} &= \underline{U}_i^n - \frac{\Delta t}{\Delta x} \{ F(\underline{U}_{i+\frac{1}{2}}^{n+\frac{1}{2}}) - F(\underline{U}_{i-\frac{1}{2}}^{n+\frac{1}{2}}) \} - \Delta t G(\underline{U}_i^n)
 \end{aligned}$$

Fig. 2.13 The Lax Wendroff scheme

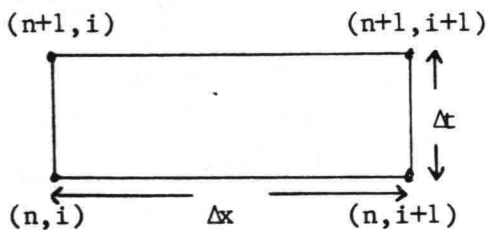
This explicit scheme has mainly been chosen because of its stability characteristics, i.e. the waves with a high frequency ($2\Delta x$ -waves) are damped out. This is important since the corrections that will be provided by the Kalman filter algorithm using measurements introduces a considerable amount of short waves on the grid. Since the physical damping (friction force) is small (great depth of the North Sea) the above mentioned numerical mechanism is necessary for the dissipation of these short waves.

Besides these essential reasons the use of an explicit scheme makes the Kalman filter more transparent than an implicit one.

As a disadvantage the strict CFL-condition may be mentioned which limits the time step to 7.5 min in this model, [Heemink, 1980].

The geometry of the estuary poses other priorities. Since physical damping is more apparent here the argument of numerical damping of high frequency waves fails.

Since in estuarine problems implicit methods are recommended [Cunge, Holly & Verwey, 1980] for their unconditional linear stability (no limitation to the time steps other than for accuracy reasons) and straightforward treatment of boundary conditions the implicit Preissmann 4 points scheme is chosen to discretize the Eastern Scheldt model [ten Brummelhuis, 1984] which is also used in the deterministic IMPLIC models.



The Partial derivatives $\frac{\partial u}{\partial t} = \frac{1}{2\Delta t} [u_i^{n+1} + u_{i+1}^{n+1} - u_i^n - u_{i+1}^n]$ are represented as

$$\frac{\partial u}{\partial x} = \frac{\theta}{\Delta x} [u_{i+1}^{n+1} - u_i^{n+1}] + \frac{1-\theta}{\Delta x} [u_{i+1}^n - u_i^n]$$

$$u = \frac{\theta}{2} [u_i^{n+1} + u_{i+1}^{n+1}] + \frac{1-\theta}{2} [u_i^n + u_{i+1}^n], \quad 0 < \theta < 1$$

Fig. 2.14 Discretization on the grid $\Omega_{\Delta x, \Delta t}$ using the Preissmann 4 points scheme

CHAPTER 3

DISCRETE FILTER THEORY

§1 Introduction

This chapter contains a description of the discrete filter theory with the emphasis on the Kalman filter theory as presented by Kalman and Bucy [1960, 1961]. The theoretical exposures will not be given via full mathematical proofs of the formulae but will be brought in a tutorial way to express the fundamental principles. The filters will be directly linked to the sets of difference equations which are derived in chapter 2. The discrete version of the filters is used since the solution of the differential equations describing the dynamics of the problem appears only possible in a numerical way, implying a discretization of the equations in both space and time.

Since the Kalman filter theory is essentially derived for linear systems, this case will be treated in §§ 2 and 3 where the characteristics and the basic assumptions of the theory are pointed out. In § 4 extensions to nonlinear problems are given, resulting in approximated filters which have proved to be useful in practical applications where filters based on a linear system description are inadequate. A frequently used approximated filter is the extended Kalman filter. Herein, the linear Kalman filter theory is applied after a local linearization in both space and time of the original nonlinear dynamical equations. The reader who is already familiar with the Kalman filter theory can immediately proceed to § 5 where (Kalman) filters are specified, based on the dynamical models stated in chapter 2.

§ 2 Linear filtering theory

Basic to the discussion below will be a deterministic system description of the form

$$(3.1) \quad \underline{x}(t_{k+1}) = \phi(t_{k+1}, t_k) \underline{x}(t_k) + \underline{u}(t_{k+1})$$

with $\underline{x}(t_k)$ the n-state vector, $\underline{u}(t_k)$ an n-input vector (boundary conditions)

for $t = t_k = k \Delta t$ and $\phi(t_{k+1}, t_k)$ the $n \times n$ state transition matrix, independent of both $\underline{x}(t_k)$ and $\underline{x}(t_{k+1})$. In many cases $\phi(t_{k+1}, t_k) = \phi(t_{k+1} - t_k)$ expressing that the actual time is not involved, only the time difference between two time levels. Eq. (3.1) can be found by either using an explicit method of discretization of the linear (partial) differential equations or after a formal inversion of eq. (3.2)

$$(3.2) \quad A(t_{k+1}, t_k) \underline{x}(t_{k+1}) = B(t_{k+1}, t_k) \underline{x}(t_k) + \underline{u}(t_{k+1})$$

which is the result of using an implicit method of discretization of these equations. Formal inversion of (3.2) yields

$$\underline{x}(t_{k+1}) = \bar{\phi}(t_{k+1}, t_k) \underline{x}(t_k) + \tilde{\underline{u}}(t_{k+1})$$

where $\bar{\phi}(t_{k+1}, t_k) = A^{-1}(t_{k+1}, t_k) \cdot B(t_{k+1}, t_k)$ and

$$\tilde{\underline{u}}(t_{k+1}) = A^{-1}(t_{k+1}, t_k) \underline{u}(t_{k+1}).$$

This procedure shows the equivalence of eq.s (3.1), and (3.2), so the method of discretization is irrelevant in this linear case.

The transformation of the deterministic system (3.1) to a stochastic system offers the opportunity to use the information provided by measurements which are related to (some components of) the state vector $\underline{x}(t_{k+1})$. If these measurements are sampled every $t = t_{k+1}$, $k \geq 0$ an m - measurement vector $\underline{z}(t_{k+1})$ can be defined which is related to $\underline{x}(t_{k+1})$ by means of the $m \times n$ -matrix M

$$(3.3) \quad \underline{z}(t_{k+1}) = M \cdot \underline{x}(t_{k+1})$$

Let $\tilde{\underline{x}}(t_{k+1})$ be an estimate of $\underline{x}(t_{k+1})$ as computed from eq. (3.1) with $\underline{x}(t_k) = \underline{x}(t_k)$ and $\hat{\underline{x}}(t_k)$ the optimal estimate of $\underline{x}(t_k)$ then the right hand side of eq. (3.3) is a prediction of $\underline{z}(t_{k+1})$ based on eq. (3.1) or eq. (3.2) and $\hat{\underline{x}}(t_k)$. The difference between the actual measurement data $\tilde{\underline{z}}(t_{k+1})$ and $M \tilde{\underline{x}}(t_{k+1})$ is due to

- measurement errors in $\tilde{\underline{z}}(t_{k+1})$,
- incomplete description, eq.s (3.1), (3.2) of the real physical system (modelled by the system noise),
- propagation errors due to uncertainties in $\hat{\underline{x}}(t_k)$

Our aim is now to extract from $\tilde{z}(t_{k+1})$ and $\tilde{x}(t_{k+1})$ a new optimal estimate $\hat{x}(t_{k+1})$ for $x(t_{k+1})$.

Example

Rewrite eq. (3.1) as $\tilde{x}(t_{k+1}) = \phi(t_{k+1}, t_k) \hat{x}(t_k) + u(t_{k+1})$ which gives an estimate $\tilde{x}(t_{k+1})$ of $x(t_{k+1})$ which is affected by errors that are mentioned above after the second and third dash. Symbolically:

$$\tilde{x}(t_{k+1}) = x(t_{k+1}) + e_{x(t_{k+1})}$$

with $x(t_{k+1})$ representing the true state.

Otherwise, the observation $\tilde{z}(t_{k+1})$ is also affected by errors:

$$\tilde{z}(t_{k+1}) = M x(t_{k+1}) + e_{z(t_{k+1})}$$

In case $M = I_n$, the identity matrix, one finds two estimations of the true state $x(t_{k+1})$. Herein, $e_{x(t_{k+1})}$ and $e_{z(t_{k+1})}$ are the unknown errors in $\tilde{x}(t_{k+1})$ and $\tilde{z}(t_{k+1})$ which are bounded by $e(x)$ and $e(z)$ respectively, so

$$\|e_{x(t_{k+1})}\| < e(x)$$

$$\|e_{z(t_{k+1})}\| < e(z) \quad \forall k > 0$$

If optimality is defined to be the minimal error in the sense that

$\|\hat{x}(t_{k+1}) - x(t_{k+1})\|$ is minimal for some suitable vector norm then the optimal estimation $\hat{x}(t_{k+1})$ can be easily be derived:

$$\begin{aligned} \hat{x}(t_{k+1}) &= \frac{e(z)}{e(x) + e(z)} \cdot \tilde{x}(t_{k+1}) + \frac{e(x)}{e(x) + e(z)} \cdot \tilde{z}(t_{k+1}) \\ &= \tilde{x}(t_{k+1}) + \frac{e(x)}{e(x) + e(z)} \{ \tilde{z}(t_{k+1}) - \tilde{x}(t_{k+1}) \} \end{aligned}$$

This procedure could be used in situations where $m = n$ and $M = I_n$. But in tidal motion problems, for instance, the most common situation is that the components of $x(t_{k+1})$ represent the water levels and the velocities in the various points but only water levels are sampled in the modelled area, so these measurements cannot influence the velocities in a formal way. Therefore, even in this simplified (= linear) case the procedure shows its shortcomings.

This can be overcome by assuming $\tilde{\underline{x}}(t_{k+1})$, $\tilde{\underline{z}}(t_{k+1})$, $\underline{e}_{\underline{x}}(t_k)$ and $\underline{e}_{\underline{z}}(t_{k+1})$ to be realisations of the random variables $\underline{X}(t_{k+1})$, $\underline{Z}(t_{k+1})$, $\underline{W}(t_k)$ and $\underline{V}(t_{k+1})$ ($\underline{u}(t_{k+1})$ is deterministic) which can be described by means of probability density functions, (p.d.f.). These functions, see for instance fig.

3.1, now define

- a measure for the errors in the various components of $\underline{X}(t_{k+1})$ in the sense of a root mean square error
- a correlation between the components for a certain time $t = t_{k+1}$ which enables us to correct all components of $\underline{X}(t_{k+1})$ using only a limited number of measurements ($m < n$).

The solution to our problem is to evaluate the p.d.f. of $\underline{X}(t_k)$ (and $\underline{Z}(t_{k+1})$) in time which will be done in two steps.

- a prediction based on the system description, including the system noise, and optimal estimate of $\underline{X}(t_k)$
- a correction step by incorporating the measurement data $\tilde{\underline{z}}(t_{k+1})$, being a realisation of the random variable $\underline{Z}(t_{k+1})$.

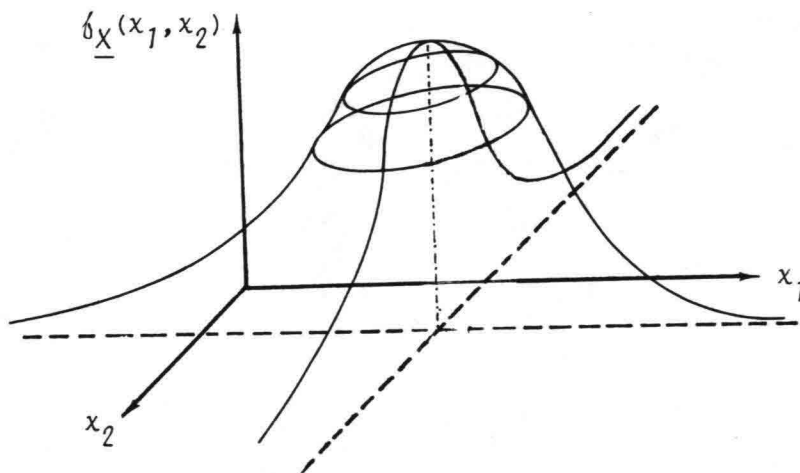


Fig. 3.1 Probability density function $f_{\underline{X}}(x_1, x_2)$ of the random variable $\underline{X} = (X_1, X_2)$

The first step towards the discrete Kalman filter algorithm now consists of an assumption about the nature of the p.d.f. of all the random variables: the p.d.f.s are Gaussian which implies that they are completely specified by two parameters: the mean or the expectation (an n -vector) and the covariance (an $n \times n$ matrix). This contrary to most p.d.f.s which are characterized by an infinite set of parameters. Although it is theoretically not necessary to restrict ourselves to p.d.f.s which are Gaussian, this assumption simplifies

the filter equations drastically [Jazwinski, 1970, Maybeck, 1979].

In terms of random variables the system description is

$$\underline{X}(t_{k+1}) = \Phi(t_{k+1}, t_k) \underline{X}(t_k) + \underline{u}(t_{k+1}) + G \underline{W}(t_k) \quad (3.4a1)$$

or:

$$(3.4) \quad A(t_{k+1}, t_k) \underline{X}(t_{k+1}) = B(t_{k+1}, t_k) \underline{X}(t_k) + \underline{u}(t_{k+1}) + C \underline{W}(t_k) \quad (3.4a2)$$

$$\underline{Z}(t_{k+1}) = M \underline{X}(t_{k+1}) + \underline{V}(t_{k+1}) \quad (3.4b)$$

Suppose for a certain time $t = t_k$ a Gaussian random variable $\underline{X}(t_k)$ is specified. The mean of $\underline{X}(t_k) = \hat{\underline{X}}(k/k)$ and the covariance = $P(k/k)$, symbolically written as $\underline{X}(t_k) \approx N(\hat{\underline{X}}(k/k), P(k/k))$. The p.d.f. of $\underline{X}(t_k)$ is based on all $\tilde{\underline{z}}(t_{k-i})$ for $t = t_{k-i}$ which are realisations of $\underline{Z}(t_{k-i})$, $0 \leq i \leq k$. The p.d.f.s of $\underline{W}(t_k)$ and $\underline{V}(t_{k+1})$ are characterized as $N(0, Q(k))$ resp. $N(0, R(k+1))$ which implies that $\underline{X}(t_{k+1})$ and $\underline{Z}(t_{k+1})$ do not suffer from systematic deficiencies due to the incompleteness of eq.s (3.4a) and (3.4b). This is expressed by the fact that the mean of both $\underline{W}(t_k)$ and $\underline{V}(t_{k+1})$ is zero. Moreover, the intensity of these noise sequences is uniformly distributed over all frequencies, which gives the explanation of the expression the $\underline{W}(t_k)$ and $\underline{V}(t_{k+1})$ are Gaussian white noise sequences.

Eq. (3.4a) now gives the relation to compute the mean $\hat{\underline{X}}(k+1/k)$ and covariance $P(k+1/k)$ of the random variable $\underline{X}(t_{k+1})$, again based on the fact that the data $\tilde{\underline{z}}(t_{k-i})$ are realisations of $\underline{Z}(t_{k-i})$, $0 \leq i \leq k$. Applying the linear mean operator E to eq. (3.4a) gives

$$(3.5) \quad \begin{aligned} \hat{\underline{X}}(k+1/k) &\stackrel{D}{=} E \underline{X}(t_{k+1}) = E \{ \Phi(t_{k+1}, t_k) \underline{X}(t_k) + \underline{u}(t_{k+1}) + G \underline{W}(t_k) \} \\ &= \Phi(t_{k+1}, t_k) E \underline{X}(t_k) + \underline{u}(t_{k+1}) + G E \underline{W}(t_k) \\ &= \Phi(t_{k+1}, t_k) \hat{\underline{X}}(k/k) + \underline{u}(t_{k+1}) \end{aligned}$$

$$(3.6) \quad \begin{aligned} P(k+1/k) &\stackrel{D}{=} E \{ \underline{X}(t_{k+1}) - \hat{\underline{X}}(k+1/k) \} \{ \underline{X}(t_{k+1}) - \hat{\underline{X}}(k+1/k) \}^T \\ &= E \{ \Phi(t_{k+1}, t_k) [\underline{X}(t_k) - \hat{\underline{X}}(k/k)] + G \underline{W}(t_k) \} \{ \cdot \}^T \\ &= \Phi(t_{k+1}, t_k) P(k/k) \Phi^T(t_{k+1}, t_k) + G Q(k) G^T \end{aligned}$$

In the calculation above an expression for both $\hat{\underline{X}}(k+1/k)$ and $P(k+1/k)$ is derived by using

- the Gaussian property of the random variables $\underline{X}(t_k)$ and $\underline{W}(t_k)$
- the mutual independence of $\underline{X}(t_k)$ and $\underline{W}(t_k)$
- The Gaussian property of $\underline{X}(t_{k+1})$ which follows from the linear relation (3.4a).

$\hat{\underline{X}}(k+1/k)$ is the optimal (in the sense of least square error) prediction of the state $\underline{X}(t_{k+1})$ regarding the available measurement data, the system noise and measurement noise. Note that the influence/information of

$\tilde{\underline{z}}(t_{k+1})$, $0 \leq i \leq k$ on $\underline{X}(t_{k+1})$ is totally transmitted via $\underline{X}(t_k)$ (more precise: via $\hat{\underline{X}}(k/k)$ and $P(k/k)$), in other words the filter is recursive:

the previous measurement data need not be stored or used to compute new predictions. This is one of the major advantages the Kalman filter offers when implemented on a computer.

To start the filtering procedure an initial condition has to be specified $\underline{X}(t_0) \sim N(\hat{\underline{X}}(0/0), P(0/0))$. This means $\hat{\underline{X}}(0/0)$ and covariance $P(0/0)$ are in many cases poorly known. Since the only available information are the data at the starting time t_0 and the knowledge of the user of the Kalman filter.

In the same way the p.d.f. of $\underline{X}(t_{k+1}) \sim N(\hat{\underline{X}}(k+1/k), P(k+1/k))$ was derived

$\underline{X}(t_{k+l})$, based on measurements $\tilde{\underline{z}}(t_{k-1})$, $0 \leq i \leq k$, can be specified using eq.s

(3.5), (3.6) with $\hat{\underline{X}}(k/k)$ and $P(k/k)$ subsequently replaced by $\hat{\underline{X}}(k+r/k)$ and $P(k+r/k)$, $1 \leq r \leq l$.

When new data $\tilde{\underline{z}}(t_{k+1})$ become available these can be used to update $\underline{X}(t_{k+1})$.

If the measurements noise $\underline{V}(t_{k+1}) \sim N(0, R(k+1))$ is independent from

$\underline{X}(t_{k+1})$, $\underline{W}(t_k)$ the new estimation of $\underline{X}(t_{k+1})$ is again Gaussian:

$\underline{X}(t_{k+1}) \sim N(\hat{\underline{X}}(k+1/k+1), P(k+1/k+1))$, where

$$(3.7) \quad \hat{\underline{X}}(k+1/k+1) \stackrel{D}{=} E \underline{X}(t_{k+1}) = \hat{\underline{X}}(k+1/k) + K(k+1) \{ \tilde{\underline{z}}(t_{k+1}) - M \hat{\underline{X}}(k+1/k) \}$$

$$(3.8) \quad P(k+1/k+1) \stackrel{D}{=} E \{ \underline{X}(t_{k+1}) - \hat{\underline{X}}(k+1/k+1) \} \{ \underline{X}(t_{k+1}) - \hat{\underline{X}}(k+1/k+1) \}^T \\ = \{ I - K(k+1)M \} P(k+1/k)$$

The $n \times m$ matrix $K(k+1)$ which is found in eq.s (3.7) and (3.8) is the so-called Kalman gain matrix and is derived according to

$$(3.9) \quad K(k+1) = P(k+1/k) M^T \{M P(k+1/k)M^T + R(k+1)\}^{-1}.$$

The derivation of this last equation tends to be complicated and is omitted here. The interested reader is referred to Jazwinski [1970].

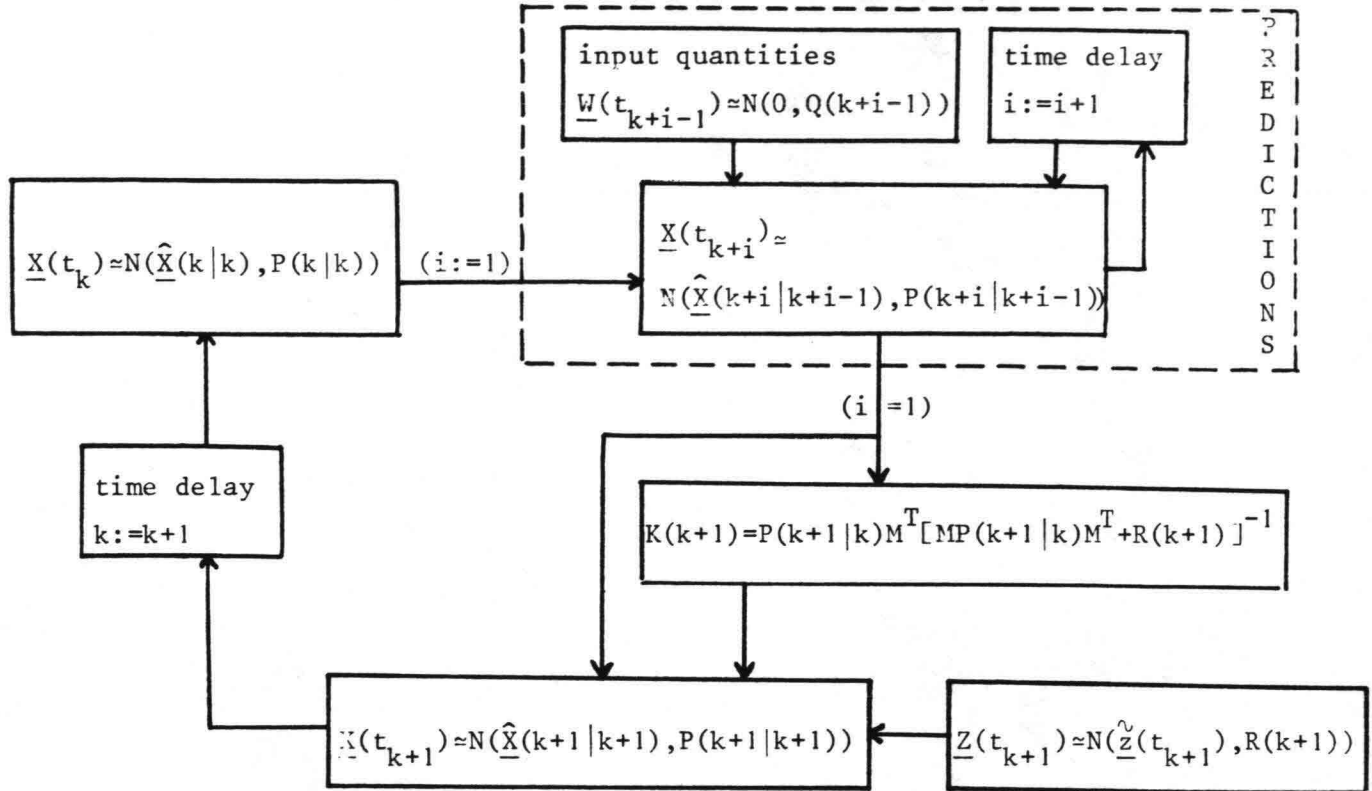


Fig. 3.2 Flow diagram of the Kalman filter

§ 3 Stability of the filter

The Kalman filter, as derived in the previous section, is said to compute optimal estimates of the random variables $\underline{X}(t_k)$. This feature does however not imply that the filter is stable.

In order to define filter stability it is useful to rewrite eq. (3.7) in

$$\begin{aligned} \hat{\underline{X}}(k+1/k+1) &= \{I - K(k+1) M\} \hat{\underline{X}}(k+1/k) + K(k+1) \tilde{\underline{z}}(t_{k+1}) \\ &= \{I - K(k+1) M\} \{\hat{\underline{x}}(t_{k+1}, t_k) \hat{\underline{X}}(k/k) + \underline{u}(t_{k+1})\} + K(k+1) \tilde{\underline{z}}(t_{k+1}) \\ &= \Psi(t_{k+1}, t_k) \hat{\underline{X}}(k/k) + \{I - K(k+1) M\} \underline{u}(t_{k+1}) + K(k+1) \tilde{\underline{z}}(t_{k+1}) \end{aligned}$$

where $K(k+1)$ is determined by eq. (3.9).

Here $\Psi(t_{k+1}, t_k)$ is the state transition matrix of the filter. The filter is said to be stable if there exists a constant $c_1 < 0$ such that

$\|\Psi(t_{k+1}, t_k)\| < c_1$, $\|\cdot\|$ being a suitable matrix norm. The filter is uniform asymptotically stable if there exist constants

$C_2, C_3 > 0$: $\|\Psi(t_{k+1}, t_k)\| < C_3 \exp\{-C_2(t_{k+1} - t_0)\}$. Uniform asymptotical stability implies that bounded inputs $\underline{u}(t_{k+1})$ and $\underline{\tilde{z}}(t_{k+1})$ produce bounded outputs $\hat{\underline{x}}(k+1/k+1)$. It guarantees that the effect of the initial condition-
 $\underline{X}(t_0) \simeq N(\hat{\underline{X}}(0/0), P(0/0))$ is forgotten as more and more information becomes available. This is important since $\hat{\underline{X}}(0/0)$ and $P(0/0)$ are often poorly known. Furthermore, uniform asymptotical stability also guarantees the dissipation of numerical errors in $P(k/k)$ which are symmetric and positive definite matrices. The significance of this characteristic is obvious since the Kalman filter algorithm is prone to numerical difficulties [Bierman, 1977].

To obtain stability criteria the common approach is to introduce the system theoretical concept of controllability and observability, both introduced by Kalman [1960, 1961]. However, in this report another approach is adopted which suits the nature of the problems considered here better. The dynamical equations are namely of the hyperbolic type which means that they can be interpreted in terms of characteristic directions, as is done in chapter 2, section 5 to derive appropriate conditions. We shall refer to this point in chapter 4. It can be shown that for the model described in chapter 2

$$\|I - K(k+1)M\| < 1 \quad \forall k > 0$$

and therefore

$$\|\Psi(t_{k+1}, t_k)\| < \|\Phi(t_{k+1}, t_k)\| \quad \forall k > 0$$

This last inequality states that the Kalman filter is (uniform asymptotically) stable if the underlying deterministic model (eq. (3.1)) is (uniform asymptotically) stable and implies that the filter is always more stable than the original system. This stability improvement property is a very desirable characteristic.

§ 4 Nonlinear filtering

As an extension to the linear Kalman filter which is described in § 2 and 3 we now turn to the nonlinear case. Although full mathematical proofs of properties like observability and filter stability are not available nonlinear filters appear to be a useful tool in cases where linear filters show an insufficient performance. This can be explained by the fact that the use of observations, deduced from essentially nonlinear physical phenomena to correct the vector of a linear system, could introduce large disturbances in the system which may easily lead to unphysical behaviour.

In this section various forms of nonlinear filters are given. The basic concept of a nonlinear filter is that the system equations (3.10)

$$(3.10) \quad \underline{f}(\Delta t_k, \underline{x}(t_{k+1})) = \underline{g}(\Delta t_k, \underline{x}(t_k)) + \underline{u}(t_{k+1})$$

with $\Delta t_k = t_{k+1} - t_k$ and \underline{f} , \underline{g} and \underline{u} are n-vectors are approximated by a Taylor series expansion around some nominal trajectory $\{\tilde{\underline{x}}(t_j)\}$, $j \geq 0$

$$(3.11) \quad \begin{aligned} & \underline{f}(\Delta t_k, \tilde{\underline{x}}(t_{k+1})) + \left[\frac{\partial \underline{f}}{\partial \underline{x}(t_{k+1})} \right]_{\tilde{\underline{x}}(t_{k+1})} (\underline{x}(t_{k+1}) - \tilde{\underline{x}}(t_{k+1})) \\ & + \frac{1}{2} \left[\frac{\partial^2 \underline{f}}{\partial \underline{x}(t_{k+1})^2} \right]_{\tilde{\underline{x}}(t_{k+1})} (\underline{x}(t_{k+1}) - \tilde{\underline{x}}(t_{k+1}))^2 \\ & + ((\underline{x}(t_{k+1}) - \tilde{\underline{x}}(t_{k+1}))^3) = \\ & = \underline{g}(\Delta t_k, \tilde{\underline{x}}(t_k)) + \left[\frac{\partial \underline{g}}{\partial \underline{x}(t_k)} \right]_{\tilde{\underline{x}}(t_k)} (\underline{x}(t_k) - \tilde{\underline{x}}(t_k)) \\ & + \frac{1}{2} \left[\frac{\partial^2 \underline{g}}{\partial \underline{x}(t_k)^2} \right]_{\tilde{\underline{x}}(t_k)} (\underline{x}(t_k) - \tilde{\underline{x}}(t_k))^2 + ((\underline{x}(t_k) - \tilde{\underline{x}}(t_k))^3) \end{aligned}$$

Here, the second order derivatives are only symbolically written as

$$\frac{\partial^2 \underline{f}}{\partial \underline{x}(t_{k+1})^2} \quad \text{and} \quad \frac{\partial^2 \underline{g}}{\partial \underline{x}(t_k)^2} \quad \text{for } n > 1.$$

A nonlinear filter can be derived if the nominal solution $\{\tilde{\underline{x}}(t_j)\}$, $j > 0$ and the order of the Taylor series expansion is specified.

The Linearized Kalman filter

Let $\{\tilde{\underline{x}}(t_j)\}$, $j > 0$ be a deterministic solution of eq. (3.10) which is computed independently from the filtering procedure. If the second order

derivatives $\frac{\partial^2 \underline{f}}{\partial \underline{x}(t_{k+1})^2}$
and $\frac{\partial^2 \underline{g}}{\partial \underline{x}(t_k)^2}$ are neglected eq. (3.11) becomes

$$\begin{aligned} (3.12) \quad & \underline{f}(\Delta t_k, \tilde{\underline{x}}(t_{k+1})) + \left[\frac{\partial \underline{f}}{\partial \underline{x}(t_{k+1})} \right]_{\tilde{\underline{x}}(t_{k+1})} (\underline{x}(t_{k+1}) - \tilde{\underline{x}}(t_{k+1})) = \\ & = \underline{g}(\Delta t_k, \tilde{\underline{x}}(t_k)) + \left[\frac{\partial \underline{g}}{\partial \underline{x}(t_k)} \right]_{\tilde{\underline{x}}(t_k)} (\underline{x}(t_k) - \tilde{\underline{x}}(t_k)) + \underline{u}(t_{k+1}) \end{aligned}$$

or, using eq. (3.10) with $\underline{x}(t_j) = \tilde{\underline{x}}(t_j) \quad \forall j > 0,$

$$(3.13) \quad \left[\frac{\partial \underline{f}}{\partial \underline{x}(t_{k+1})} \right]_{\tilde{\underline{x}}(t_{k+1})} (\underline{x}(t_{k+1}) - \tilde{\underline{x}}(t_{k+1})) = \left[\frac{\partial \underline{g}}{\partial \underline{x}(t_k)} \right]_{\tilde{\underline{x}}(t_k)} (\underline{x}(t_k) - \tilde{\underline{x}}(t_k))$$

which is equivalent with eq. (3.2) $\left\{ \begin{aligned} A &= \left[\frac{\partial \underline{f}}{\partial \underline{x}(t_{k+1})} \right]_{\tilde{\underline{x}}(t_{k+1})} \\ B &= \left[\frac{\partial \underline{g}}{\partial \underline{x}(t_k)} \right]_{\tilde{\underline{x}}(t_k)} \end{aligned} \right.$

The linear Kalman filter can now be applied to eq. (3.14) where a white system noise sequence $\underline{W}(t_k)$ is added and random variables $\delta \underline{x}(t_j) = \underline{x}(t_j) - \tilde{\underline{x}}(t_j)$ are introduced

$$(3.14) \quad \underline{A} \delta \underline{x}(t_{j+1}) = \underline{B} \delta \underline{x}(t_j) + \underline{W}(t_j) \quad \text{with } A, B \text{ defined above.}$$

The optimal estimate of the mean and covariance of $\underline{x}(t_{k+1})$, based on eq. (3.14) and measurement data $\underline{z}(t_j)$, $1 < j < k$ are now found according to

$$\begin{aligned}
 \hat{\underline{x}}(k+1/k) &= \hat{\underline{\delta x}}(k+1/k) + \tilde{\underline{x}}(t_{k+1}) = A^{-1}B \hat{\underline{\delta x}}(k/k) + \tilde{\underline{x}}(t_{k+1}) \\
 (3.15a) \qquad &= A^{-1}B \{ \hat{\underline{x}}(k/k) - \tilde{\underline{x}}(t_k) \} + \tilde{\underline{x}}(t_{k+1})
 \end{aligned}$$

$$(3.15b) \quad P(k+1/k) = A^{-1} \{ B \cdot P(k/k) \cdot B^T + Q(k) \} A^{-T}$$

The next step in the filter algorithm to compute $\hat{\underline{x}}(k+1/k+1)$ and $P(k+1/k+1)$ are performed according to eq.s (3.7)-(3.9) which can be applied without resumption. Crucial to the application of this filter algorithm is that $\| \underline{x}(t_k) - \tilde{\underline{x}}(t_k) \|$ is small for all $k \geq 0$. This assumption can however easily be violated. If for example in tidal motions a phase shift appears between the computed water levels represented in $\tilde{\underline{x}}(t_k)$ and their true value $\| \underline{x}(t_k) - \tilde{\underline{x}}(t_k) \|$ will grow substantially.

The extended Kalman filter

is more suited to provide that $\| \underline{x}(t_k) - \tilde{\underline{x}}(t_k) \|$ is small since $\tilde{\underline{x}}(t_k)$ is not calculated in advance but is derived from

$$(3.16) \quad \tilde{\underline{x}}(t_k) = \hat{\underline{x}}(k/k), \quad \underline{f}(\Delta_k, \tilde{\underline{x}}(t_{k+1})) = \underline{g}(\Delta_k, \hat{\underline{x}}(k/k)) + \underline{u}(t_{k+1})$$

which implies that the nominal solution $\{ \tilde{\underline{x}}(t_j) \}$ is influenced by the measurement data $\tilde{\underline{z}}(t_i)$ as soon as these are available. The filter algorithm is essentially the same as the linearized Kalman filter but the approach is rather different. So in first order $\hat{\underline{x}}(k+1/k) = \tilde{\underline{x}}(t_{k+1})$. This follows from eq. (3.15a) with $\tilde{\underline{x}}(k/k) = \hat{\underline{x}}(k/k)$. The other filter equations are equivalent with eq.s (3.15b), (3.7)-(3.9).

This extended Kalman filter is widely used in nonlinear filtering problems. The ability of this filter to reconstruct the state from noisy initial data and observations however can only be deduced from numerical experiments with so-called "truth - models", examples can be found in the next section.

Second order filters

The first order filters are based on a set of linear system equations which are derived by a local and instantaneous linearization of the original

nonlinear eq.s (3.10) to apply the linear Kalman filter algorithm. It is therefore that no difference is found whether an explicit or implicit method of discretization is used: the derived system is linear on both time levels. This analogy disappears when in the Taylor series expansion terms up to second order are retained.

Take again $\tilde{\underline{x}}(t_k) = \hat{\underline{x}}(k/k)$, $\underline{f}(\Delta t_k, \tilde{\underline{x}}(t_{k+1})) = \underline{g}(\Delta t_k, \hat{\underline{x}}(k/k)) + \underline{u}(t_{k+1})$. Then eq. (3.17) is found.

$$\begin{aligned}
 (3.17) \quad & \left[\frac{\partial \underline{f}}{\partial \underline{x}}(t_{k+1}) \right]_{\tilde{\underline{x}}(t_{k+1})} (\underline{x}(t_{k+1}) - \tilde{\underline{x}}(t_{k+1})) + \\
 & + \frac{1}{2} \left[\frac{\partial^2 \underline{f}}{\partial \underline{x}^2}(t_{k+1}) \right]_{\tilde{\underline{x}}(t_{k+1})} (\underline{x}(t_{k+1}) - \tilde{\underline{x}}(t_{k+1})) (\underline{x}(t_{k+1}) - \tilde{\underline{x}}(t_{k+1}))^T = \\
 & = \left[\frac{\partial \underline{g}}{\partial \underline{x}}(t_k) \right]_{\hat{\underline{x}}(k/k)} (\underline{x}(t_k) - \hat{\underline{x}}(k/k)) + \\
 & + \frac{1}{2} \left[\frac{\partial^2 \underline{g}}{\partial \underline{x}^2}(t_k) \right]_{\hat{\underline{x}}(k/k)} (\underline{x}(t_k) - \hat{\underline{x}}(k/k)) (\underline{x}(t_k) - \hat{\underline{x}}(k/k))^T
 \end{aligned}$$

In case of an explicit discretization: $\underline{f}(\Delta t_k, \underline{x}(t_{k+1})) = \underline{x}(t_{k+1})$ eq. (3.17) reduces to eq. (3.18)

$$\begin{aligned}
 (3.18) \quad & \underline{x}(t_{k+1}) - \tilde{\underline{x}}(t_{k+1}) = \left[\frac{\partial \underline{g}}{\partial \underline{x}}(t_k) \right]_{\hat{\underline{x}}(k/k)} (\underline{x}(t_k) - \hat{\underline{x}}(k/k)) + \\
 & + \frac{1}{2} \left[\frac{\partial^2 \underline{g}}{\partial \underline{x}^2}(t_k) \right]_{\hat{\underline{x}}(k/k)} (\underline{x}(t_k) - \hat{\underline{x}}(k/k)) (\underline{x}(t_k) - \hat{\underline{x}}(k/k))^T
 \end{aligned}$$

Application of the E operator to eq. (3.18) results in

$$(3.19) \quad \hat{\underline{x}}(k+1/k) = \tilde{\underline{x}}(t_{k+1}) + \frac{1}{2} \left[\frac{\partial^2 \underline{g}}{\partial \underline{x}^2}(t_k) \right]_{\hat{\underline{x}}(k/k)} P(k/k)$$

For common nonlinear $\underline{f}(\Delta_k, \underline{x}(t_{k+1}))$ eq. (3.17) leads to

$$\begin{aligned}
 (3.20) \quad & \left[\frac{\partial \underline{f}}{\partial \underline{x}(t_{k+1})} \right]_{\underline{\hat{x}}(t_{k+1})} (\hat{\underline{x}}(k+1/k) - \tilde{\underline{x}}(t_{k+1})) + \\
 & + \frac{1}{2} \left[\frac{\partial^2 \underline{f}}{\partial \underline{x}(t_{k+1})^2} \right]_{\underline{\hat{x}}(t_{k+1})} \{ P(k+1/k) + [\hat{\underline{x}}(k+1/k) - \tilde{\underline{x}}(t_{k+1})]^2 \} = \\
 & = \frac{1}{2} \left[\frac{\partial^2 \underline{g}}{\partial \underline{x}(t_k)^2} \right]_{\underline{\hat{x}}(k/k)} P(k/k)
 \end{aligned}$$

A comparison between eq.s (3.19) and (3.20) learns that eq. (3.19) computes $\hat{\underline{x}}(k+1/k)$ independently from $P(k+1/k)$ whereas $\hat{\underline{x}}(k+1/k)$ and $P(k+1/k)$ are coupled in eq. (3.20). Moreover, the equation associated with eq. (3.20) to compute $P(k+1/k)$ is nonlinear with respect to $P(k+1/k)$ and contains terms like $[\hat{\underline{x}}(k+1/k) - \tilde{\underline{x}}(t_{k+1})]^2$ which are not easy to deal with. These difficulties do not arise when $\underline{f}(\Delta_k, \underline{x}(t_{k+1})) \equiv \underline{x}(t_{k+1})$, requiring

$$\begin{aligned}
 (3.21) \quad P(k+1/k) = & \left[\frac{\partial \underline{g}}{\partial \underline{x}(t_k)} \right]_{\underline{\hat{x}}(k/k)} P(k/k) \left[\frac{\partial \underline{g}}{\partial \underline{x}(t_k)} \right]_{\underline{\hat{x}}(k/k)}^T + Q(k) + \\
 & + \alpha \cdot \left[\frac{\partial^2 \underline{g}}{\partial \underline{x}(t_k)^2} \right]_{\underline{\hat{x}}(k/k)} P(k/k)^2 \left[\frac{\partial^2 \underline{g}}{\partial \underline{x}(t_k)^2} \right]_{\underline{\hat{x}}(k/k)}^T
 \end{aligned}$$

with $\alpha = \frac{1}{2}$ (resulting in the Gaussian second order filter) or $\alpha = \frac{1}{4}$ (Truncated second order filter) [Maybeck, 1982].

The second order filters require much more computational time and memory if compared with the extended kalman filter, whereas the benefits are not always clear. The full second order filter algorithm is therefore seldom used, especially not when $\underline{f}(\Delta_k, \underline{x}(t_{k+1}))$ is nonlinear in $\underline{x}(t_{k+1})$.

A compromis in applying the second order effects is achieved by neglecting the quadratic forms of $P(k+1/k)$ and $P(k/k)$ in the relation to compute $P(k+1/k)$ which means that this approximated relation equals the extended Kalman filter algorithm. Now, the for greater part of the computational efforts to

incorporate the second order effects has vanished but the essence is retained. This approximation introduces the "bias correction terms"

$$\frac{1}{2} \left\{ \left[\frac{\sigma_g^2}{\partial \underline{x}(t_k)^2} \right] \hat{\underline{x}}(k/k) P(k/k) - \left[\frac{\sigma_f^2}{\partial \underline{x}(t_{k+1})^2} \right] \tilde{\underline{x}}(t_{k+1}) P(k+1/k) \right\}$$

in eq. (3.20).

The effects of these second order terms will be pointed out according to the numerical results in the tidal motion problem which can be found in chapter 4.

§ 5 Specification of the filter

The difference equations, derived in chapter 2, form the basis of the system description to be used in the filter. The nonlinearity of these equations necessitates the use of the extended Kalman filter algorithm where possibly bias correction terms can be added.

The state vector $\underline{x}(t_k)$ contains components which represent the water level and the velocity at the various grid points. However, there are more unknown quantities in the system, for example the (chezy) parameter μ in the friction term, the reflection coefficients ρ and η in the boundary conditions and the wind stress coefficient C_d . All these parameters are to some extent unknown and can be conceived as random variables. The evolution in time is assumed to be very simple: it is expected that they behave like system constants, so the relation between a parameter $p(t = t_{k+1})$ and $p(t = t_k)$ is $p(t = t_{k+1}) = p(t = t_k) + W(t_k)$, $W(t_k)$ being a component of the white noise sequence $\underline{W}(t_k) \simeq N(0, Q(k))$. By adding the noise a random character of the parameter can be taken into account.

Model along the coast (Model I)

Based on the system representation, compare eq. (3.10),

$$\underline{x}(t_{k+1}) = \Phi(\Delta t_k, \underline{x}(t_k)) + \underline{u}(t_{k+1})$$

the stochastic model to describe the propagation in time of the stochastic proces $\{\underline{x}(t_k)\}$ is

$$(3.14) \quad \underline{X}(t_{k+1}) - \tilde{\underline{X}}(t_{k+1}) = \Phi(\Delta t_k, \hat{\underline{X}}(k/k))(\underline{X}(t_k) - \hat{\underline{X}}(k/k)) + \underline{W}(t_k)$$

where $\underline{W}(t_k)$ is the white noise and $\tilde{\underline{X}}(t_{k+1}) = \phi(\Delta t_k, \hat{\underline{X}}(k/k))$.

In deriving the measurement equation one has to consider that, in general, the sampling points or tide gauges where the water level is measured, are not located exactly on the x-axis. However, by means of eq. (2.10) it is possible to correct the water level perpendicular to the x-axis, taking into account the effects of the wind in the y-direction and the Coriolis force. Using this equation we can express the sampled water level as a nonlinear function of the state $\underline{X}(t_k)$. Suppose $\tilde{z}(t_k)$ is a scalar measurement data and a realisation of the scalar random variable $Z(t_k)$ taken at the sampling point, see fig. 3.3

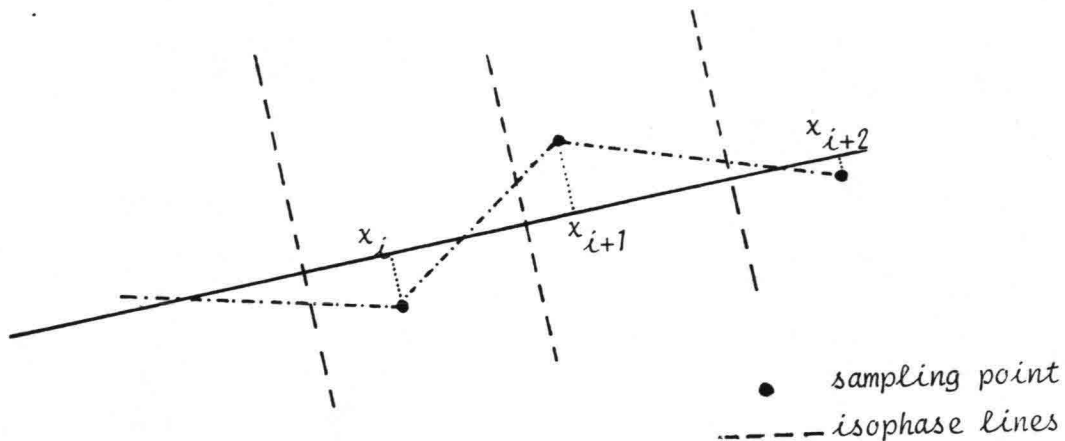


Fig. 3.3 Location of sampling points with respect to the x-axis.

In this case the measurement equation is

$$(3.22) \quad \begin{aligned} Z(t_k) &= m^i(\underline{X}(t_k)) + V(t_k) \\ &= h(x_m, t_k) + \frac{1}{g} \{-f \cdot u(x_m, t_k) - C_d \frac{V^2 \sin \phi}{D(X_m) + h(x_m, t_k)}\} \Delta y + V(t_k) \end{aligned}$$

Here Δy is the distance between the measurement station and the x-axis, see fig. 3.3, and $V(t_k)$ the scalar measurement noise. Since in general

$$\left| C_d \frac{V^2 \sin \phi}{D+h} \right| \ll |fu| \quad \text{the term dealing with the wind effect has been}$$

omitted. To account for local effects a parameter a^i is introduced in the measurement equation:

$$(3.23) \quad \begin{aligned} Z(t_k) &= m^i(\underline{X}(t_k)) + V(t_k) \\ &= (1+a_i) h(x_m, t_k) - \frac{f}{g} u(x_m, t_k) \cdot \Delta y \end{aligned}$$

with $a_i \ll 1$.

Generalizing this scalar case yields the vector measurement equation

$$(3.24) \quad \underline{Z}(t_k) = \underline{m}(\underline{X}(t_k)) + \underline{V}(t_k) \text{ where } \underline{m}(\underline{X}(t_k)) = \begin{bmatrix} m^1(\underline{X}(t_k)) \\ \vdots \\ m^n(\underline{X}(t_k)) \end{bmatrix}$$

and $m^i(\underline{X}(t_k))$ defined by eq. (3.23), $i > 1$.

The x -axis is chosen such that the sampling point at $x = x_1$ is located exactly on the x -axis, this

$$(3.25) \quad m^1(\underline{X}(t_k)) = h(x_1, t_k)$$

As mentioned before, the μ , C_d and also the a^i are not constant but have essentially a random character. Therefore, these parameters are estimated together with the water levels and velocities by augmenting the n -state vector:

$$\underline{X}(t_k) = [h^k, u_1^k, h_2^k, a_2^k, u_2^k, h_3^k, \dots, h_m^k, a_m^k, u_m^k, s^k, \mu, C_d]$$

In order to apply the filter equations (3.7)-(3.9) we must find a constant $m \times n$ - measurement matrix M . This matrix M can be found in a similar way the nonlinear eq. (3.10) is linearized (locally and instantaneously by means of $\tilde{\underline{X}}(t_{k+1})$ and $\hat{\underline{X}}(k/k)$) to use in the extended Kalman filter algorithm. Here, this linearization leads to

$$(3.26) \quad \begin{aligned} \underline{Z}(t_{k+1}) - \underline{m}(\tilde{\underline{X}}(t_{k+1})) &= \left[\frac{\partial \underline{m}}{\partial \underline{X}(t_{k+1})} \right]_{\tilde{\underline{X}}(t_{k+1})} (\underline{X}(t_{k+1}) - \tilde{\underline{X}}(t_{k+1})) + \underline{V}(t_{k+1}) \\ &= M(\underline{X}(t_{k+1}) - \tilde{\underline{X}}(t_{k+1})) + \underline{V}(t_{k+1}) \end{aligned}$$

In chapter 2, section 5 the boundary conditions were prescribed:

$x = x_1$: an oscillating water level to "drive" the model,

$x = x_m$: a weakly reflective boundary condition, eq. (2.17) with $\eta = 0$

$$u - 2\sqrt{g \frac{A}{b}} = \text{constant}$$

If, for $t = t_k$, predictions of the water levels and velocities are required, eq (3.14) is solved (repeatedly), see also fig. 3.2. As initial conditions the estimate of the state $\underline{X}(t_k)$ is used. However, at the boundary ($x = x_1$) Nieuwpoort the water level has to be predicted too. This can be established by performing a harmonic analysis of the water level at this location [Dronkers, 1964, 1975]:

$$(3.27) \quad h_1(t) = \sum_i A_i \cos(2\pi v_i t + \phi_i) + s(t)$$

where A_i , v_i and ϕ_i are respectively the amplitude, frequency and phase of the i -th harmonic constituent, and $s(t)$ the non tidal part of the water level, i.e. mainly determined by meteorological effects. Now $s(t_k)$ is a component of the state vector $\underline{X}(t_k)$ and can be predicted using eq. (2.18). Therefore, the prediction of $h_1(t)$, $t > t_k$ is given by

$$(3.28) \quad \begin{aligned} h_1(t) &= \sum_i A_i \cos(2\pi v_i t + \phi_i) + s(t) \\ &= h_1(t_k) + \sum_i A_i \cos(2\pi v_i t + \phi_i) - \sum_i A_i \cos(2\pi v_i t_k + \phi_i) \\ &\quad + s(t) - s(t_k) \\ &= h_1(t_k) + \sum_i A_i [\cos(2\pi v_i t + \phi_i) - \cos(2\pi v_i t_k + \phi_i)] \\ &\quad + \gamma V^2(t - \tau) \cos(\tilde{\psi}(t - \tau) - \tilde{\psi}_0) - s(t_k) \end{aligned}$$

where eq. (2.18) is substituted. Since both $h_1(t_k)$ and $s(t_k)$ are components of $\underline{X}(t_k)$ they are estimated by the filter and can be used to predict the water level $h_1(t)$, $t > t_k$ by means of eq. (3.28).

The Eastern Scheldt model (Model II)

Comparing this model with the model along the coast, the following differences can be noted:

- a simpler (= linear) relationship between $\underline{Z}(t_k)$ and $\underline{X}(t_k)$ because the dependence of the water level on the y-direction may be neglected in the estuary, so the sampling points are identified with grid points. Therefore, the parameters a_i are absent.
- Random friction parameters are assigned to every channel branch between two sampling points. The fact that in Model I only one random friction parameter μ is introduced depends on the necessary random parameters a_i which represent already some frictional effects.
- In the boundary conditions, random variables η , ρ estimated by the filter.

This gives the n-state vector

$$\underline{X}(t_k) = [h_1^k, u_1^k, h_2^k, \dots, h_r^k, u_r^k, \eta_1^k, \eta_2^k, \rho_1^k, \rho_2^k, C_d^k, \mu_1^k, \dots, \mu_s^k]$$

with r = number of grid points in Model II

s = number of channel branches.

In deterministic sense the linking of the two models is quite simple: in Model I the water level in O.S.10 is computed which serves as the boundary condition for Model II. In our stochastic approach this cannot be applied without modification. One of the assumptions is that the two models are stochastically independent which implies that the set of available measurements must be divided in two disjoint subsets, are is used in Model I the other in Model II. Since the grid point which represents O.S.10 occurs in both models, see fig. 2.9. This measurement can only be used in I or II. This independency is suggested by the fact that the tidal motion in the Eastern Scheldt does not influence the water movement in the area outside the estuary. So, if the measurements from O.S.10 are used to correct the predicted solution in Model I, these cannot be used in Model II. This of course has less practical than theoretical significance. Our solution to this problem, which somewhat violates the assumed stochastic independence, is to use the estimate $\hat{h}(k/k)$ in model I of the water level at O.S.10 as artificial measurements with the associated measurement noises found from the covariance $P(k/k)$.

CHAPTER 4

APPLICATION TO TIDAL MOTION PROBLEMS

§ 1 Introduction

In the previous part of this report a stochastic model was formulated to describe the tidal motion in the Dutch coastal area. Now, the results obtained with this model will be commented. An essential feature of the filtering procedure is the computation of (sub)-optimal estimates of the state vector using all available information, both from the mathematical model and the measurement data. The performance of the filter is judged by checking whether the residuals possess their theoretical statistical properties which can be derived from the model. To fulfil this criterion unknown quantities should be specified which is accomplished by the so-called tuning of the filter, i.e. the assignment of values to the variances of the system- and measurement noise. Usually this is a rather complicated process that is carried out by trial and error. In addition to these variances the initial state should be prescribed. Since the dynamical equations are of the hyperbolic type every signal (expressed in terms of Quasi Riemann Invariants) entering the system will vanish after a limited period of time. Consequently, the specification of the initial state is less important than the variances of the noise sequences.

Earlier in this report we mentioned several applications to use the filter

- as a descriptive model in which certain parameters are estimated simultaneously,
- as an algorithm to optimize the location of sampling points in a network
- as a system to predict the water levels (and velocities) in the considered geometrical area.

With this last application one has to remember that variations in quantities as the water velocity and height propagate through the system in a limited time. This property restricts the length of the time interval predictions are still influenced by the (sub)-optimal estimates of the state vector which acts now as an initial condition to perform the predictions. This time interval is

rather simply derived by considering characteristic lines in the (x,t) -domain, see chapter 2, section 4.

In the following sections attention will be paid to all these aspects, illustrated with numerical results using real data. The data from 11-13 September '75 are used to tune the filter in circumstances without significant meteorological effects. However, it is important to study the necessary adaptations in the variances of the noise sequences in periods when meteorological effects are strongly influencing the tidal motion. As will be pointed out later only minor changes are needed to optimize the performance of the filter which means that the system- and measurement noise sequences are relatively time-invariant, a very convenient property when the model is used to predict the water levels on-line.

The availability of measurement data during the 5 weeks period from 11 January - 15 February '83 made it possible to test the filter behaviour extensively, also under extreme situations with wind velocities up to 24 ms^{-1} and water levels above $3.5 \text{ m} + \text{N.A.P.}$ in the mouth of the Eastern Scheldt. This long period also enabled us to analyze the estimates, particularly those which represent parameters. These parameters appear as random variables in system equations, based on certain physical concepts. The analysis may show the random character of the parameters, e.g. whether or not it has a white noise behaviour. For example it is possible to derive the dependence of a wind stress coefficient on the wind velocity, or how the phase of the tide is correlated with the estimates of the friction coefficients.

One of the first studies relating to tidal motions in seas and estuaries has been performed by Budgell and Unny [1982]. Their study considered the following aspects:

- a description of the water movement in a tidal river in Canada,
- computational aspects of the filter algorithm.

Although the geometrical configuration and the dynamical equations are to a certain extent identical with the model of the Eastern Scheldt, some differences in the implementation should be noted:

- the parameter estimation is not included in the (extended Kalman) filter algorithm, but the parameters are adapted by means of a separate maximum

- likelihood estimation procedure,
- the occurrence of matrices of high dimension (the covariance matrices) can easily lead to numerical operations which require huge computation time and memory assess, as is also stated in chapter 3. The use of an implicit method of discretization is even worsening the case because matrix inversions are necessary when the extended Kalman filter is applied, eq.(3.4a2). The use of matrix partitioning techniques, as performed by Budgell and Unny, makes it is possible to approximate the algorithm by substituting the matrix inversion by an inversion operation on a matrix of a much smaller dimension,
 - their primary attention was not to perform predictions over longer periods of time (only predictions, half an hour ahead were computed) while further meteorological influences on the tide were only of minor significance.

§ 2 The filter as a descriptive model

The stochastic model requires, besides a formulation of the dynamics, an interpretation of the geometry which is expressed in terms of the cross-sectional area (A), the channel width (b), the wetted perimeter (P) and the depth (D). These geometrical functions are specified for each grid point. The crude grid makes it difficult to attain certain geometrical influences on the tidal motion that are due to local variations of the bottom surface between the grid points, despite a possible correct prescription of the geometry in these points. The effect of these model errors can be studied by using "truth-models". In literature it is indicated [Chiu, 1978] that these tests are on effective way to study the filter behaviour. These experiments yield information with respect to the following points:

- the way in which certain errors are compensated by the filter. A question to be posed is whether or not reliable values for the water levels can be reproduced from noisy data, in case the geometry is disturbed and how these disturbances effect the simultaneous estimated quantities.
- the ability of the filter to reconstruct all states. This necessary property limits the number and the character of the quantities that we wish to estimate. If we focus our attention on the parameter estimation it will be clear that not every parameter, conceived as a random

variable, can be reconstructed from measurements of water levels: there has to be a correlation between the water levels and the particular parameters via the correlation coefficient from $P(k+1/k)$. Moreover, only an overall effect can be derived from the measurements, e.g. a frictional effect between two sampling points. Difficulties arise when between two sampling points also a wind effect has to be estimated. The associated water levels do not provide enough information to decompose the residual into its correct components. The introduction of such unreconstructable parameters does not reduce the r.m.s. error of the residual and makes the parameter estimation less transparent, so this should be omitted.

The importance of these tests is even more stressed by the lack of mathematical proofs concerning the convergent behaviour of the estimates in time in the case of nonlinear filters and the complications due to the hyperbolic character of the dynamical equations.

After this preliminary step was carried out [Heemink, 1980, ten Brummelhuis, 1984] real data from 11-13 September 1975 were used to tune the filter. Representative results of the predictions, half an hour ahead, are shown in fig.s 4.1-4.4 where the high- and low waters of the astronomical tide are also indicated to mark the meteorological influences. To compare the accuracy of the half hour predictions, the r.m.s. errors

$$(4.1) \quad \sigma_j = \frac{1}{N} \sum_{k=1}^N \{h_j(k+1/k) - m_j(t_{k+1})\}^2, \quad j = 1, 2, \dots, 8$$

are calculated with - $h_j(k+1/k)$ the predictions at point j
 - $m_j(t_{k+1})$ the sampled water level

α (cm)	0.S.4	0.S.9	Zierik- zee	Stave- nisse	Steenb. Sas	Rak Zuid	Wemel- dinge	Bergen op Zoom
σ_j	5.1	6.2	3.3	6.8	3.7	4.7	5.5	7.0
$(\sigma_p)_j$	4.1	5.3	1.7	6.1	2.3	3.6	4.6	6.3

Table I: The r.m.s. errors according to eq.s (4.1) and (4.2)

PERIOD 11 - 13 September '75

— water level, predicted 9.5 hrs. ahead

o sampled data

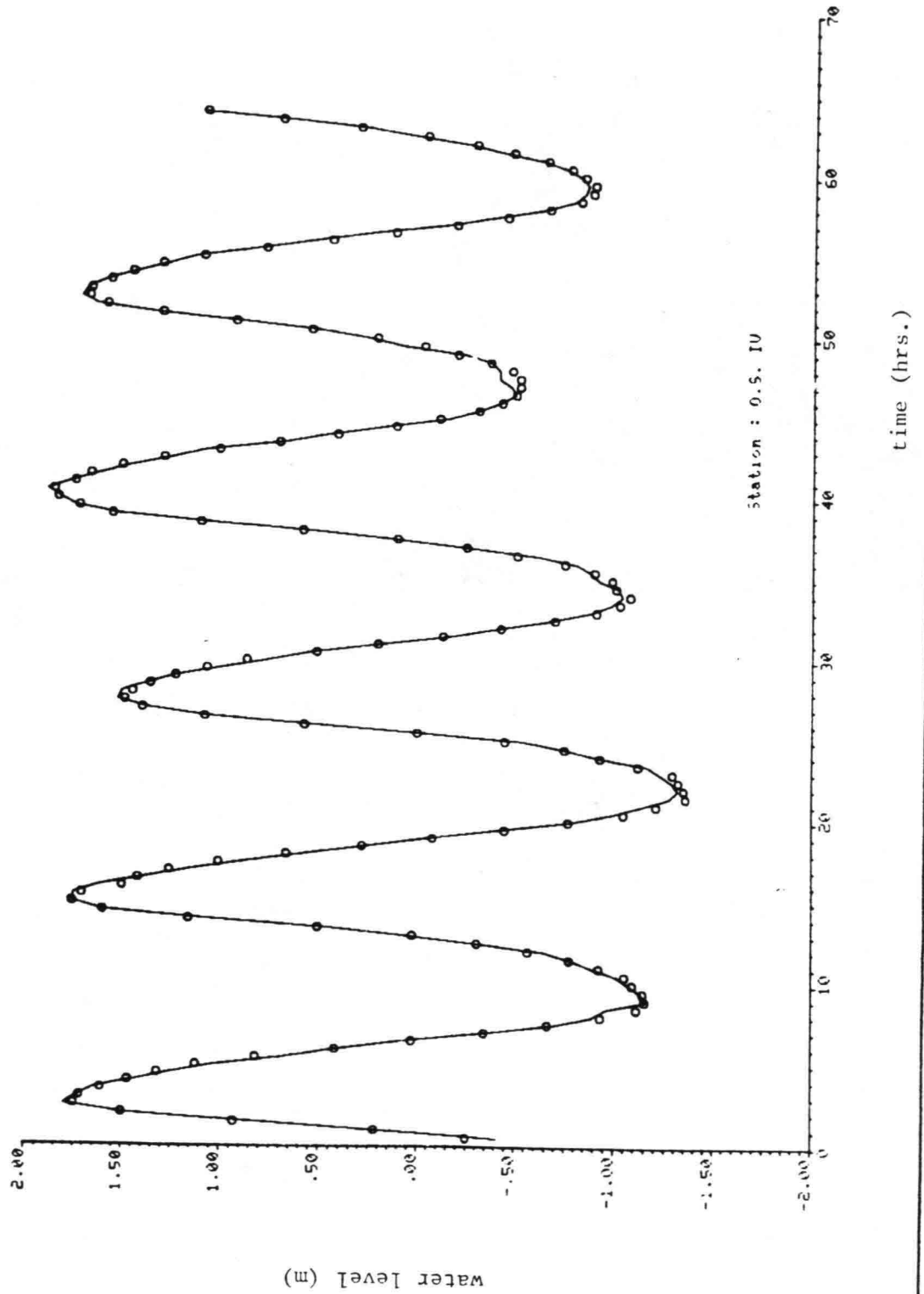


Fig. 4.1

PERIOD 11 - 13 September '75
— water level, predicted 0.5 hrs. ahead
o sampled data

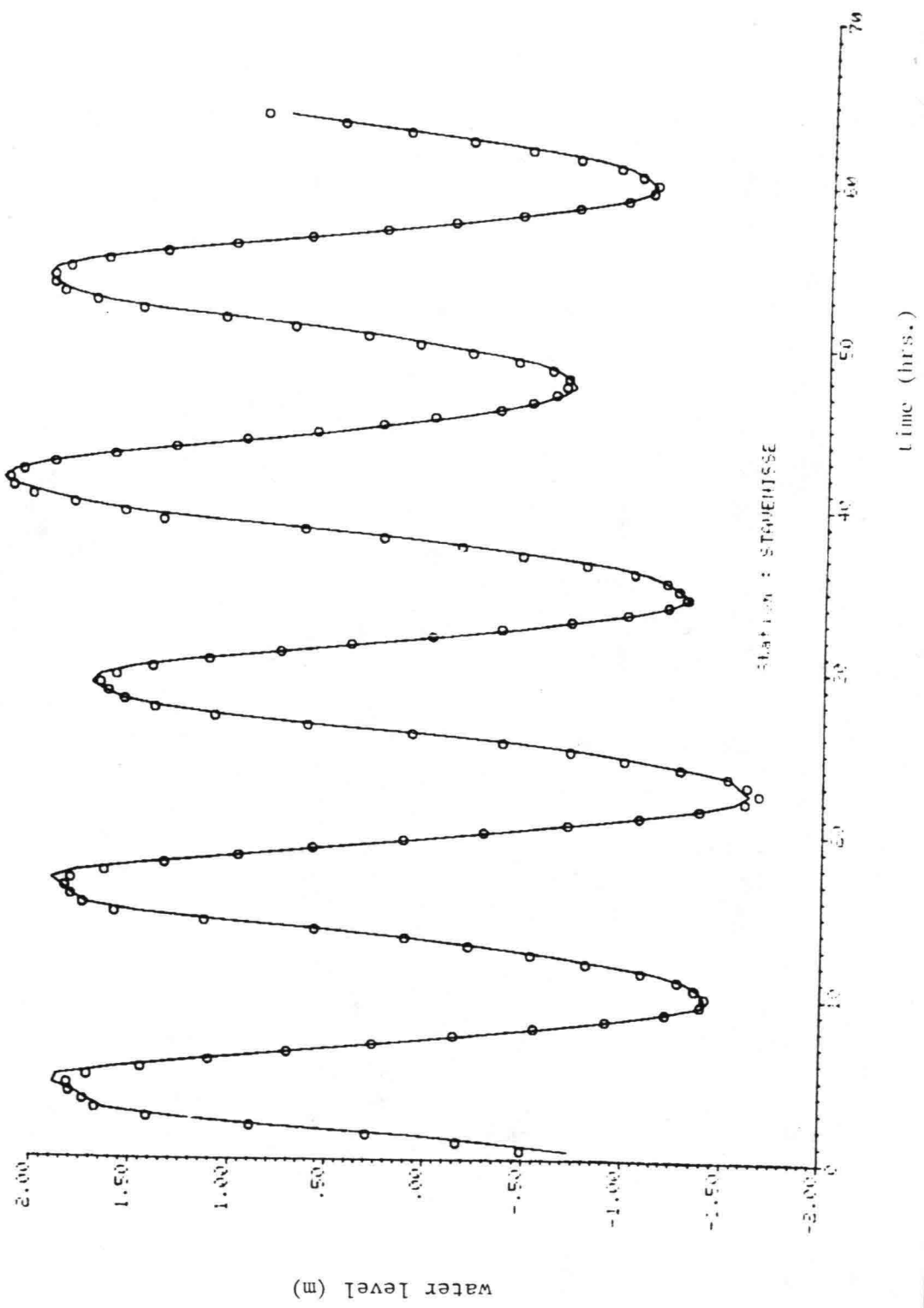


Fig. 4.2

PERIOD 11 - 13 September '75
water level, predicted 0.5 hrs. ahead

o sampled data

—

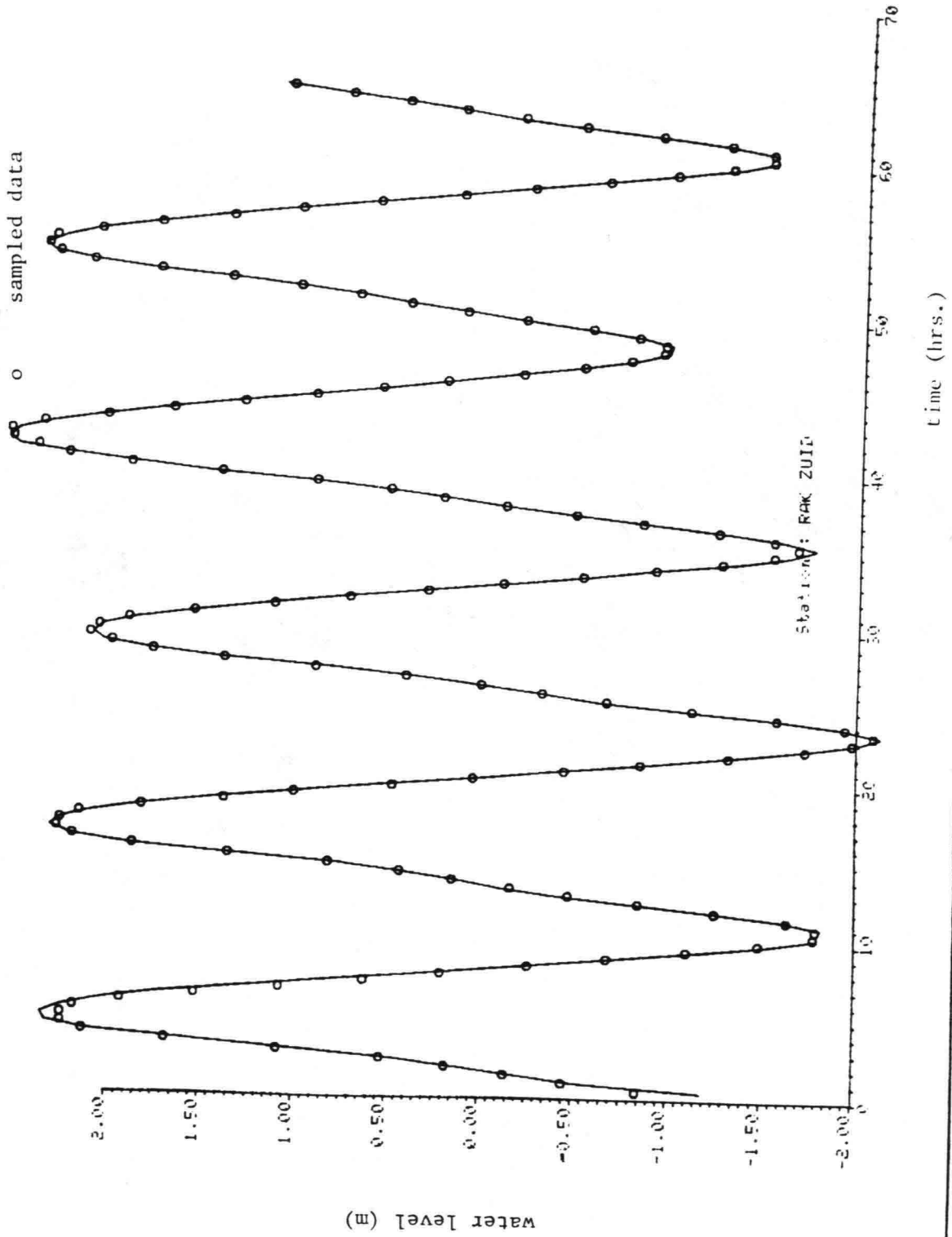


Fig. 4.3

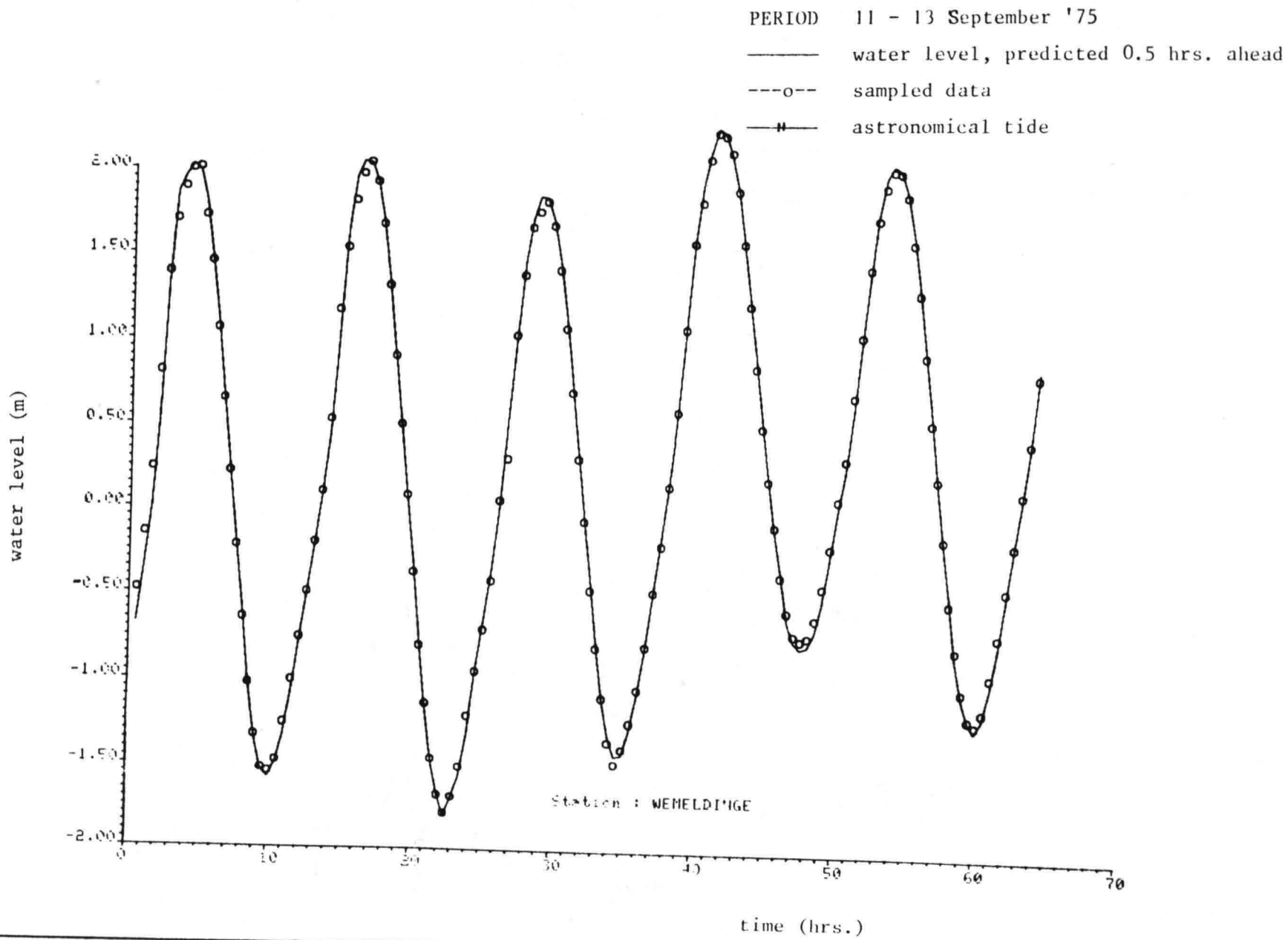


Fig. 4.4

The standard deviation of the measurement errors (σ_m) are assumed to be 2.8 - 3.0 cm in this period, so the error of the predicted water levels can be derived from

$$(4.2) \quad (\sigma_p)_j^2 = \sigma_j^2 - (\sigma_m)_j^2$$

and are given in the last row of table I. The filter is said to be tuned when the residual satisfies its theoretical statistical properties which can be derived from the model.

First, the residual bias shift, derived from

$$(4.3) \quad B(\text{ias}) = \frac{1}{N} \sum_{k=1}^N \{z(t_k) - \hat{h}(k/k-1)\}$$

should be zero.

The second property is that values of $\tilde{\sigma}_j^2$, eq. (4.4), and σ_j^2 , calculated from eq. (4.1) must match: $\tilde{\sigma}_j^2 = \sigma_j^2$

$$(4.4) \quad \tilde{\sigma}_j^2 = P_{jj} + (\sigma_m)_j^2$$

with P_{jj} the variance of $h_j(k+1/k)$, $P_{jj} \in P(k+1/k)$

To achieve the (sub)-optimal behaviour of the filter the statistical properties of the system- and measurement noise sequences must be specified.

The variance of $\underline{X}(t_{k+1}) \simeq N(\hat{X}(k+1/k), P(k+1/k))$ has two components

- the variance, propagated by means of the state transition matrix $\Phi(t_{k+1}, t_k)$ or $A^{-1}(t_{k+1}, t_k) B(t_{k+1}, t_k)$, eq. (3.4a)
- the variance of the system noise $\underline{W}(t_k)$.

A global measure of the variance of the components of $\underline{W}(t_k)$ can be found by assuming that $P(k/k)$ is only weakly amplified by the state transition matrix to derive $P(k+1/k)$, since the eigenvalues of $\Phi(t_{k+1}, t_k)$ are ≤ 1 (in absolute sense) for stability reasons. Therefore, the local error (which is represented by the system noise) varies between 1 - 5 cm for the water levels.

The system noise can be used in different ways. Essentially, a system noise sequence is associated with a dynamical equation or a boundary - c.q. compatibility condition to represent its local error. If an explicit method of discretization is used to derive a system of nonlinear difference equations, this noise is assigned to a specific random variable which is computed by means of this equation. When the method of discretization necessitates a number of computational time steps Δt to cover the interval $\Delta \tau$ between two measurements (for accuracy reasons or a strict CFL - condition) the system noise can be applied every Δt .

Via implicit methods of discretization the system noise is introduced in the expressions by means of the terms

$$(4.5) \quad A^{-1} Q(k) A^{-T}, \text{ using eq. (3.4a2) to compute } P(k+1/k).$$

The transformation (4.5) makes the effect of the system noise correlated in space, even if $Q(k)$ is chosen as a diagonal matrix. Another effect of the implicit formulation is that the variance of the noise sequence of a dynamical equation is equally distributed over the water levels and the velocities in the neighbouring grid points of the stream section.

After investigating the various ways our conclusion with respect to the use of the system noise is that the system noise acts like an integrated quantity over the time interval $[\tau, \tau + \Delta \tau]$ and that it is favourable to assume that the system noise sequences are correlated in space. This can be achieved by introducing in $Q(k)$ off-diagonal elements $\neq 0$ or by means of eq. (4.5) in case of implicit methods of discretization.

Another way to deal with model errors is to conceive system parameters as random variables. In the estimates of these parameters oscillations can be noted which are the model corrections the filter carries out to reduce the r.m.s. error of the residual. In the next section this aspect will be treated more explicit.

The results, acquired with data from the 11 Januari - 15 Februari '83 period are well comparable to the results obtained with the data from the tuning period. However, the instationary behaviour of the tide (in this period 2 major storms occurred) will influence the residuals to some extent. The speci-

fication of the system noise variance is the same as in the tuning period. Examples of the half hour predictions are shown in fig.s 4.5 - 4.10 where the meteorological influences are apparent. The r.m.s. errors, according to eq. 4.1, are presented in table II, where a distinction is made between periods with

- (I) weak
 - (II) moderate
 - (III) strong
- } meteorological influences

σ (cm)	O.S.4	Zierikzee	Steenb. Sas	Rak Zuid	Wemeldinge
σ (I)	5.5	3.7	5.1	5.2	5.7
σ (II)	6.0	4.7	5.7	5.9	6.3
σ (III)	7.0	6.2	5.8	7.4	6.8
σ (average)	6.0	4.6	5.4	6.3	6.1
σ (tuning)	5.1	3.3	3.7	4.7	5.5

Table II: The r.m.s. errors for sampling points in the Eastern Scheldt.

PERIOD 20 - 22 January '83

— water level, predicted 0.5 hrs. ahead

o sampled data

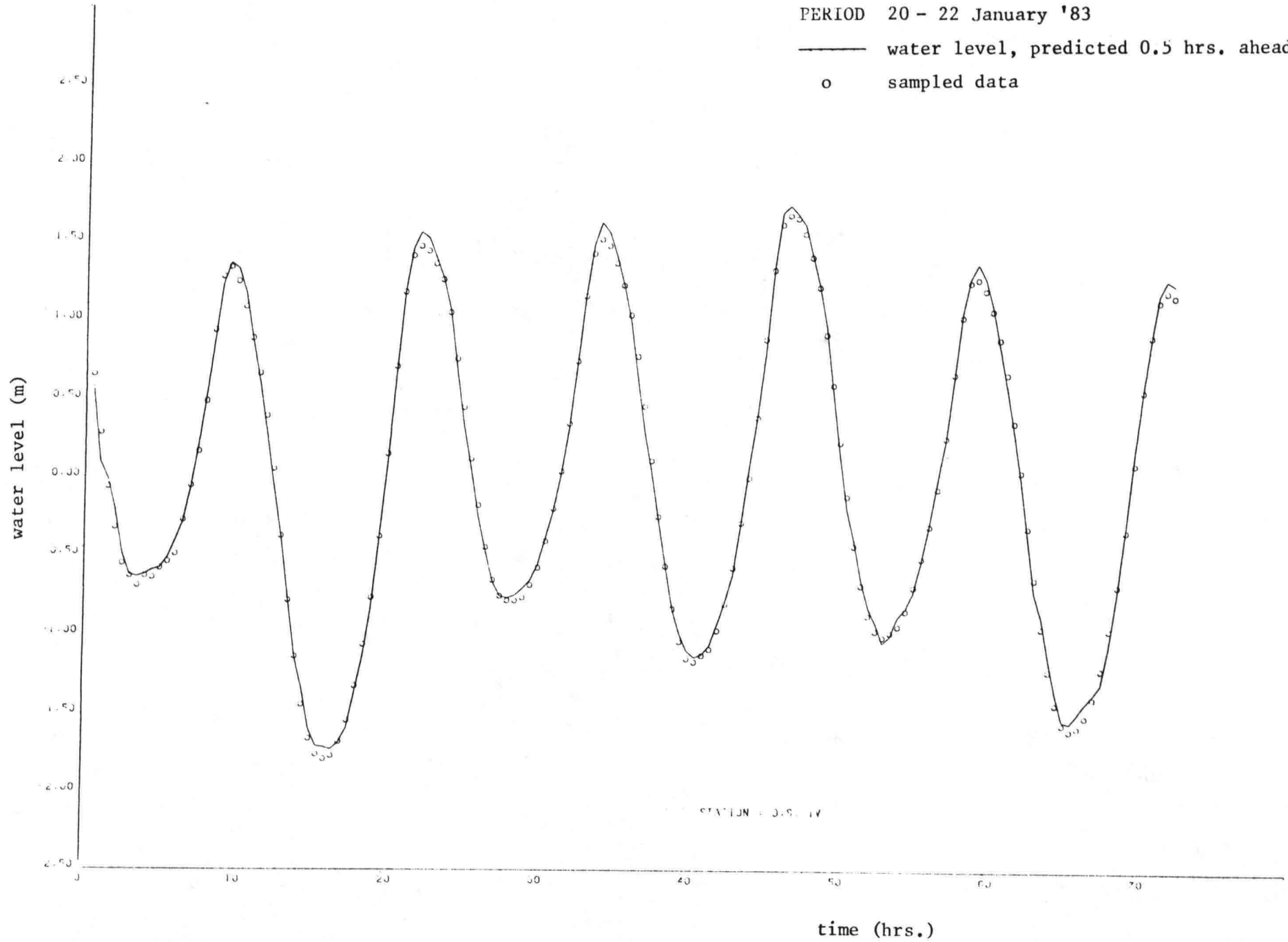


Fig. 4.5a

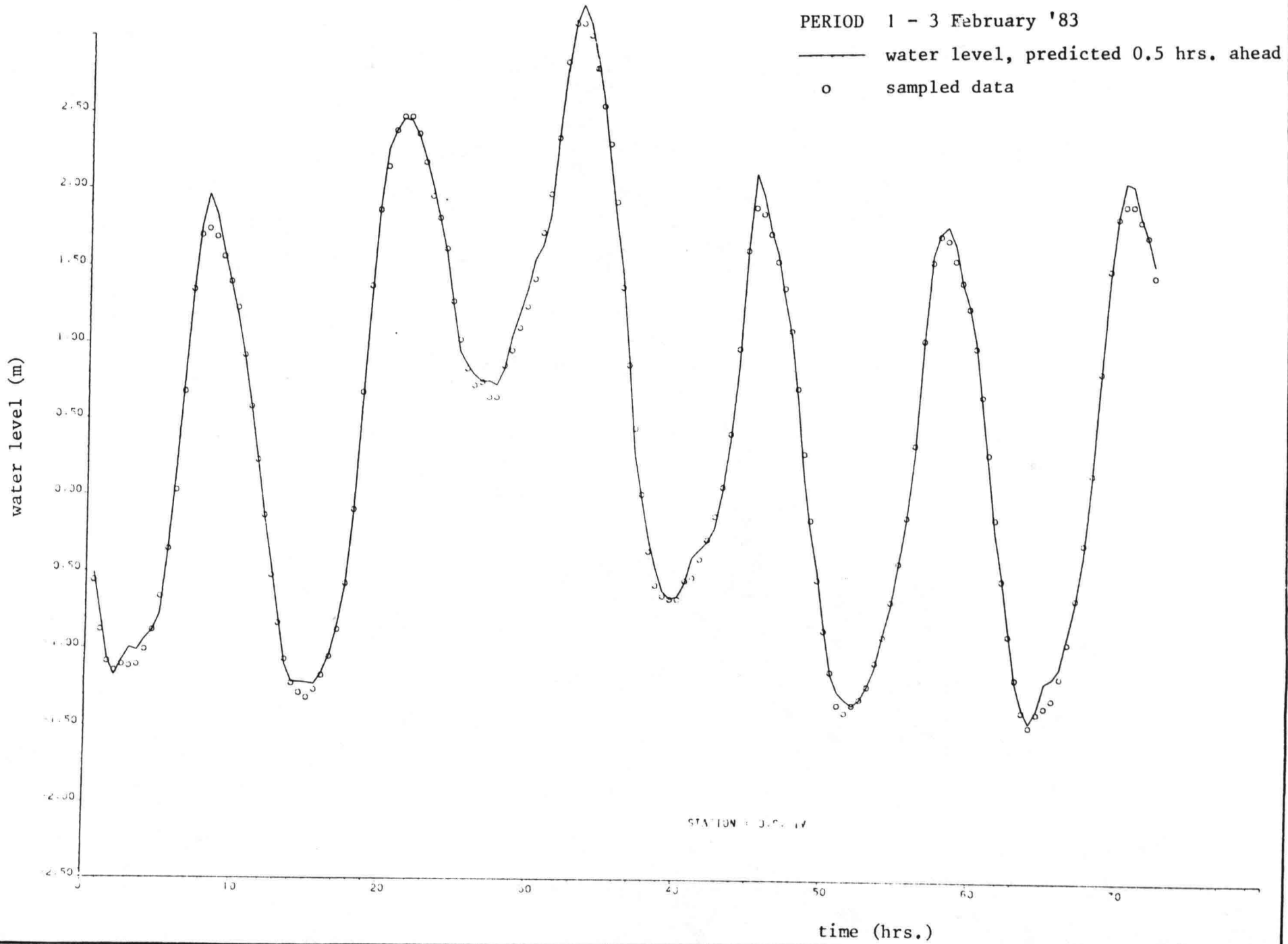


Fig. 4.5b

PERIOD 20 - 22 January '83

— water level, predicted 0.5 hrs. ahead

o sampled data

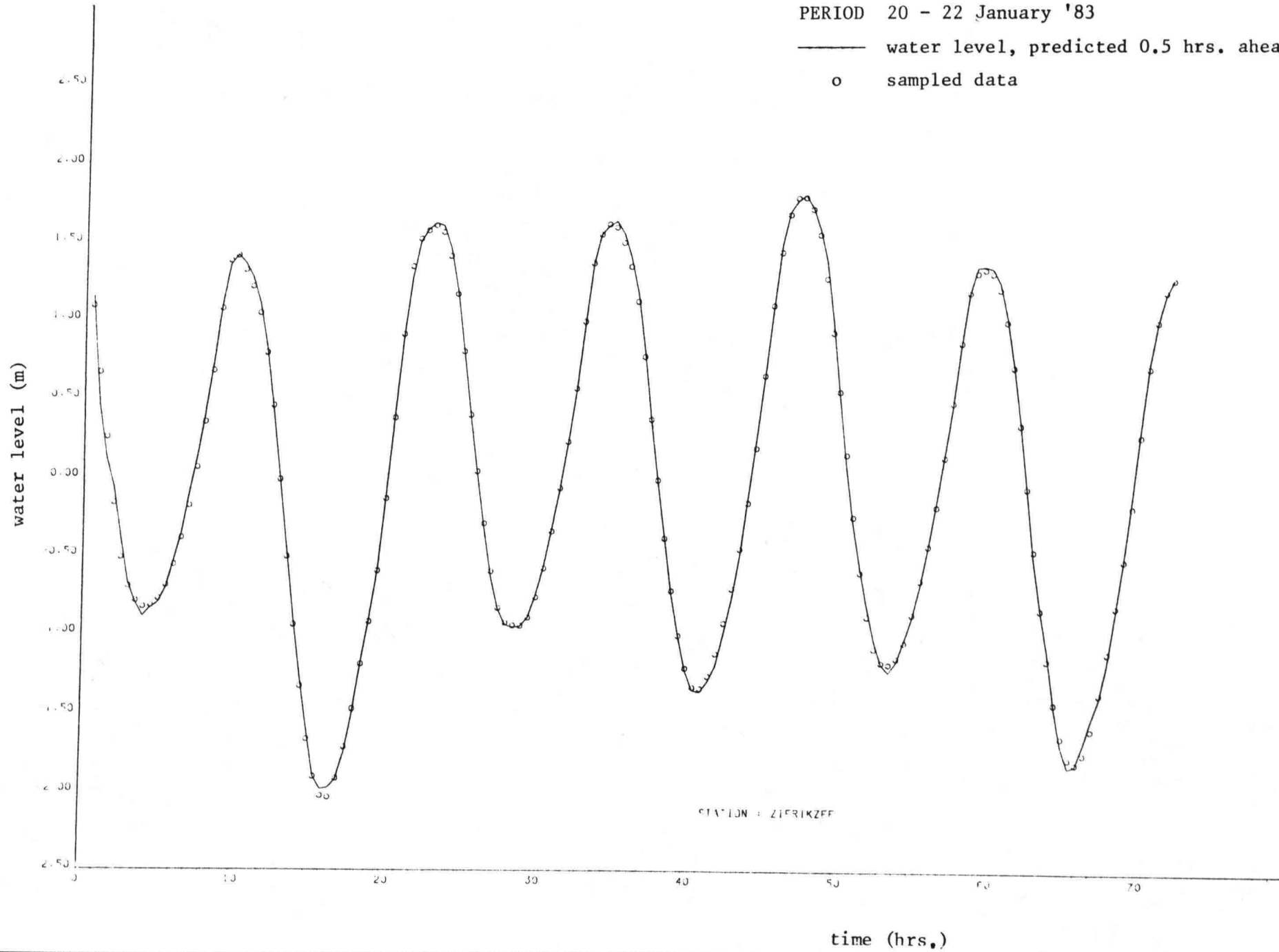


Fig. 4.6a

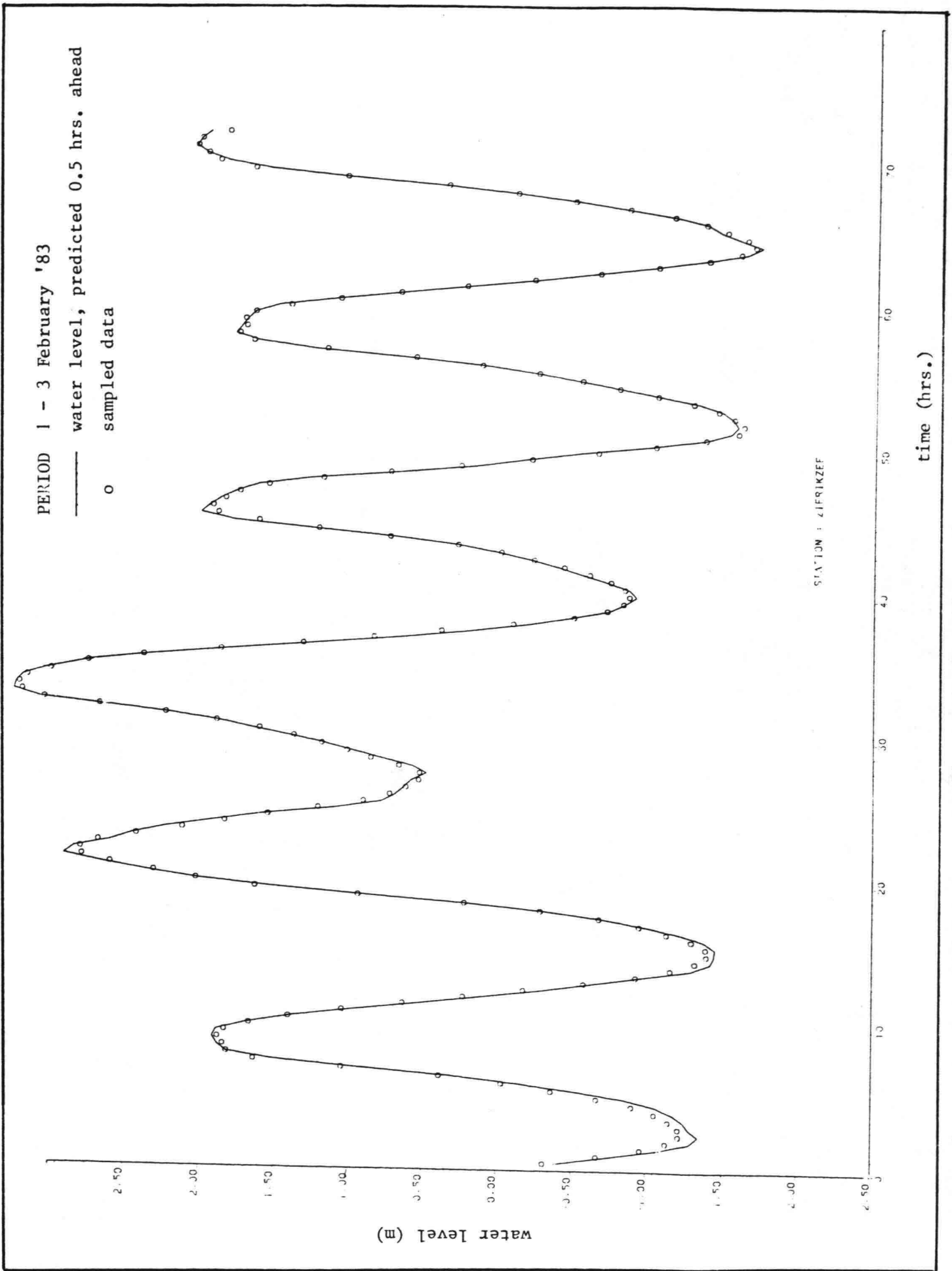


Fig. 4.6b

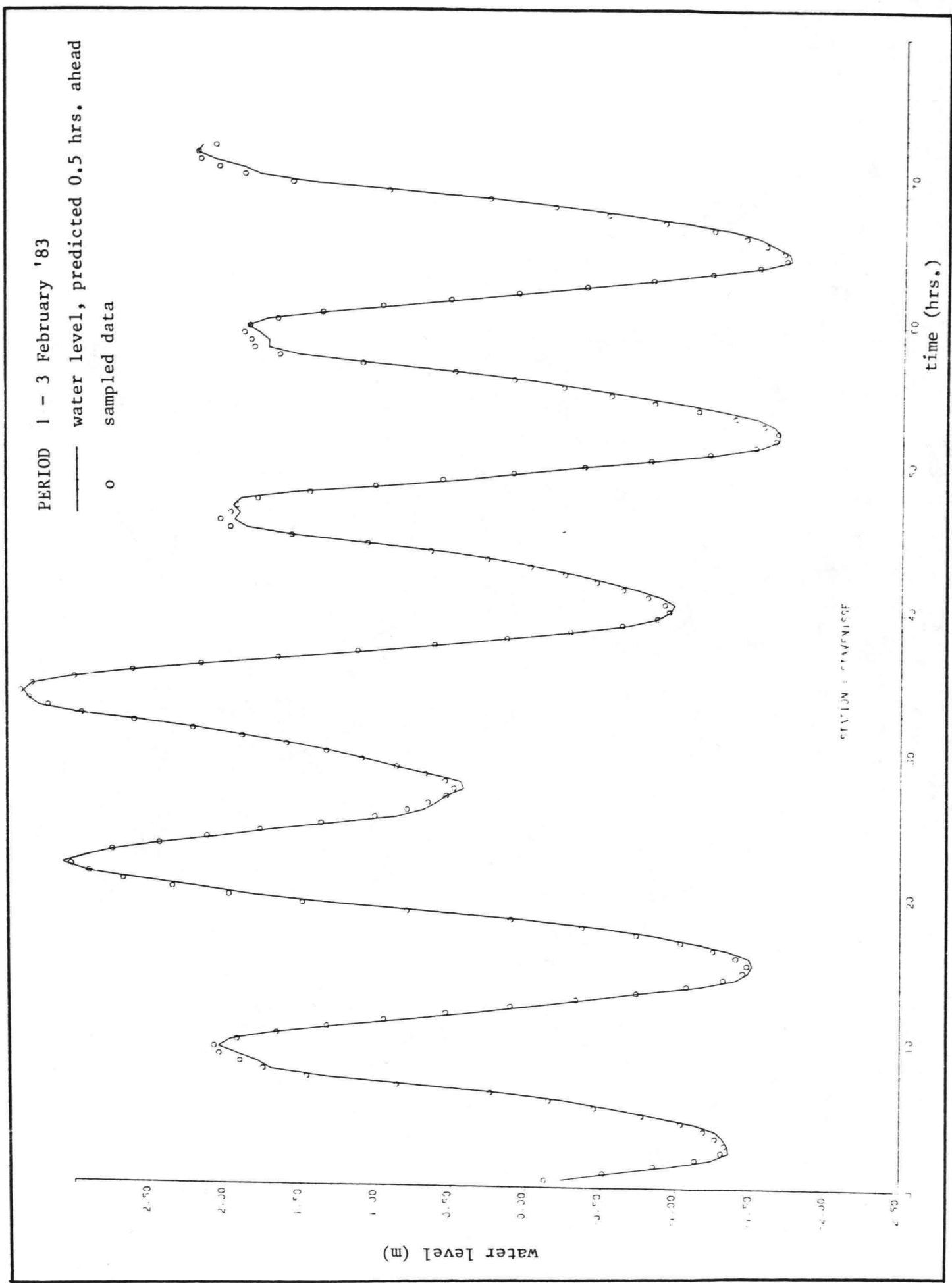


Fig. 4.7a

PERIOD 4 - 6 February '83

— water level, predicted 0.5 hrs. ahead

o sampled data

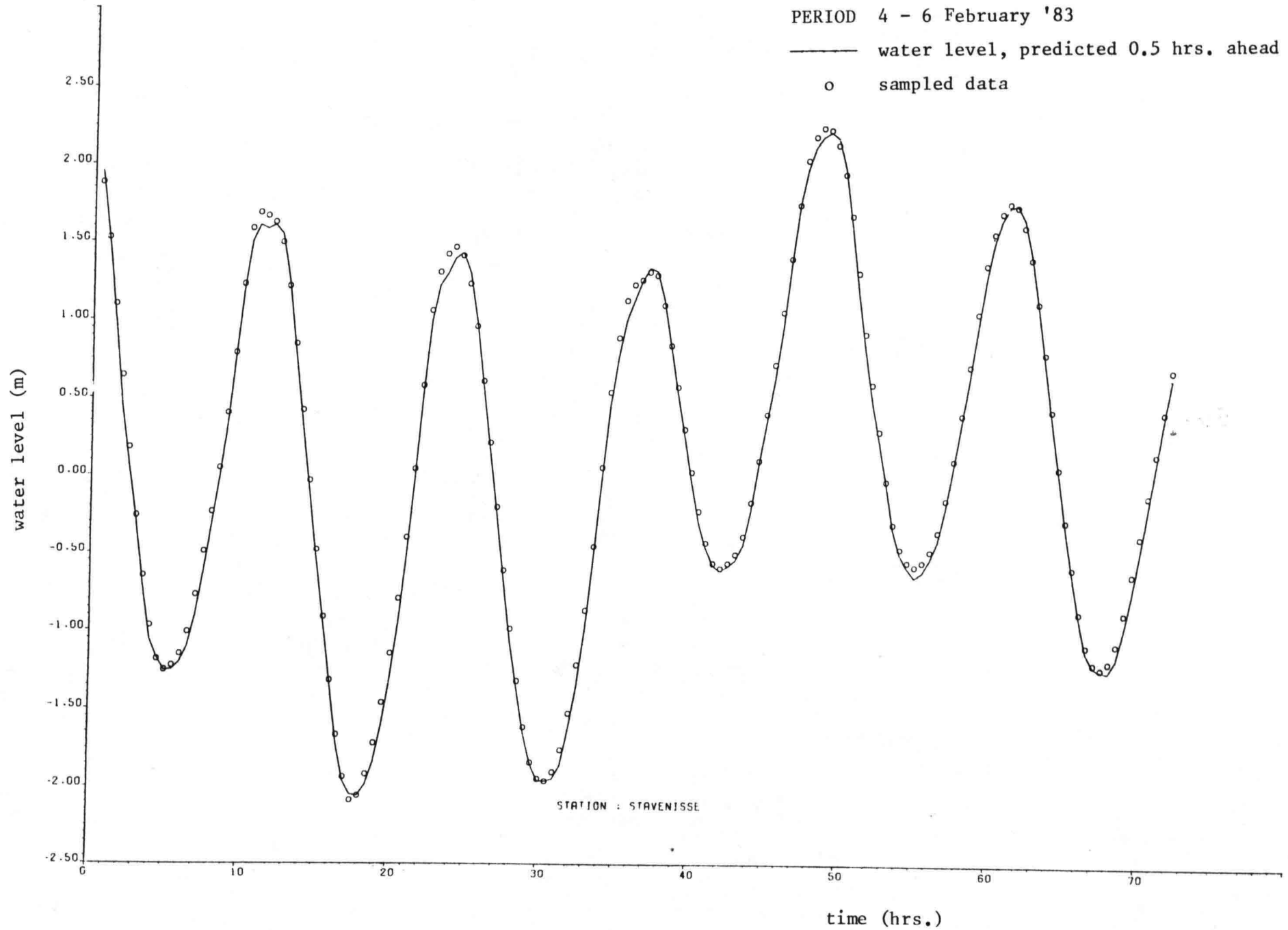
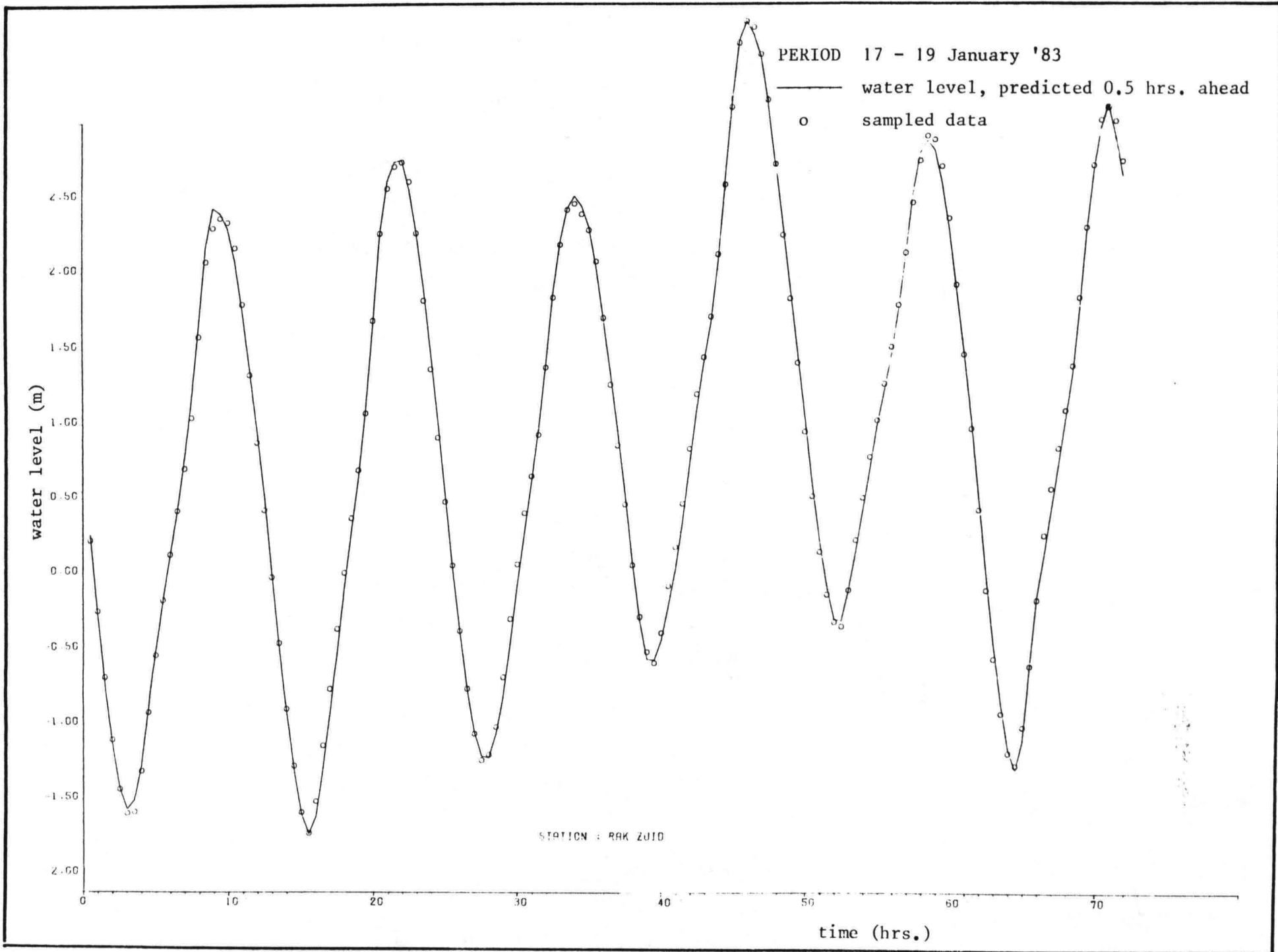


Fig. 4.7b

Fig. 4.8a



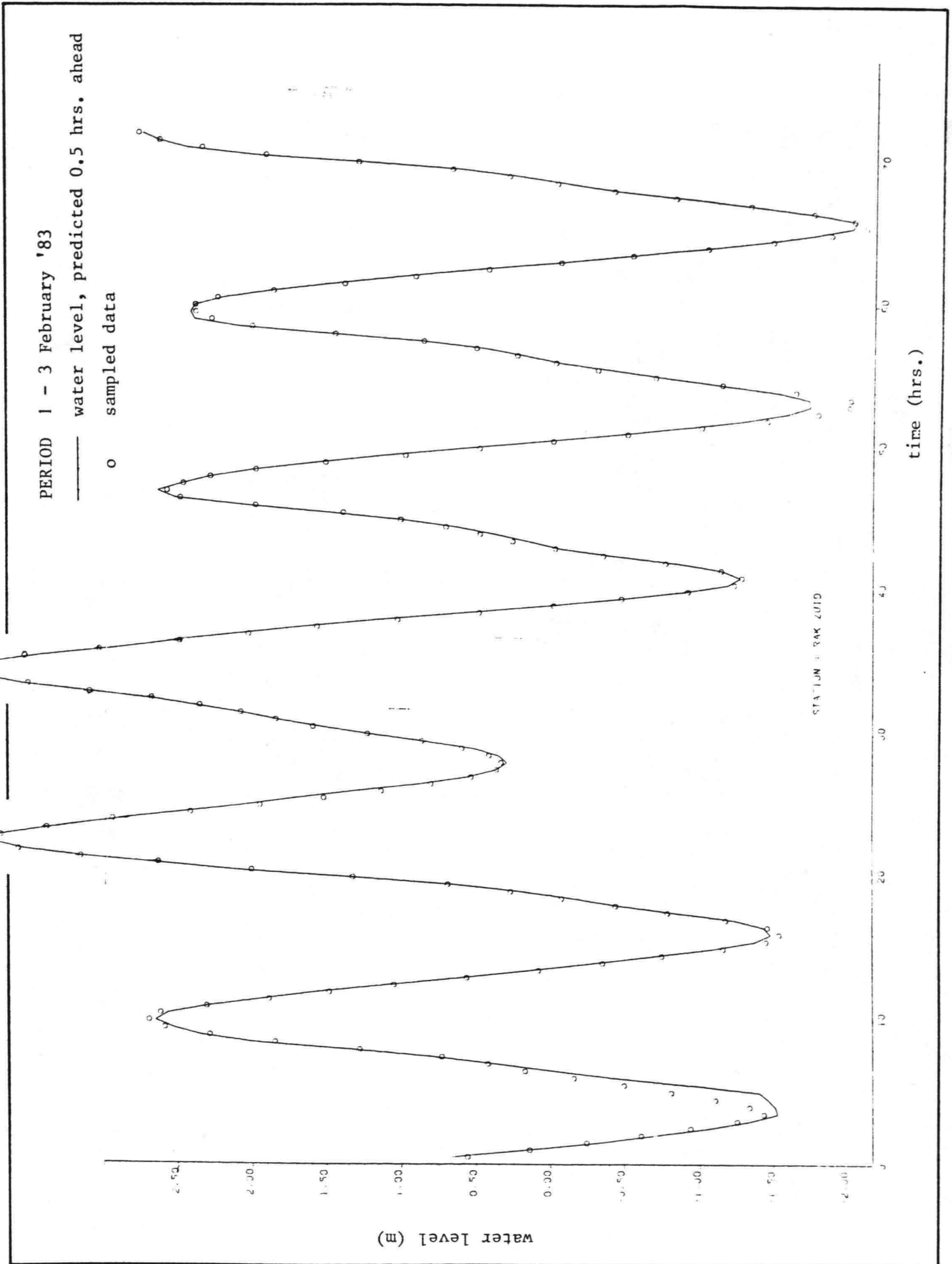


Fig. 4.8b

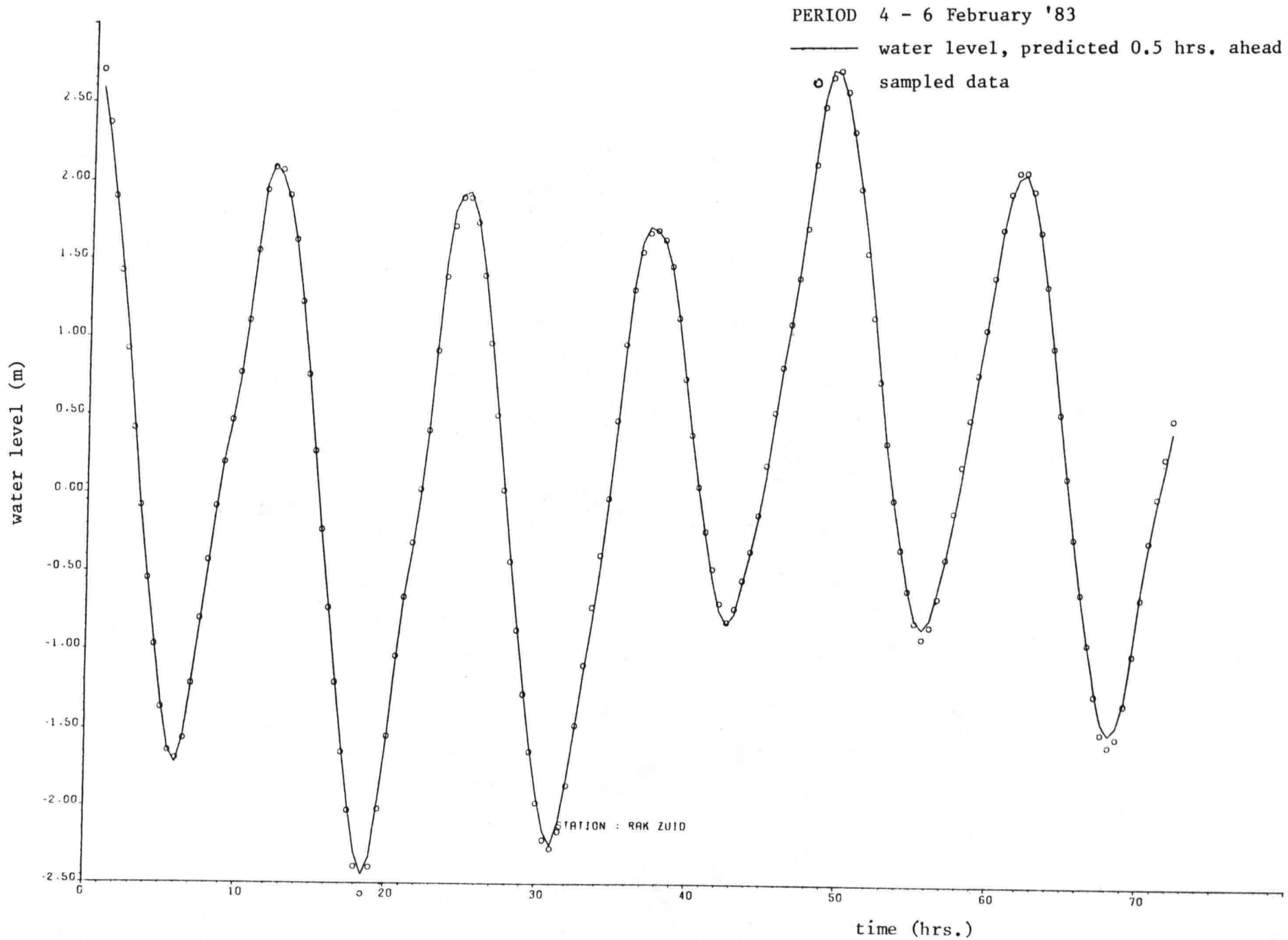
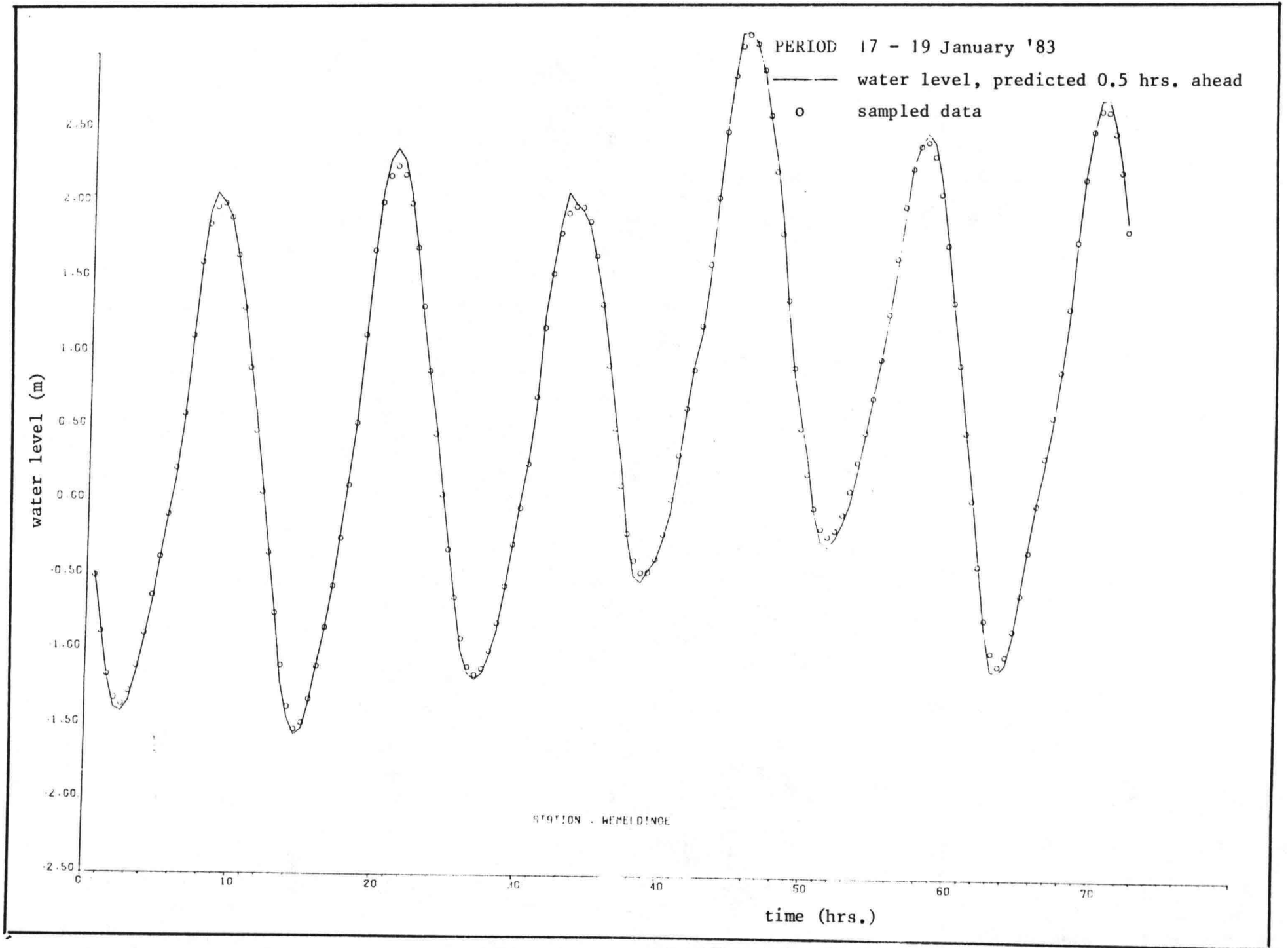


Fig. 4.8c

Fig. 4.9a



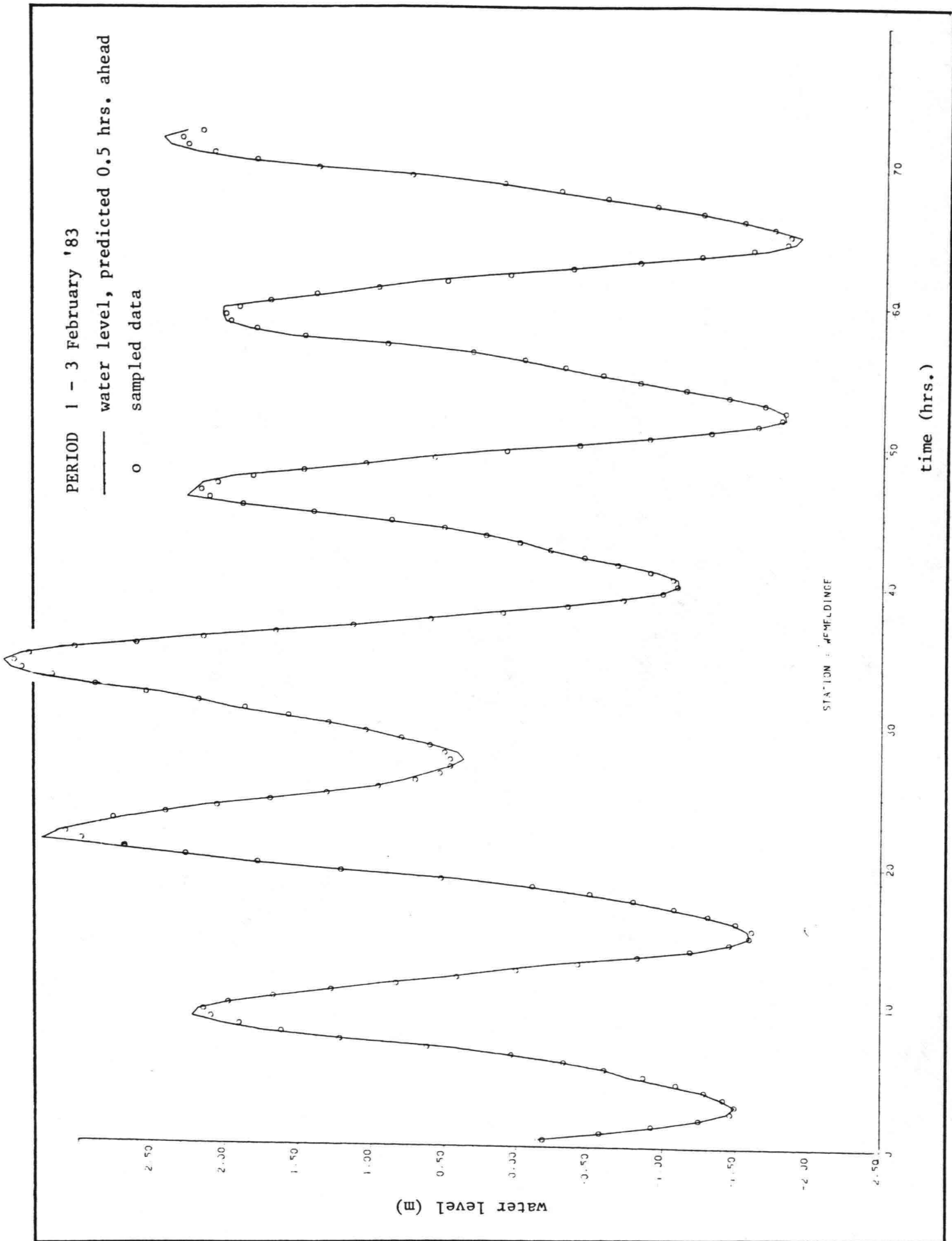


Fig. 4.9b

PERIOD 23 - 25 January '83

— water level, predicted 0.5 hrs. ahead

o sampled data

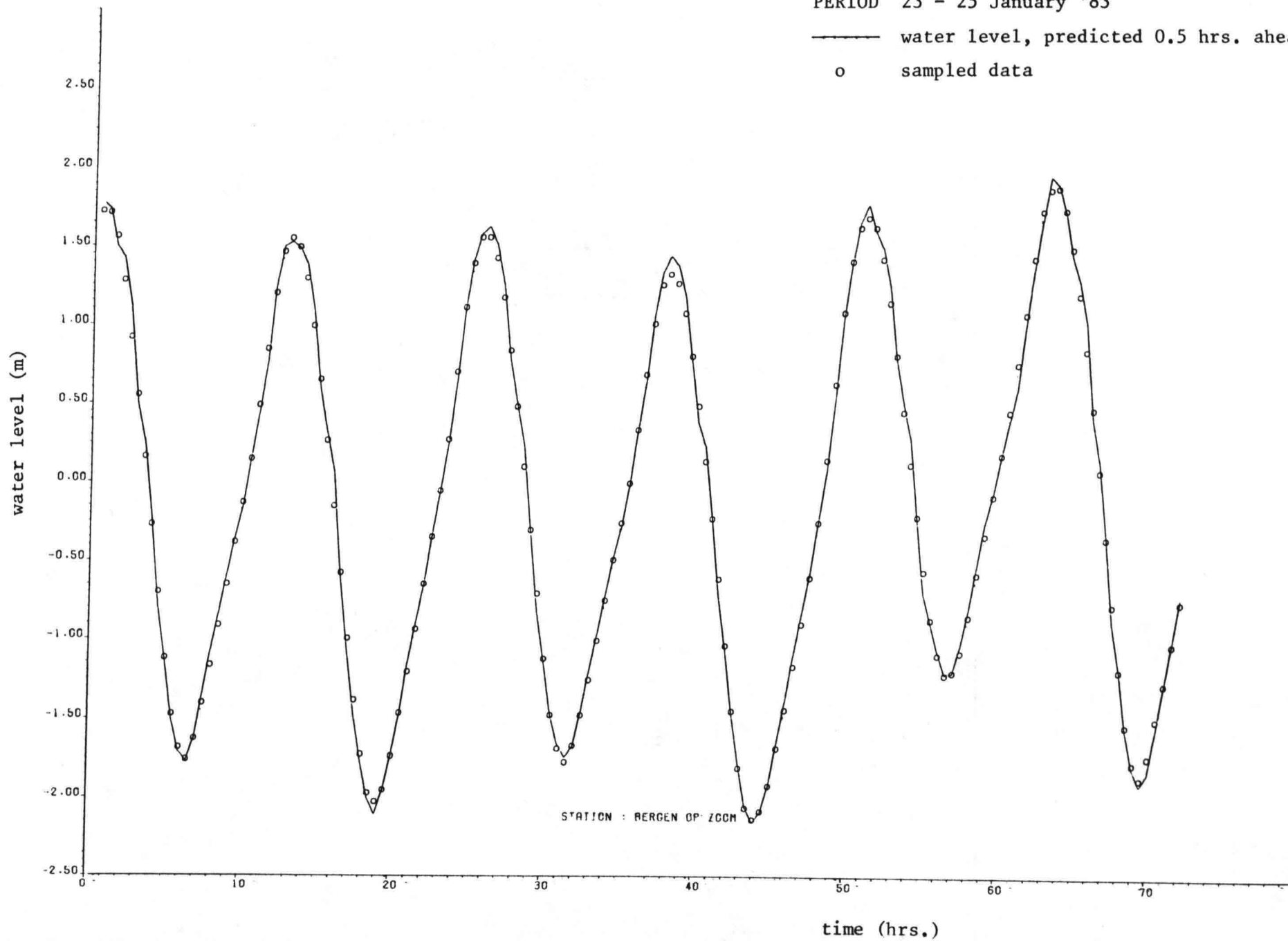


Fig. 4.10a

PERIOD 10 - 12 February '83

— water level, predicted 0.5 hrs. ahead

o sampled data

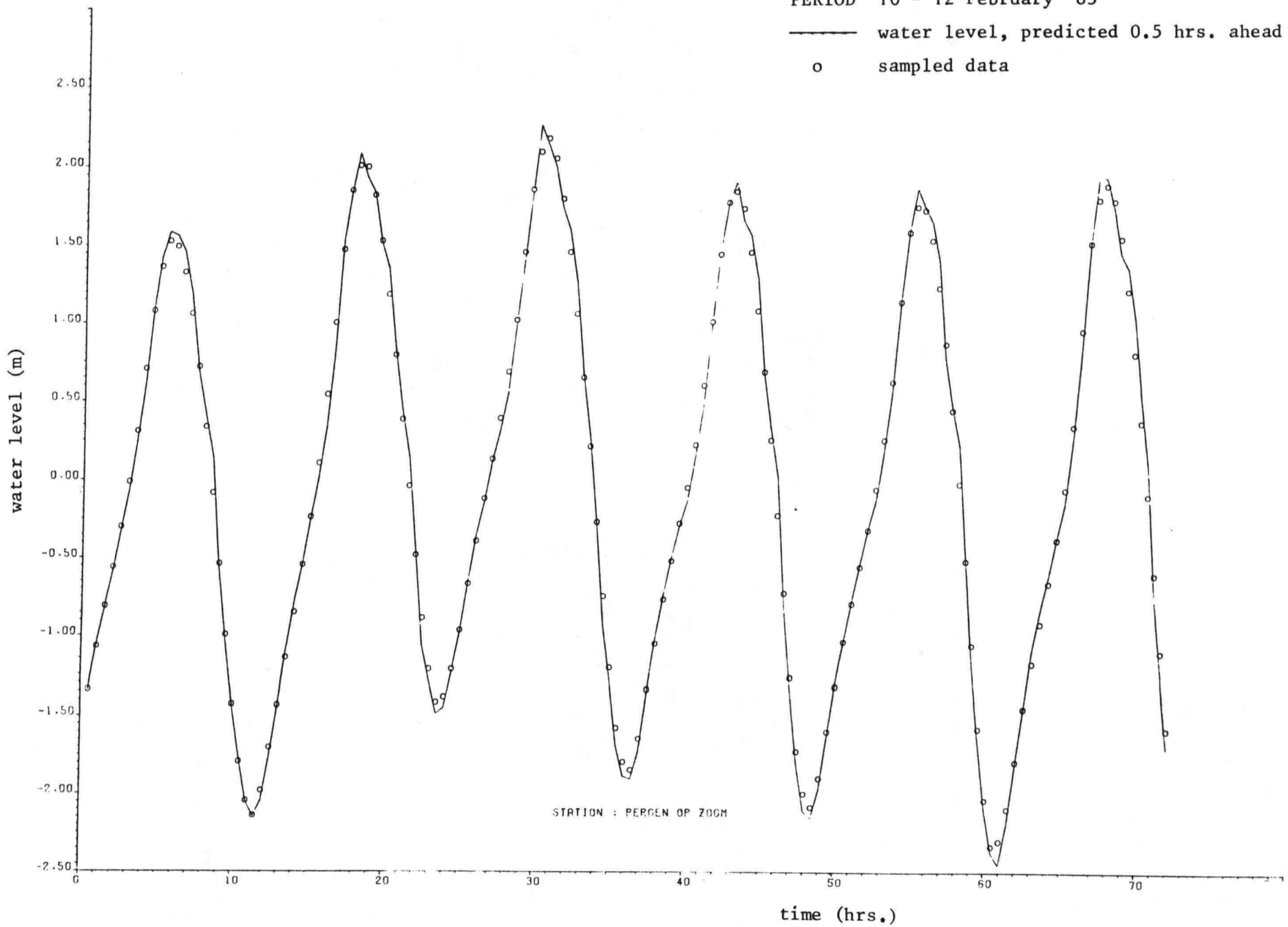


Fig. 4.10b

The r.m.s. errors of the residuals are increased if compared to those of the tuning period (last row in table II). In absolute sense the increase varies between 0.4 and 1.4 cm. The effect of the meteorological circumstances is also seen in these results: the r.m.s. error is enlarged, but not dramatically, if rather strong wind velocities occur, having values up to 24 ms^{-1} .

Another quantity which reflects the filter behaviour is the residual bias shift, defined by eq. (4.3). For the far greater part of the residuals the calculated B is only some mm, but occasionally it can increase to 1.0-1.2 cm (averaged over a days period) when the meteorological circumstances change.

In chapter 3 it is explained that several forms of the filter algorithm easily lead to computational difficulties. For this reason the full second order approximation is seldom used. After the extended Kalman filter was tuned the bias correction terms, eq. (3.20) are added. As expected, the r.m.s. errors of the residuals are diminished, about 3 - 7%. The nonlinear effects are therefore non-dominant which is mainly due to the crude grid that makes the geometry smooth: the nonlinearity, expressed by the second order terms, are strongly influenced by the prescribed geometry.

§ 3 Parameter estimation

The system noise represents in the stochastic model the model errors which determine the reliability of the estimates to some extent. The so-called adaptive filtering is used to compensate these errors by estimating several system parameters simultaneously. Since a large number of estimates is available we are able to employ an harmonic analysis [Dronkers, 1964, 1975, Godin, 1972].

This method describes the time dependent behaviour of the parameter estimates by a series of independent harmonic functions:

$$(4.6) \quad c(t) = c_0 + \sum_{i=1}^N f_i(t) A_i \cos(\omega_i t + \phi_i + u_i(t))$$

with

- $c(t)$ = parameter
 c_0 = mean level
 A_i = amplitude of the i -th harmonic constituent
 $f_i(t)$ = nodal correction for A_i
 ϕ_i = phase of the i -th harmonic constituent
 $u_i(t)$ = nodal correction for ϕ_i
 ω_i = astronomical frequency of the i -th harmonic constituent.

The most important constituents were selected by a harmonic analysis of the water levels registered at O.S.4 using a time serie of one year (1983). From the 5 weeks period we selected a 3 weeks period, large enough to distinguish the important M_2 and S_2 components in the estimates of reflection - and friction coefficients, see fig. 4.11 - 4.13. In table III the results of the analysis are shown for the reflection coefficient ρ at Rak Zuid.

ω_i		A_i (*10 ⁻²)	ϕ_i (degr.)
name	degr./hour		
MFM	1.64	4.13	166.6
O1	13.94	1.37	20.2
K1	15.04	0.38	0.4
MU ₂	27.97	0.57	199.3
M ₂	28.98	2.01	10.9
S ₂	30.00	1.14	37.2
MN ₄	57.42	0.59	276.1
M ₄	57.97	0.59	285.9
MS ₄	58.98	0.48	214.8
M ₆	86.96	0.23	101.5
2MS ₆	87.97	0.05	81.9
Mean level = 0.980		energy ratio 56%	

Table III: Harmonic analysis of the reflection coefficient at Rak Zuid.

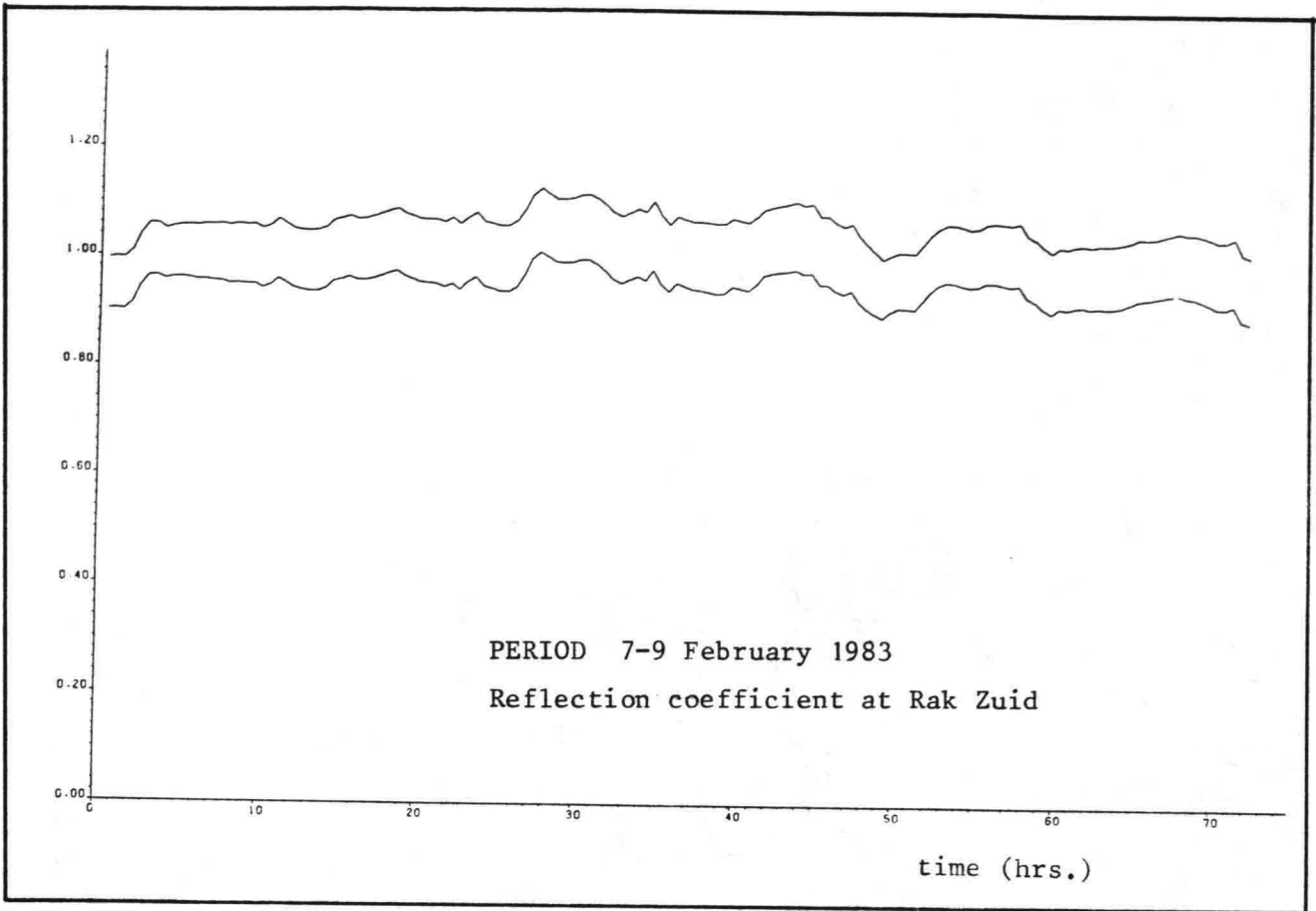


Fig. 4.11a

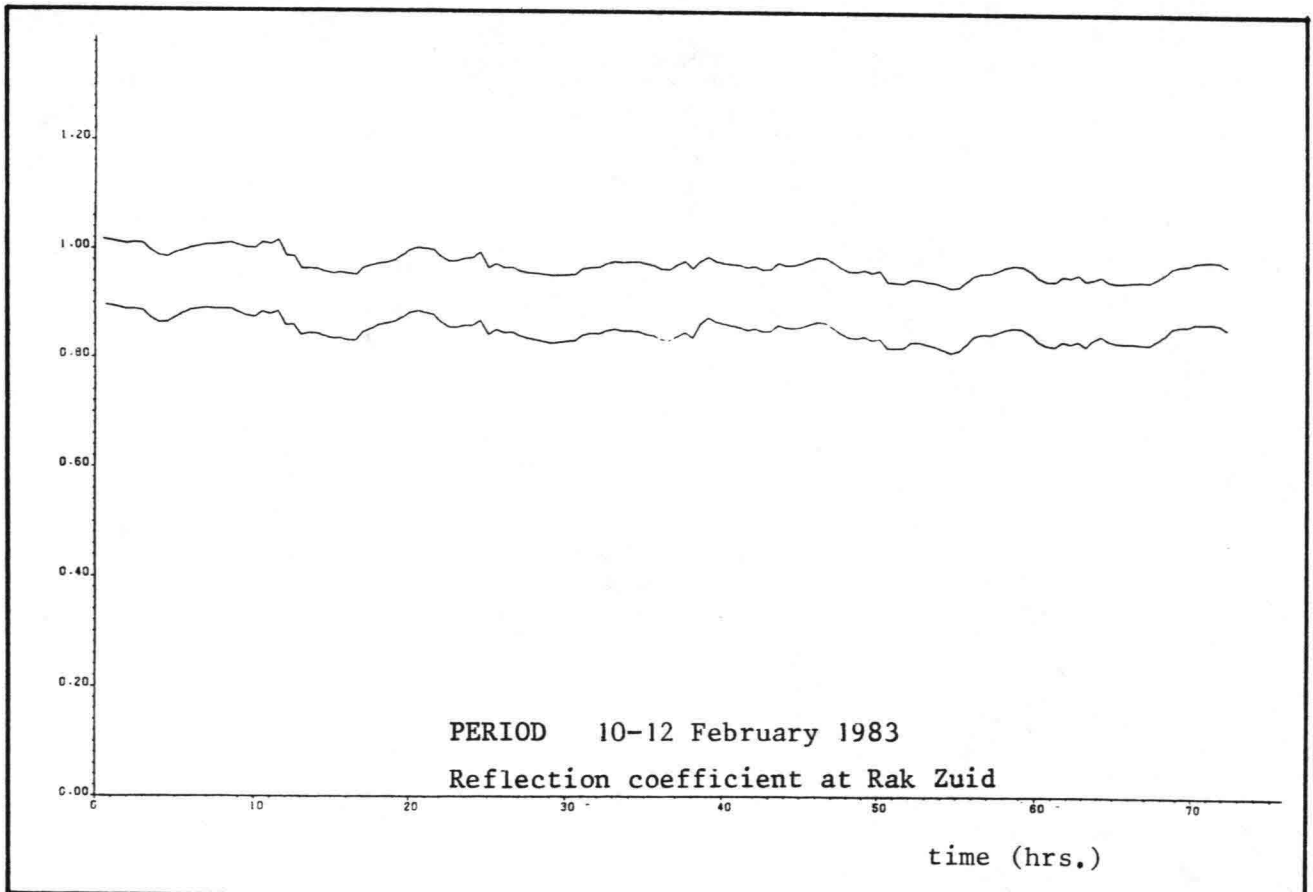


Fig. 4.11b

The M_2 and M_4 components are apparently used to amplify the M_4 tidal constituent in the water levels (and velocities) near the boundary. The occurrence of these specific harmonics indicated that our assumption of the noise sequence being white is violated somewhat: the energy is not equally distributed over the whole frequency domain. The mean level of ρ is very close to the unit value nl. 0.980 so the boundary at Rak Zuid is said to be almost totally reflective and the velocities are, in absolute sense, smaller than 0.2 ms^{-1} .

A similar behaviour should be expected for the reflection coefficient at Bergen op Zoom. Since the geometry of the estuary branch between Zierikzee and Bergen op Zoom is much more complicated than the geometry between Stavenisse and Rak Zuid, greater model errors and to be expected, so the estimates of ρ possess harmonics with an amplitude that are greater than those in the former case. The mean level is also different from the unit value (0.890), accomplished by the fact that the sampling point is not exactly located near a closed boundary.

For the friction coefficients the results are summarized in table IV. It can be noted that there is a remarkable difference between the energy ratios. Only 13% of the energy in the estimates of the friction coefficient between O.S.4 and Zierikzee is found in the tidal constituents whereas 40% for the friction coefficient between Zierikzee and Stavenisse. From this difference one may not draw the conclusion that in one of the cases the model errors are greater than in the other, but something can be said about the nature of the model errors. First, a white noise sequence may be interpreted here as a sequence of harmonics without dominant tidal constituents. The low energy ratio (13%) therefore accounts for model errors that are due of the incompleteness of the prescribed dynamics.

ω_i		A_i ϕ_i (degr.)		A_i ϕ_i (degr.)	
name	degr./hour	(* 10 ⁻⁶)		(* 10 ⁻⁶)	
MFM	1.64	154.4	177.1	82.0	2.3
O1	13.94	9.9	74.6	22.4	230.4
K1	15.04	13.5	155.0	13.1	257.8
MU ₂	27.97	10.0	80.0	18.8	116.8
M ₂	28.98	12.6	24.3	73.0	243.4
S ₂	30.00	12.4	45.2	36.0	339.5
M ₄	57.97	6.2	236.8	7.9	252.7
MS ₄	58.98	1.9	277.9	3.0	116.4
M ₆	86.95	1.0	305.0	11.2	11.0
2MS ₆	87.97	3.0	309.8	13.0	110.9
mean level		1.48* 10 ⁻⁴		2.03* 10 ⁻⁴	
energy ratio		13.0%		40.0%	
streamsection		O.S.4 - Zierikzee		Zierikzee - Stavenisse	

Table IV Harmonic analysis of the coefficients $\frac{\mu}{g}$, ($\frac{\mu}{g} = \hat{\mu} \text{ Chezy}^{-2}$)

In chapter 2 (page 20) it has been noticed already that the dynamics of the tidal motion in the mouth of the Eastern Scheldt cannot easily be represented in a one-dimensional model which causes the "whiteness" of the estimates of the friction coefficient between O.S.4 and Zierikzee. On the other hand wrong or insufficient prescription of the dynamics will cause systematic oscillations of the estimates. For example, the frictional effect is modeled as $\mu|u|P$ with u the velocity, averaged over over the cross-sectional area A . But the friction is essentially related in the local velocity u_b at the bottom, so the harmonical behaviour of μ could be interpreted as a correction for this discrepancy*. However, an incorrect prescription of the geometry may also cause harmonics of tidal frequencies.

* Recount the dependence of μ via the logarithmic rule: $\mu \sim \ln \frac{D+h}{D}$

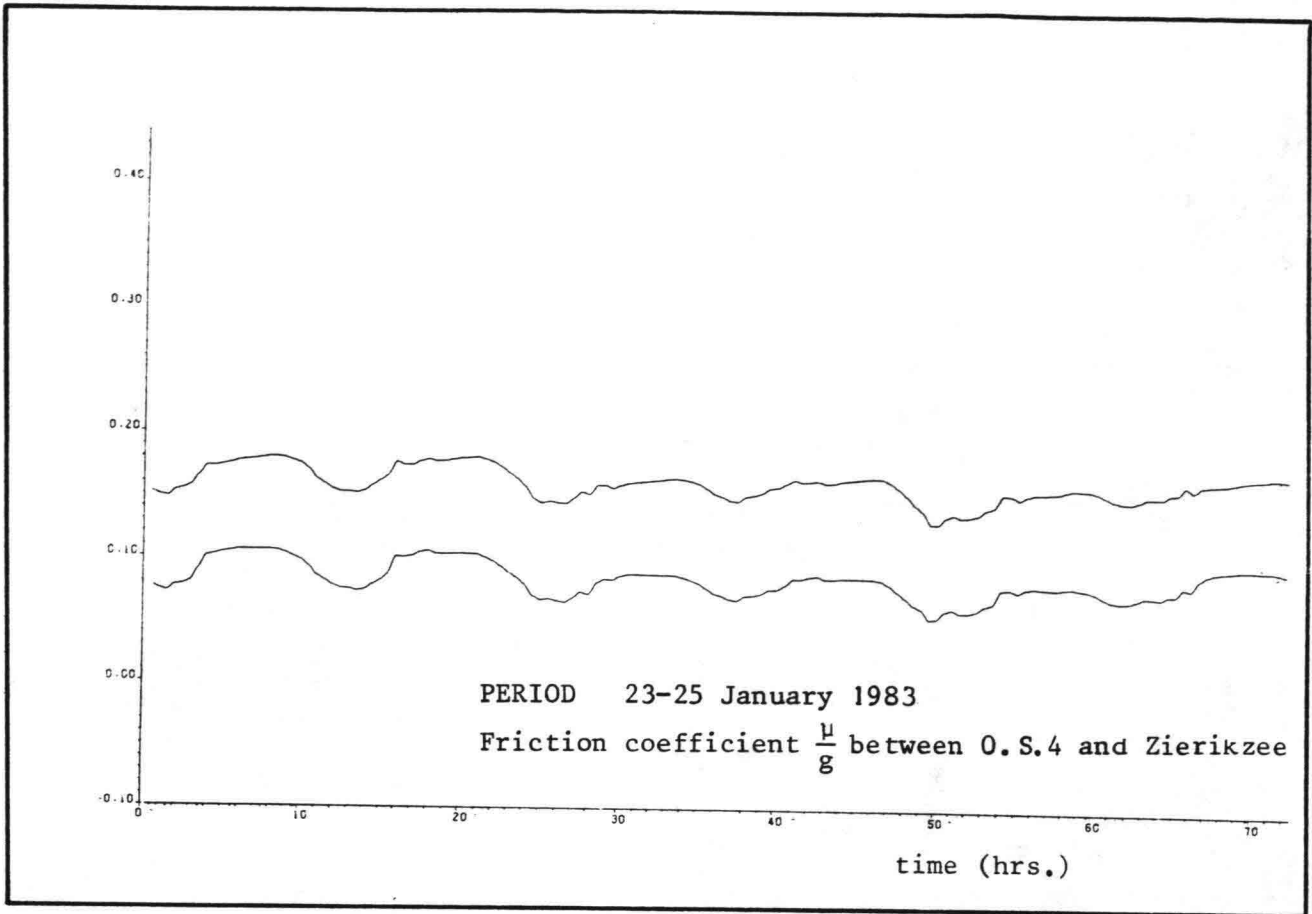


Fig. 4.12a

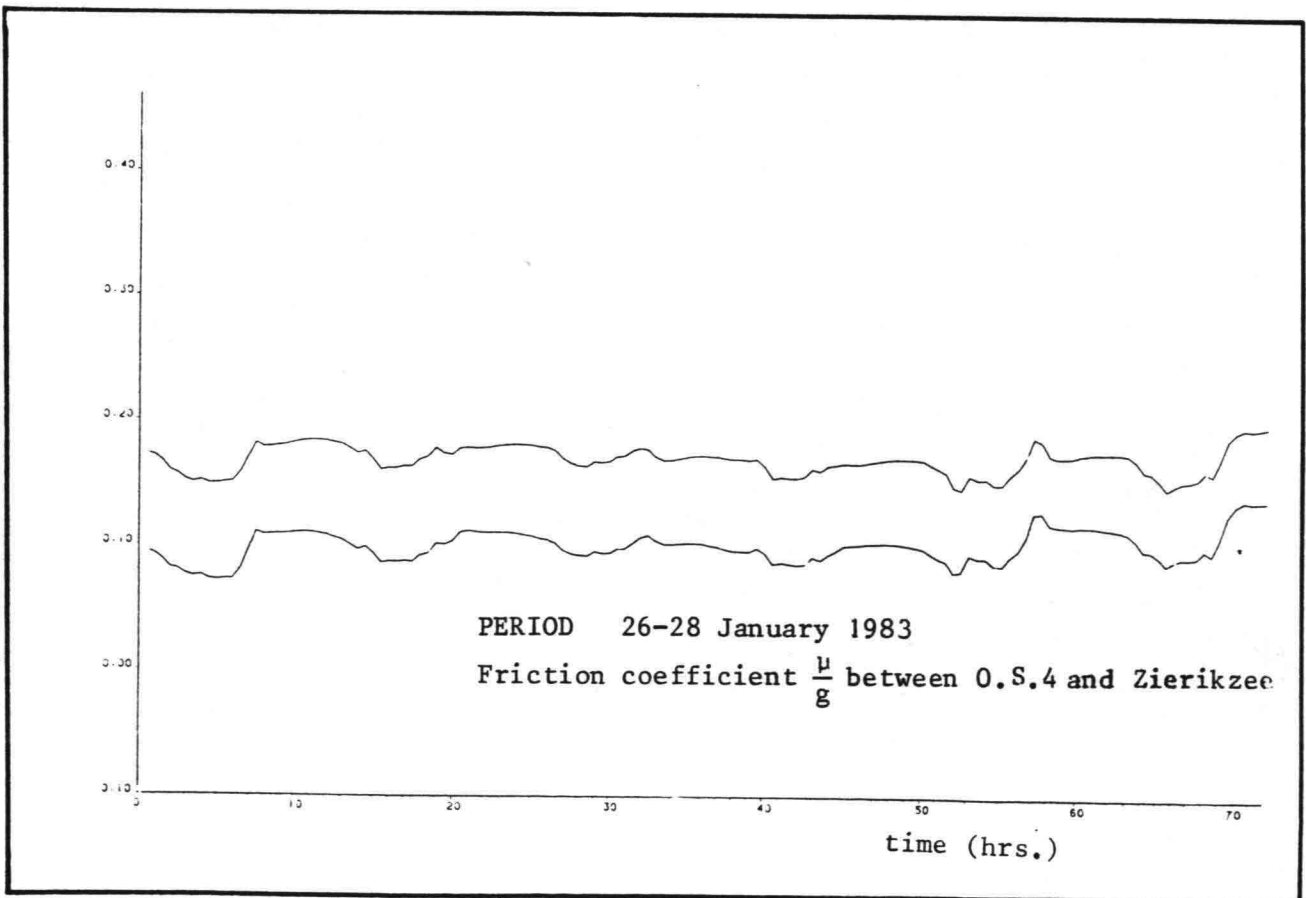


Fig. 4.12b

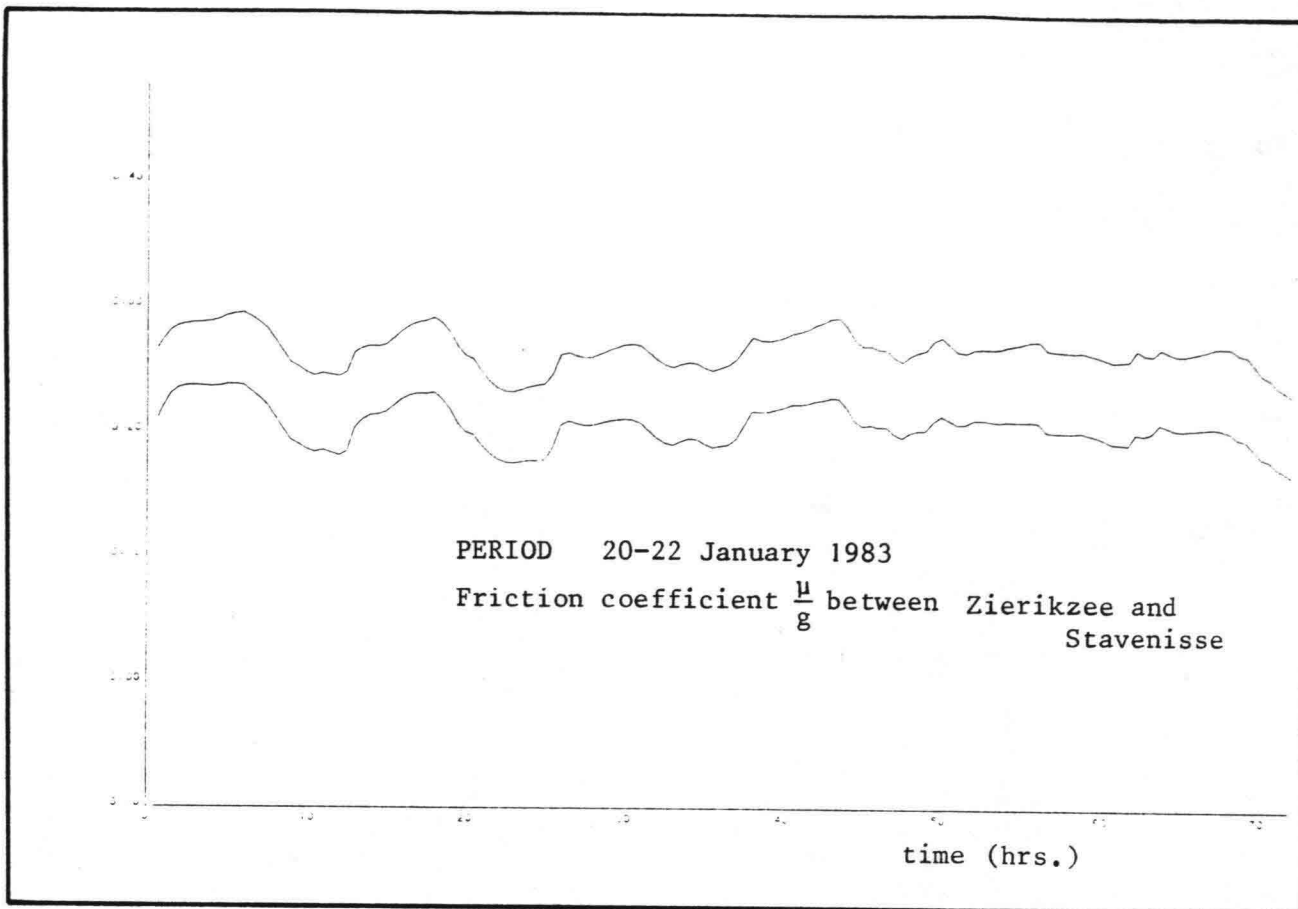


Fig. 4.13a

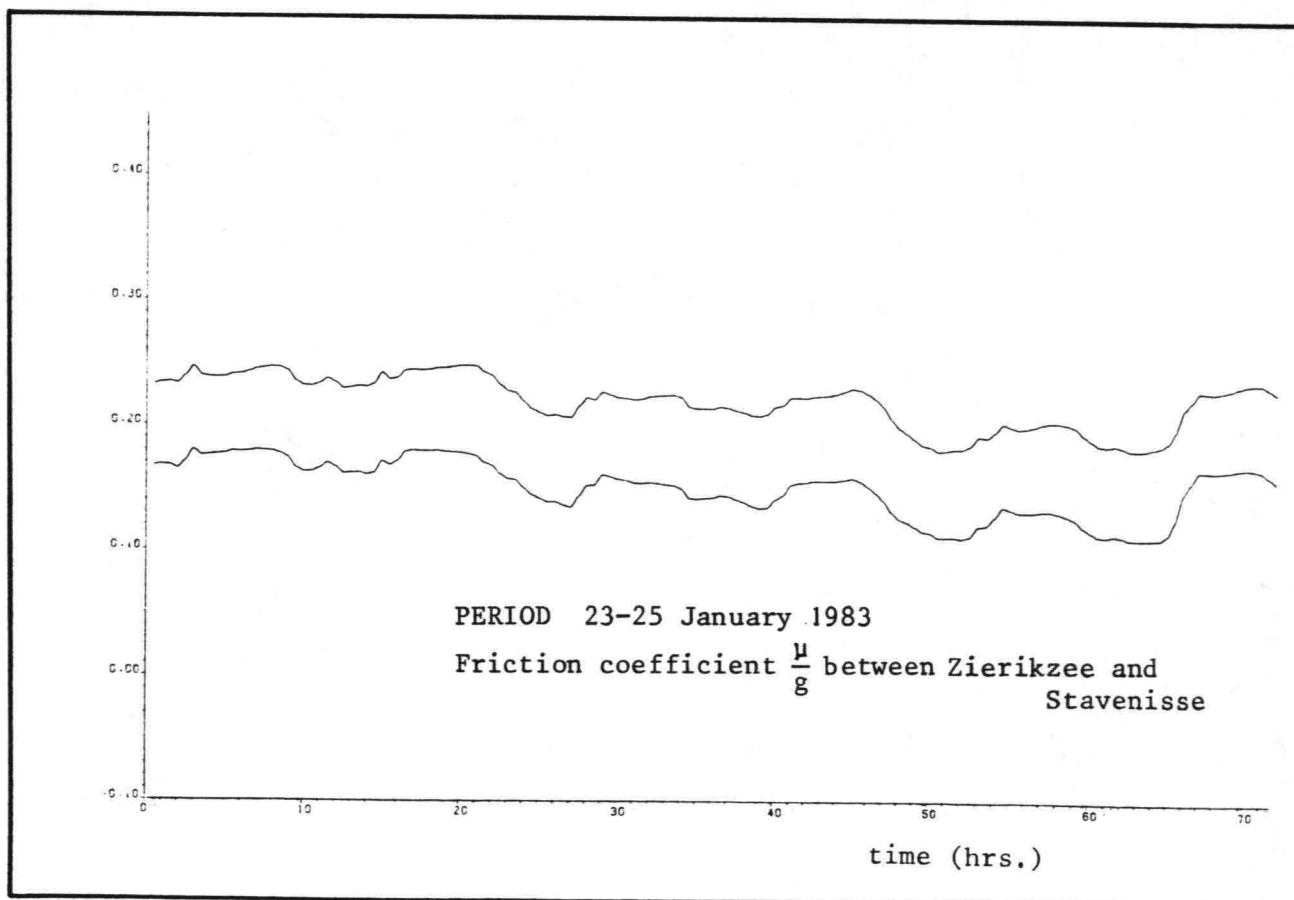


Fig. 4.13b

From table IV it can also be seen that the amplitudes of the MFM constituent are significant, suggesting that the coefficients μ at neap tide differ from those at spring tide. However, for all these points, no definitive conclusions can be drawn whether or not this behaviour is due to changing effects (in the physical sense) or to model errors, but it would seem correct to remark that the results which are achieved in this way can be used to improve the model.

For the representation of the exchange of momentum between a wind field and the water the empirical relation

$$(4.7) \quad C_d V^2 b \cos \psi \quad \text{or} \quad C_d \frac{V^2 \cos \psi}{D+h} \quad \text{is used, see eq. (2.6)}$$

In literature it is a well-known fact that the wind stress coefficient depends on V (and ψ), which are treated as input quantities in the filter. Since C_d is estimated the indirect influence of V and ψ may be found by analyzing the computed estimates of C_d . If we restrict ourselves to the C_d in the Eastern Scheldt model, the procedure is as follows: A main direction is chosen as a reference to define a windangle ψ_a . We should further note that the C_d is a global parameter which is determined by a total of factors relating both to the physical properties of the mathematical model, see fig. 4.14.

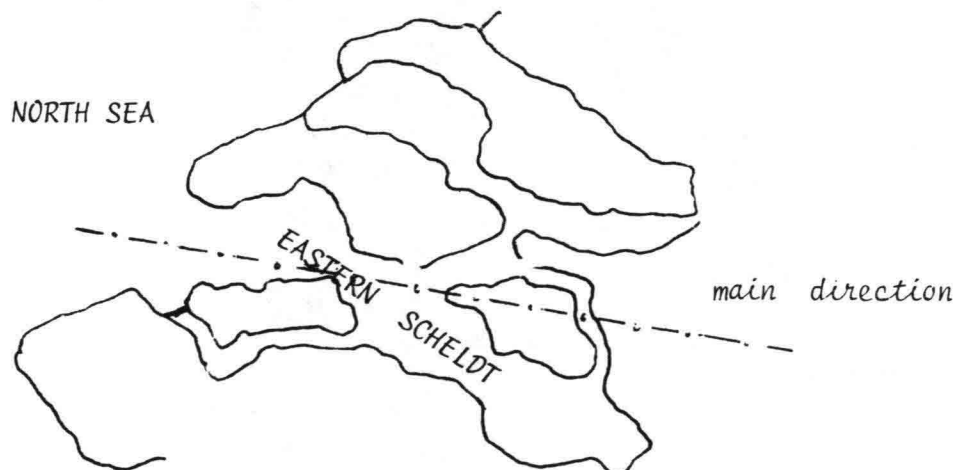


Fig. 4.14

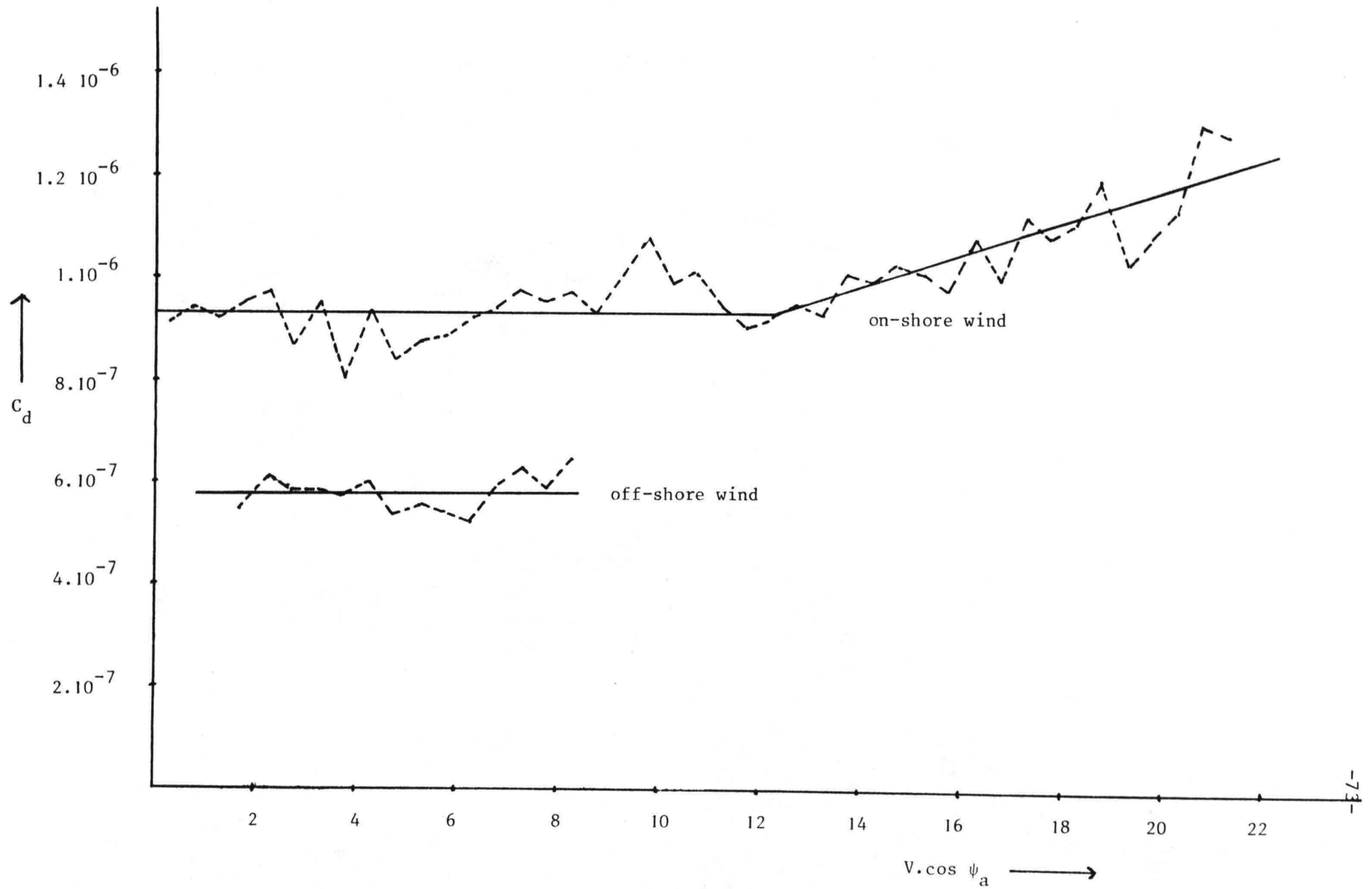


Fig. 4.15 The relation between the averages of the estimated C_d coefficient and the component of the wind velocity, registered at B.G.2

Fig. 4.15 shows the relation between C_d and $V \cos \psi_a$ when the horizontal axis is partitioned in 50 subintervals of length $\Delta V = 0.5 \text{ ms}^{-1}$ and the corresponding C_d value is just the average value of C_d which is found of wind velocities between V and $V + \Delta V$. This treatment assumes in fact an uncorrelated sequence of estimates for C_d in time, which is of course not the case, i.e. the Kalman filter derives corrections for the instantaneous (sub)- optimal estimates. The argument to justify the analysis is that due to the large number of estimates ($N = 1680$) systematic trends in the correlations are removed.

In case of on-shore wind the C_d coefficient is relatively constant at a value $9.3 \cdot 10^{-7}$ for wind velocity components below 12 ms^{-1} , and increases linear with $V \cos \psi_a > 12 \text{ ms}^{-1}$. If one takes into account that the wind velocity, observed in the Eastern Scheldt, is approximately 80% of the value, registered at B.G.2, for on-shore winds [Langerak, 1984] the shape of this curve and the scale of the axes are very similar to those, found from other experiments [Timmerman, 1975] and illustrates the physical behaviour of the filter that can be adequately used in the area of model research.

The estimates of the C_d coefficient for the off-shore wind velocity components deviate largely from the average estimates for on-shore winds, although also a constant value ($5.8 \cdot 10^{-7}$) is found. This striking difference can be explained by two reasons: first, the exchange of momentum is different for off- and on-shore winds, or secondly, which is more plausible, the measured wind velocities at B.G.2 and in the Eastern Scheldt are differently correlated in the considered cases. In that case the results illustrate an input errors, and if an equal C_d coefficient is assumed the 80% correction for on-shore winds must be replaced by an 63% correction in case of off-shore winds.

From eq. (4.7) it is seen that the exchange of momentum is assumed to be independent of the water velocity u . A further analysis of the C_d estimates for on-shore winds is pursued, by dividing the estimates into two categories:

- C_d for ebb ($u_{\text{Zierikzee}} < 0$)
- C_d for flood ($u_{\text{Zierikzee}} > 0$)

and than averaging the C_d -values for the two categories separately. However, this procedure does not provide any argument to reformulate the empirical relation, eq. (4.7), and to introduce a relative wind velocity between V and u instead of V . The absence of a correlation with ebb or flood states that the described interaction is a local effect at the water surface and also suggests that wind fields can influence the flow pattern within the water, causing a

counter current along the bottom of the stream section to maintain potential energy. The effect of ebb and flood is possibly noted in the estimates of the friction coefficients, but will only be measurable if V exceeds 25 ms^{-1} [Langerak, 1984].

§4 Optimization of sampling networks.

One of the interesting applications of Kalman filters can be found in optimizing sampling networks, as indicated in chapter 1. Although a complete treatise of an optimization procedure is beyond the scope of this report, the basic idea of filter interpolation is illustrated. Filter interpolation deals with the influence (domain) of information provided by measurement data, and which is dependent on

- the location of the sampling points in a network,
- the sampling quantity, and
- the associated measurement error.

Now consider a network, as shown in fig. 4.16 where the

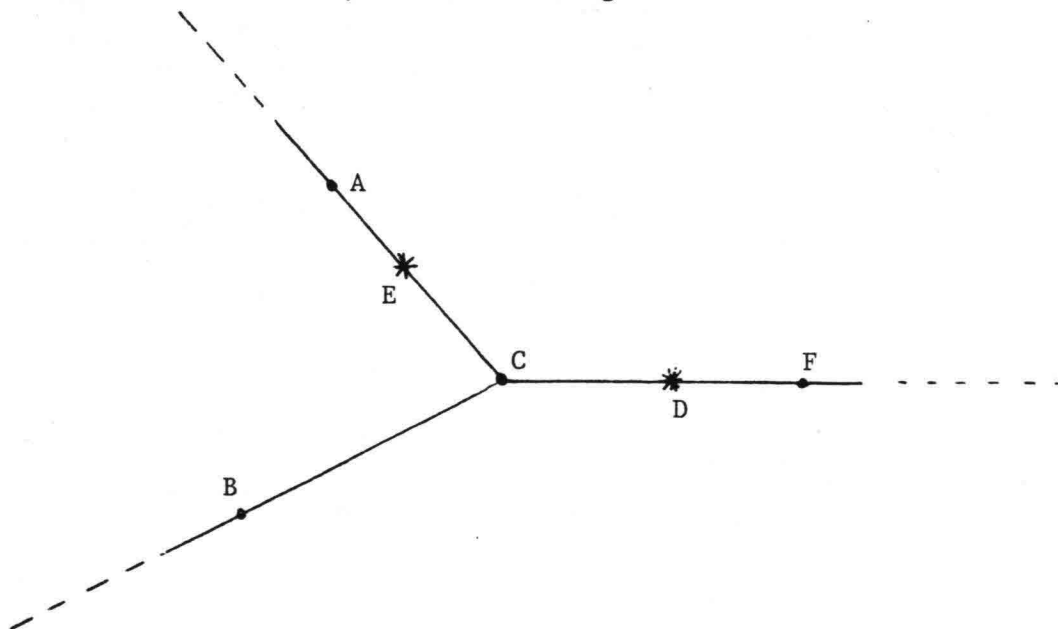


fig. 4.16

gridpoints A, B, C and F are also sampling points. The estimations $\tilde{X}(k+1/k+1)$ which result from the filter algorithm are based on the measurement data from A, B, C and F. These data however also influence the estimated states in D and E, which are obtained by interpolation. This based on the discrete dynamical equations.

Returning to the tidal motion problem, one can identify, for instance, C with Zierikzee, D with Stavenisse and F with Steenbergse Sas. In "normal" situations, the measurement data from Stavenisse are used to correct the half hour predictions. A measure for the information provided by these data can be deduced by comparing the estimates in a "normal" situation with those obtained from experiments where the measurement data from Stavenisse are not processed in the filter, see fig.s 4.17 - 4.18. These examples show that in the considered period the role of these data cannot be fully overtaken by the remaining data. To specify this difference the r.m.s. errors are calculated, table II, III.

$$(4.8) \quad \begin{aligned} (\sigma_p)^2 &= \frac{1}{N} \sum_{k=1}^N \{ \tilde{z}(t_k) - \hat{h}(k/k-1) \}^2 \\ (\sigma_c)^2 &= \frac{1}{N} \sum_{k=1}^N \{ \tilde{z}(t_k) - \hat{h}(k/k) \}^2 \\ (\sigma_1)^2 &= \frac{1}{N} \sum_{k=1}^N \{ \tilde{z}(t_k) - [\xi \hat{h}_z(k/k) + (1-\xi) \hat{h}_{st}(k/k)] \}^2 \end{aligned}$$

with

N	= number of time steps
$\tilde{z}(t_k)$	= measurement data from Stavenisse, $t = t_k$
$\hat{h}(k/k+1)$	= predicted water level at Stavenisse, $t = t_k$
$\hat{h}(k/k)$	= estimated water level at Stavenisse, $t = t_k$
$\hat{h}_z(k/k)$	= estimated water level at Zierikzee, $t = t_k$
$\hat{h}_{st}(k/k)$	= estimated water level at Steenbergse Sas, $t = t_k$
ξ	= weighting parameter, $0 < \xi < 1$

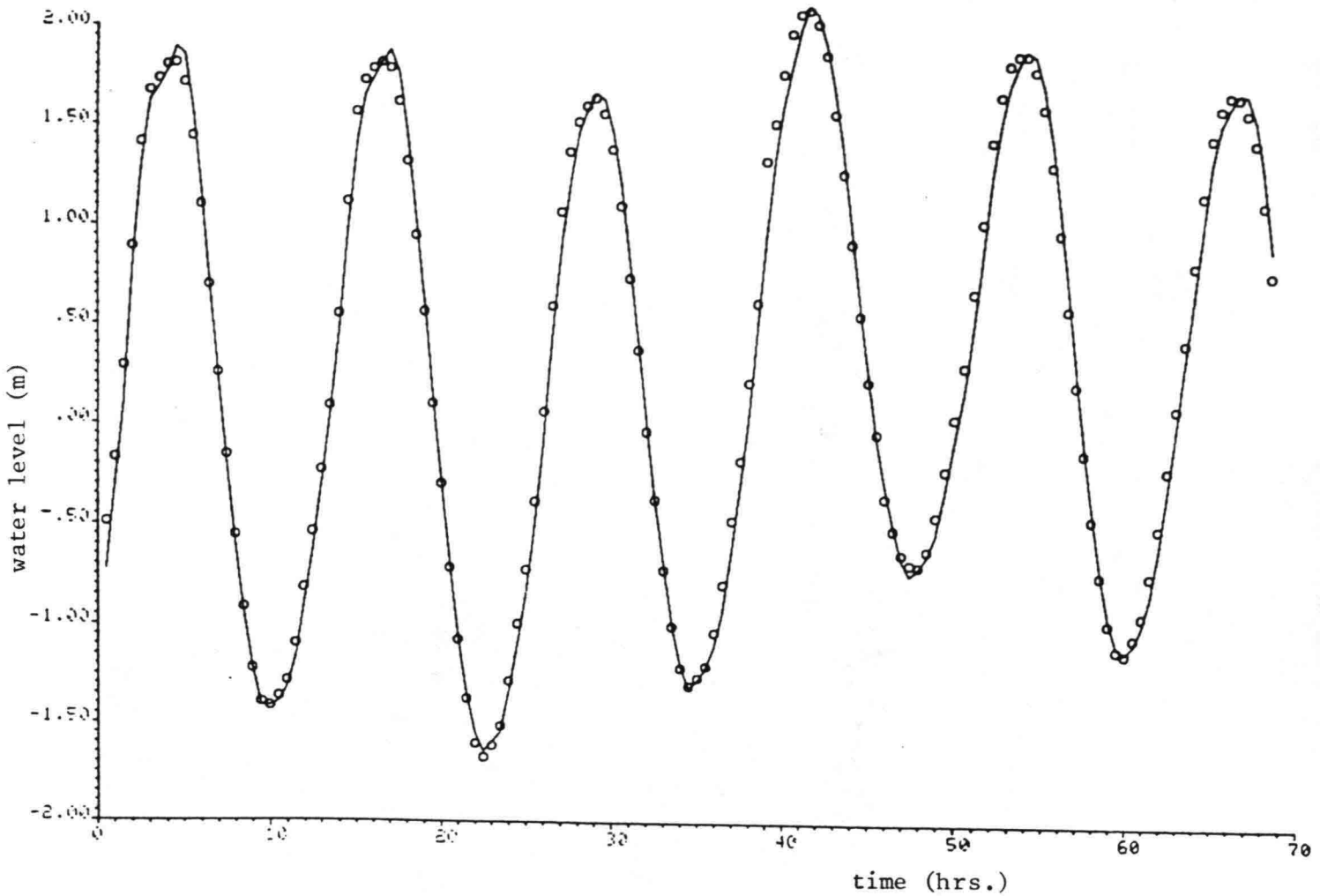


Fig. 4.17 Half hour predictions of the water level at Stavenisse in case the local measurements are neglected.

		σ_p (cm)
With	processing the data $\tilde{z}(t_k), k = 1, 2, \dots, N$	6.5
Without		8.3

Table II: The r.m.s. errors σ_p of the predictions at Stavenisse

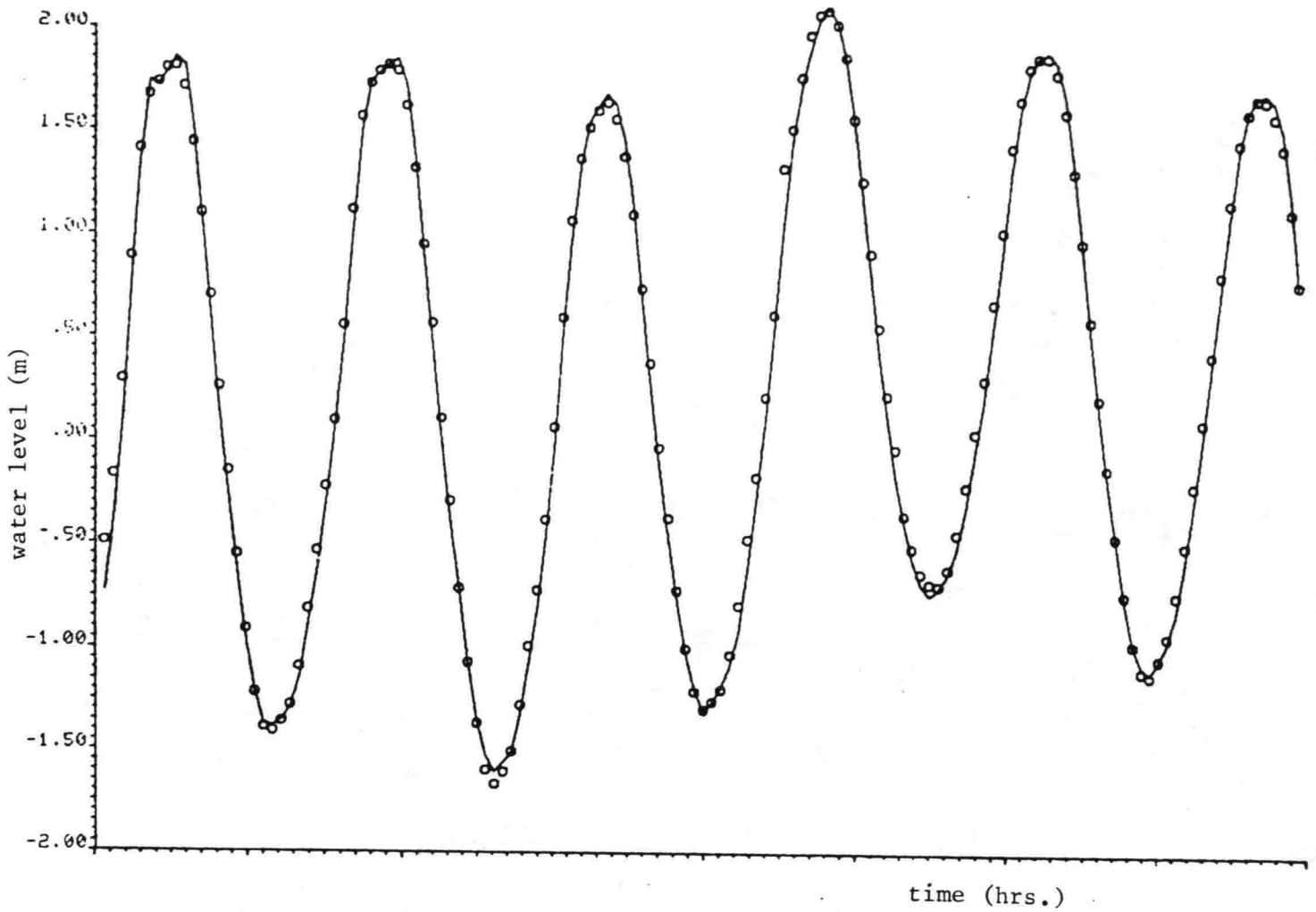


Fig. 4.18 The estimates $\hat{h}(k/k)$ of the water level at Stavenisse in case the local measurements are neglected.

		σ_c (cm)	σ_l (cm)
With	processing the data $\tilde{z}(t_k), k = 1, 2, \dots, N$	< 2.8	-
Without		4.3	5.9

Table III The r.m.s. errors σ_c and σ_l of the estimates at Stavenisse.

The neglect of the measurement data from Stavenisse induces an increase of the standard deviations, both of the predictions as well as the estimates, see fig.s 4.17-4.18, which is most obvious in the periods before high tide. The effect of the filter interpolation is seen in table III: although we may conclude that the processing of the data $\tilde{z}(t_k)$, $k = 1, 2, \dots, N$ gives the best result (a r.m.s. error smaller than the standard deviation of the measurement error), the interpolation based on the discrete dynamical equations is superior to the linear interpolation between Zierikzee and Steenbergse Sas.

These experiments can be performed for all sampling points to study the necessity of keeping a particular tide gauge in operation*, once maximal allowable r.m.s. errors are established. This procedure assumes that the three quantities, determining the information contained in the measurement data are invariable. On the other hand however, the installation of new sampling points requires experiments (now using simulated data) to answer the following questions to achieve a maximal benefit of the investments:

- where should the sampling point be located,
- what quantity should be sampled,
- within what accuracy should the sampling be performed?

§ 5 Short-term predictions

In predicting the water level and velocities in the Dutch coastal area the boundary condition at point 1 (Nieuwpoort) has to be extrapolated. This is done by harmonic analysis of the tide and by estimating the set-up, see chapter 2, section 6. Since, in general, the extrapolation will not be accurate, this restricts the prediction capability of the filter. Therefore, before discussing the medium range predictions, we define a prediction horizon. This prediction horizon is the maximum length of the time interval during which the computed predictions are uninfluenced by the extrapolated boundary condition at Nieuwpoort (grid point 1 in the model).

* Note that the removal of sampling points can mathematically be simulated by introducing a large standard deviation of the measurement error for certain data, so its reliability approximates zero.

The dynamical equations (2.7) - (2.8) and (2.11) - (2.12) are of the hyperbolic type so every signal (expressed as Q.R.I.s) propagates along the characteristics in the (x,t)-domain with a limited velocity, eq.s (2.13, (2.14). The extrapolated boundary condition can be conceived as a disturbed signal which implies that the prediction horizon is determined by the path of the characteristic which enters the (x,t)-domain at point 1 at a time following the time τ the most recent data are sampled, see fig. 4.19. Consequently, the predictions which are based on measurements at time $t \leq \tau$ can be computed in the shaded area. It is seen that the limited propagation speed accounts for a space dependent prediction horizon: it is limited to 2.0 hrs at O.S.4, O.S.9, to 2.5 hrs at Zierikzee and 3.5 hrs at Rak Zuid en Bergen op Zoom. Related to this prediction horizon we can now apply a concept of stochastic observability which restricts the observability domain to all points P with a domain of dependence (for $t \geq \tau$) which lies within the area, limited by the curve C, the line $t = \tau$ and the boundaries, and coincides with the shaded area in fig. 4.19 [Goodson, 1970] .

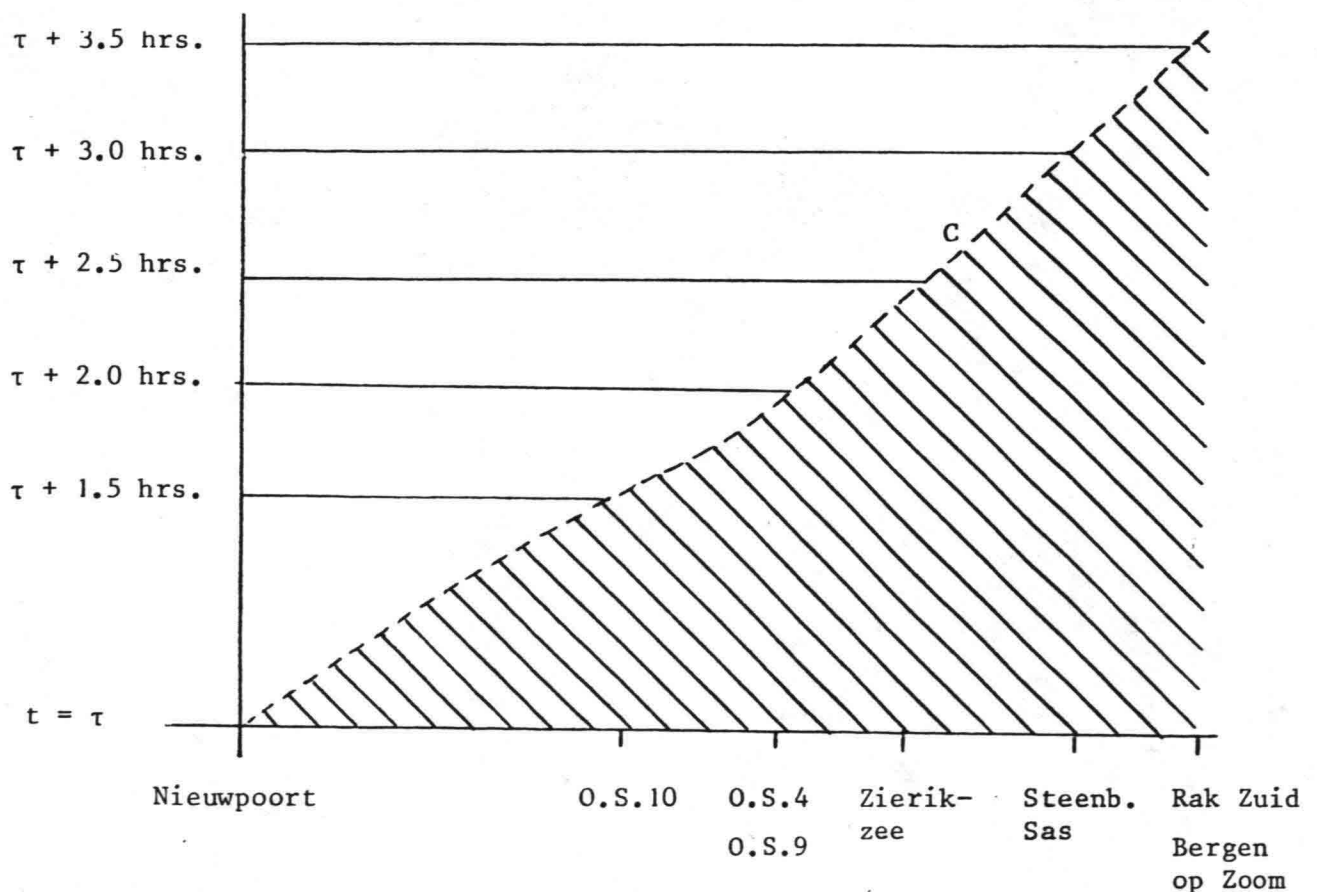


Fig. 4.19 The space dependent prediction horizon. The curve C is determined

$$\text{by } \frac{dx}{dt} = u \sqrt{g(D+h)}.$$

In the fig.s 4.20-4.37 representative examples are shown of the short term predictions of the water levels in levels in the sampling points. The fig.s 4.20-4.24 are drawn from the results during the tuning period (11-13 September '75) whereas the remaining are derived from the two storm periods 18-20 Januari '83 and 31 Januari - 2 February '83. The influence of the storm is again marked by the difference between the actual and the astronomical tide.

The performance of the filter with respect to the prediction of water levels in the Eastern Scheldt depends on several aspects such as

- the prediction of the boundary condition, derived from the model along the coast,
- the changing meteorological circumstances,
- the variations of the estimated parameters in time.

The most striking difference between the sampled data and the predictions of the water level at point 7, see fig. 2.11, which serves as the boundary condition is the apparent phase shift of the M_4 constituent at low tide. This deviation is more obvious during the storm periods than during the tuning period, compare fig. 4.20 and fig.s 4.25-4.26, 4.32-4.33, and it propagates through the Eastern Scheldt as a disturbance wave along the characteristics. The errors of the Eastern Scheldt model can amplify these disturbances, while in other cases the interaction with disturbance waves from Rak Zuid or Bergen op Zoom accounts for a smaller deviation. This is seen at the second high tide at Steenbergse Sas, fig.s 4.28a-4.28c, where the prediction, 3 hrs. ahead, is more closely following the actual tide than the prediction, computed 2 hrs. ahead.

The fact that the errors of the predictions from the model along the coast seem to be relatively large is mainly due to the influence of the meteorological circumstances which is much greater at open sea than in the estuary. The meteorological effects must actually be deduced from the action of a wind field on the water surface. But since the measurements, registered at B.G.2, were the only available data from the 5 weeks period we had to take the local registration to be valid for the entire area. However, this is highly improbable. In order to relate the deviations to the meteorological influence a vector quantity is indicated which denotes the wind registration at B.G.2, a vector length of 1 cm corresponds to a wind velocity of 15 ms^{-1} . The local character of the wind field at B.G.2. is illustrated by the

diviations that occur at the second low tide (31 Januari '83) and originates in the areas at the boundaries. The reason of this interpretation is based on the rapid and strong variation of the C_d coefficient while the wind registration changes marginally during a period of several hours and the other estimated parameters do not indicate any sudden adaptation. So, we must assume that the registered wind field is not globally correct and obviously causes large errors.

Another source of errors with respect to the meteorological effects is the orientation of the coordinate axis, e.g. if a front enters the southern part of the North Sea from the North Western direction it shows up earlier at the mouth of the estuary than it does at Nieuwpoort and therefore the predictions, computed several hours ahead, are in error, as is also seen in the period 18-20 Januari '83. This is a shortcoming of our 1-D approach to model the propagation of the tidal wave in storm periods.

In case of considerable variations of the parameter values, as compared to the prediction period, we may also expect rapid growth of the deviations of the predicted water levels in time. This is illustrated by the behaviour of the reflection coefficient ρ at Rak Zuid. In storm periods, ρ changes occasionally by 10% within 1.5 hrs. just before high tide and the same change in reverse in the next 1.5 hrs. This affects the short term predictions at Rak Zuid, see fig.s 4.29a-4.29c while a similar behaviour is noticed at Bergen op Zoom. From the fig.s 4.28a-4.28d it is seen that the disturbance, initiated at Rak Zuid propagates backward and is first noticed in the predictions at Steenbergse Sas computed 1.0 hour ahead.

For the friction coefficients the above mentioned effect is only minor. First, the variations of μ are smaller and second, their influence is more globally. If the short term predictions are of primary importance this could suggest to specify the variance of the system noise component $W(t_k)$, associated with the solution equation

$$P(t_{k+1}) = P(t_k) + W(t_k) ,$$

at a lower level to dissipate and retardate the effect of the residuals on the correction of the parameter by influencing the Kalman gain matrix.

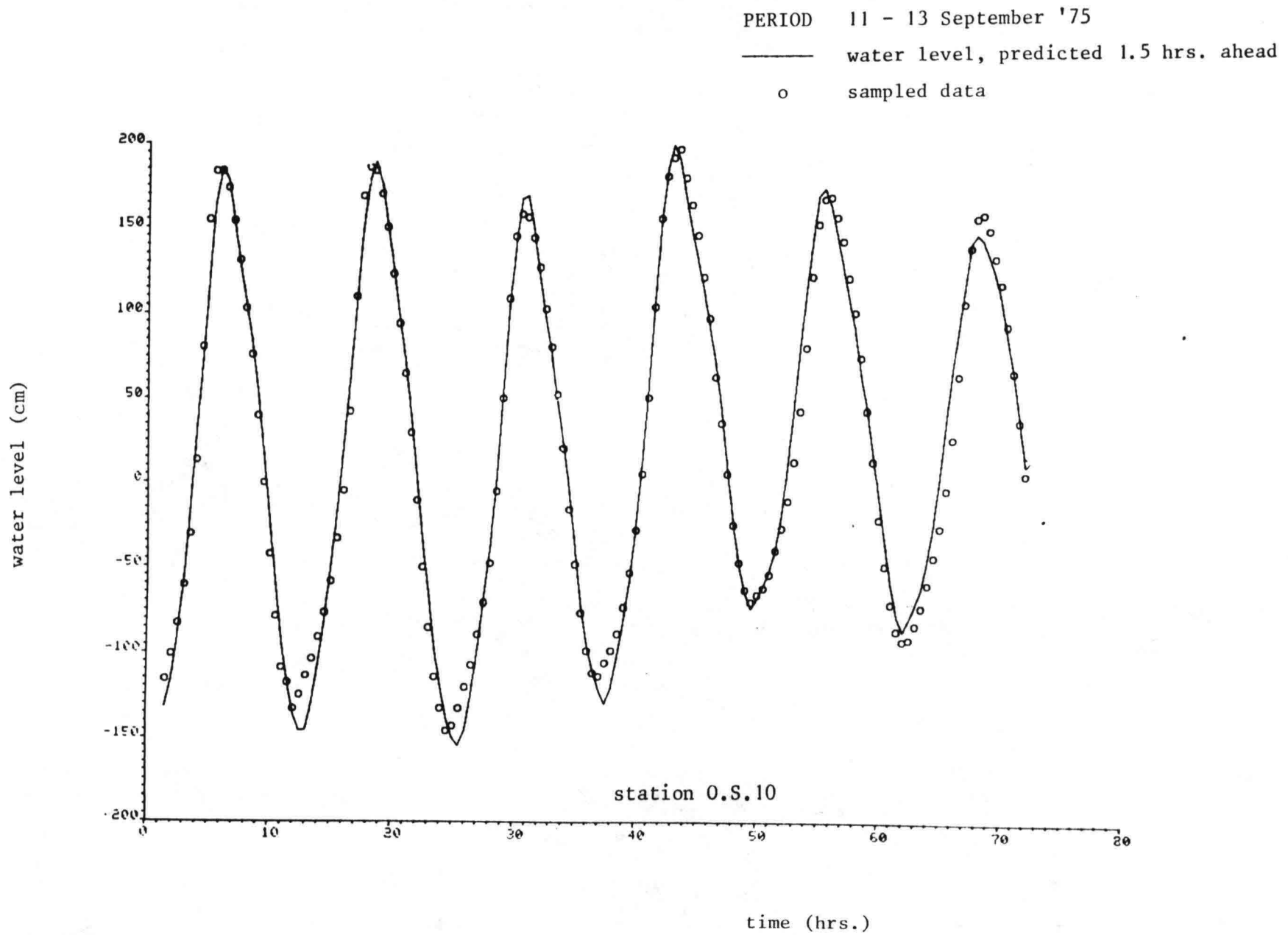


Fig. 4.20

PERIOD 11 - 13 September '75

— water level, predicted 1.0 hrs. ahead

o sampled data

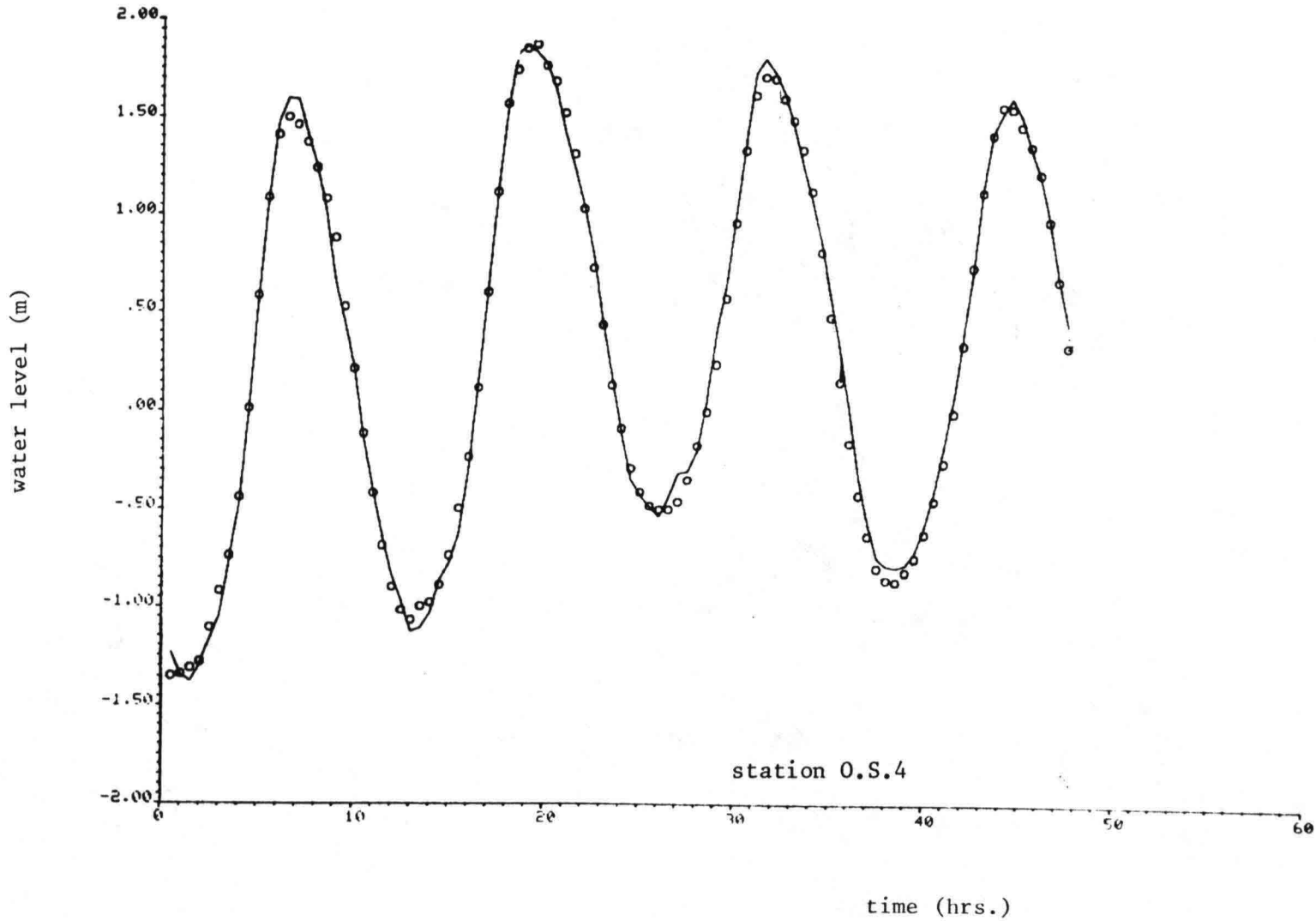


Fig. 4.21a

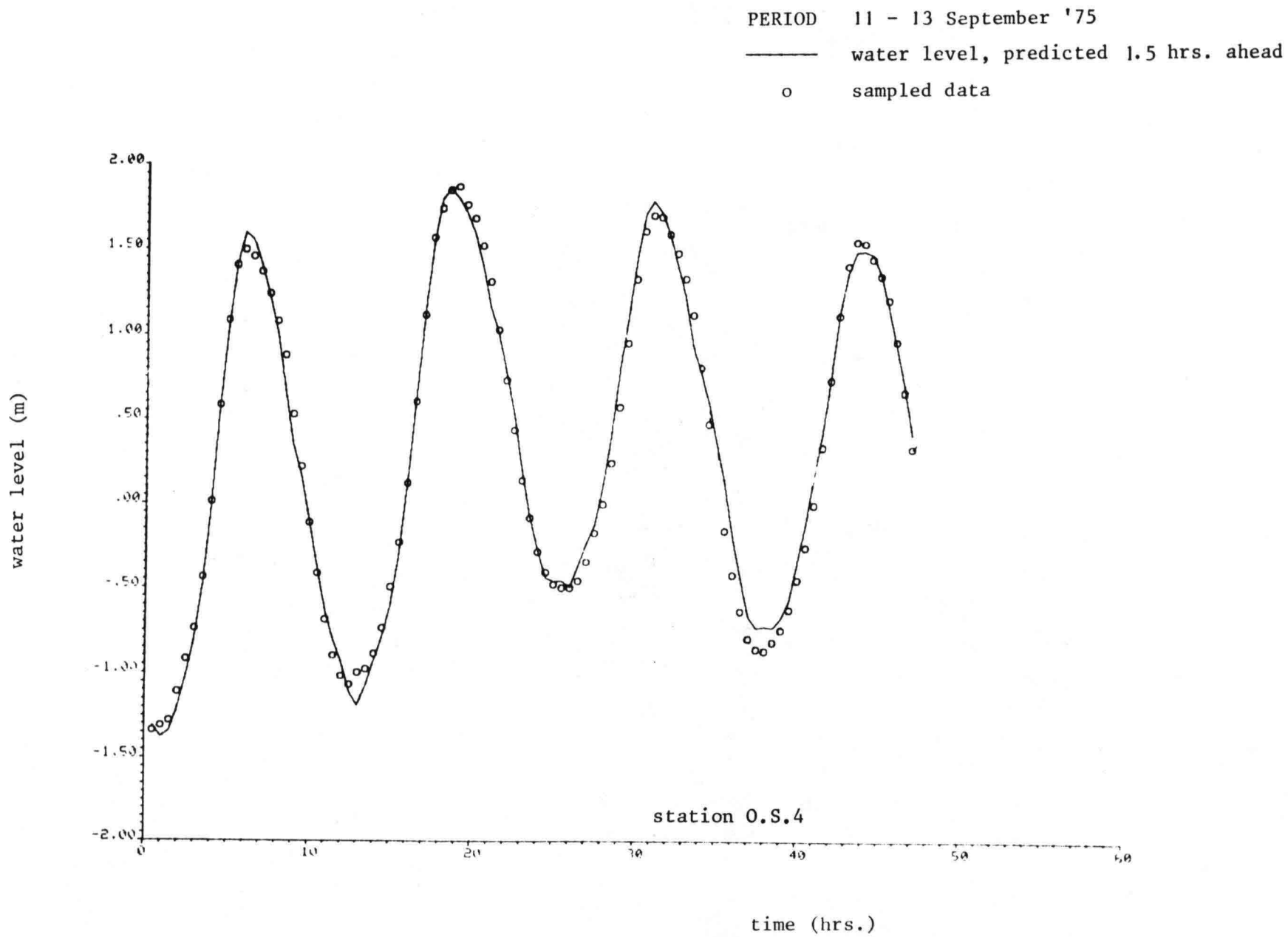


Fig. 4.21b

PERIOD 11 - 13 September '75

— water level, predicted 1.0 hrs. ahead

o sampled data

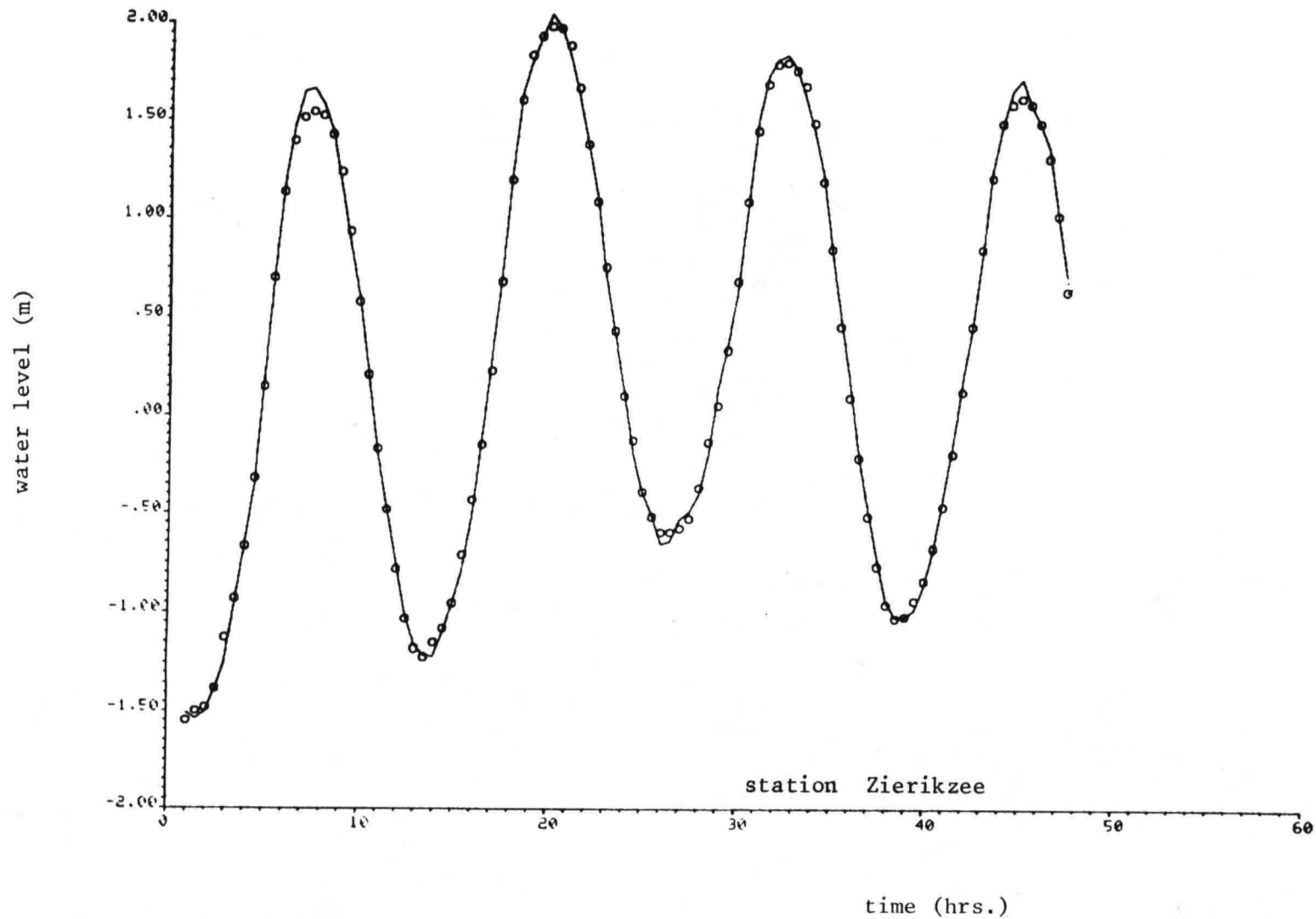


Fig. 4.22a

PERIOD 11 - 13 September '75

— water level, predicted 2.0 hrs. ahead

o sampled data

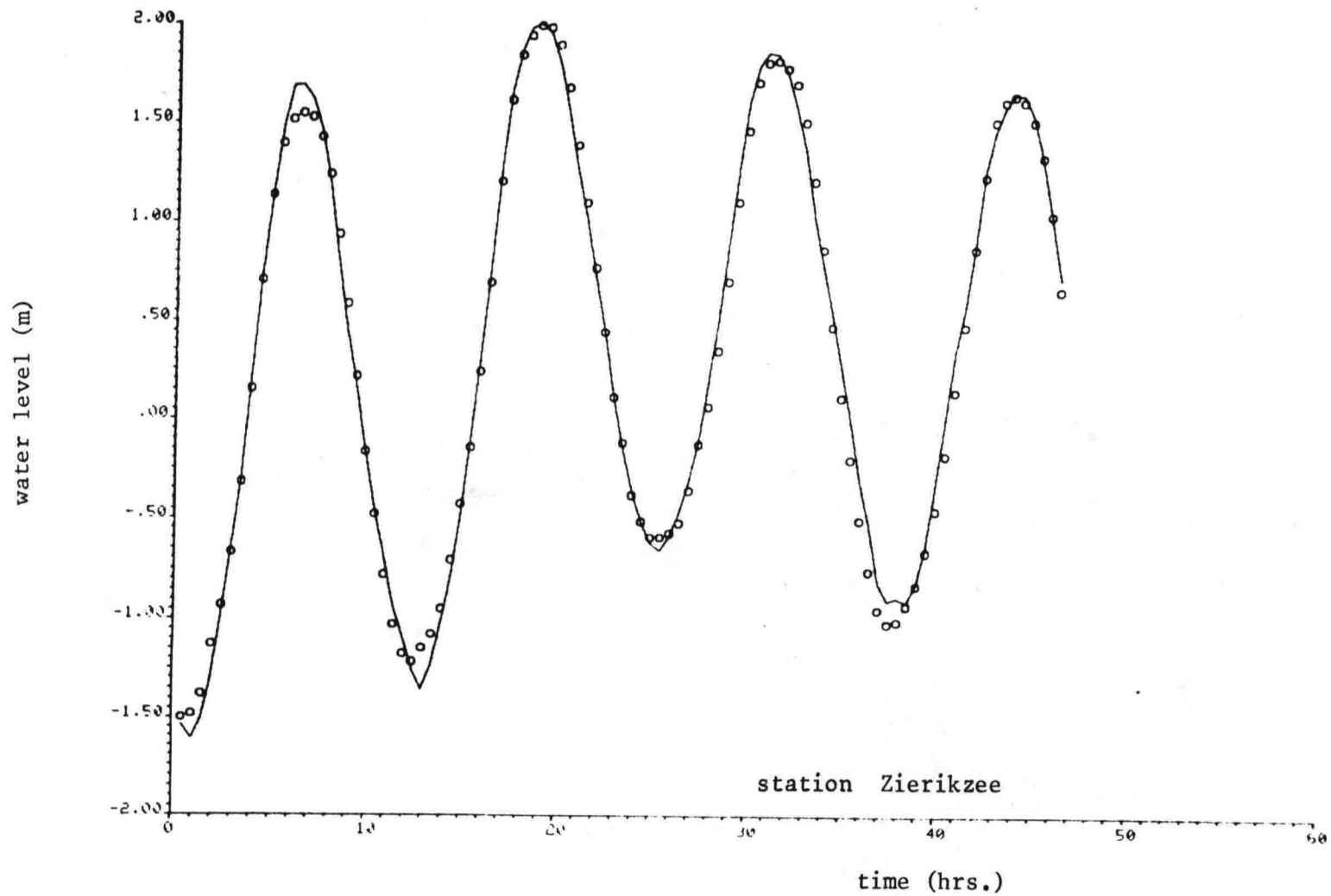


Fig. 4.22b

PERIOD 11 - 13 September '75
— water level, predicted 2.0 hrs. ahead
o sampled data

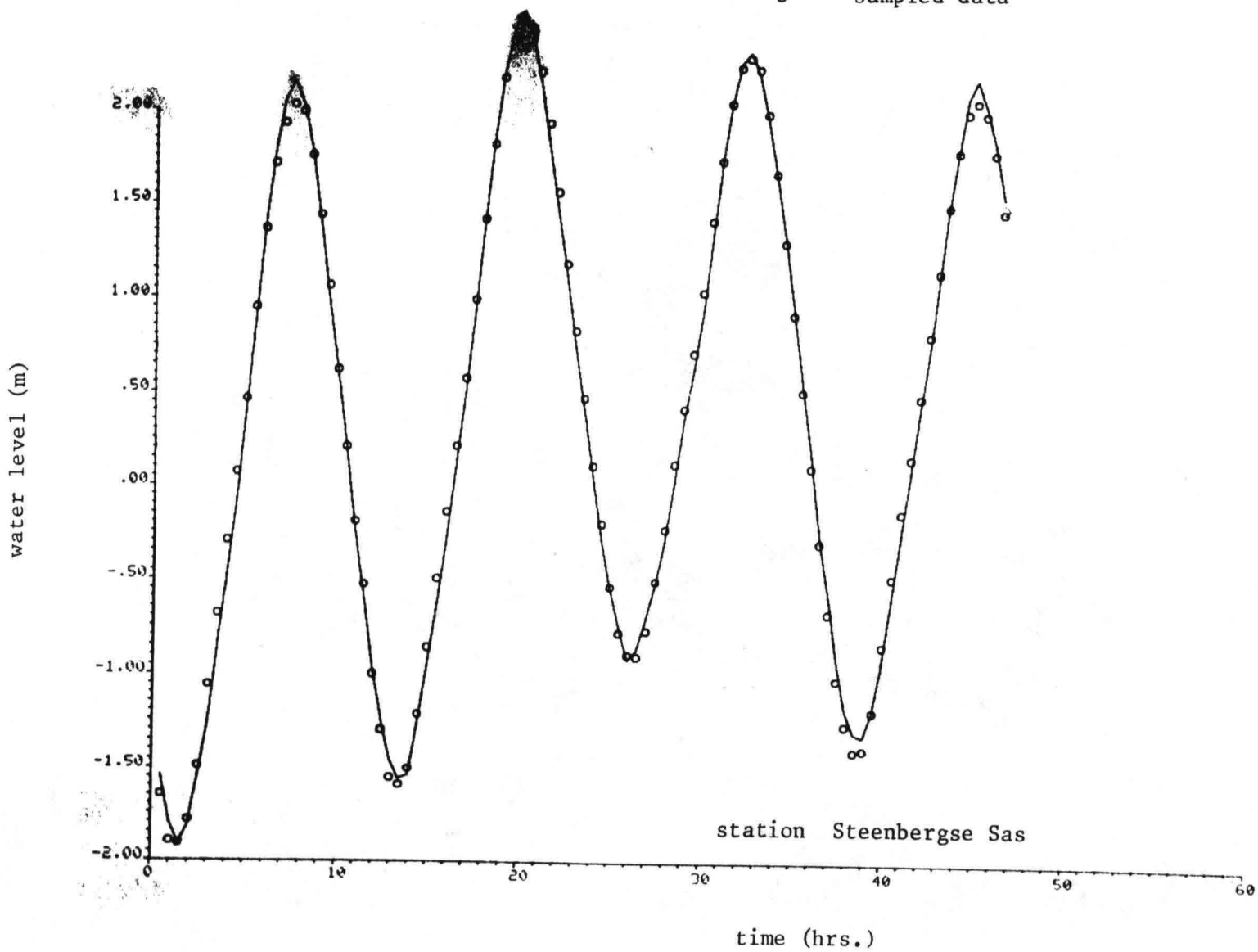


Fig. 4.23a

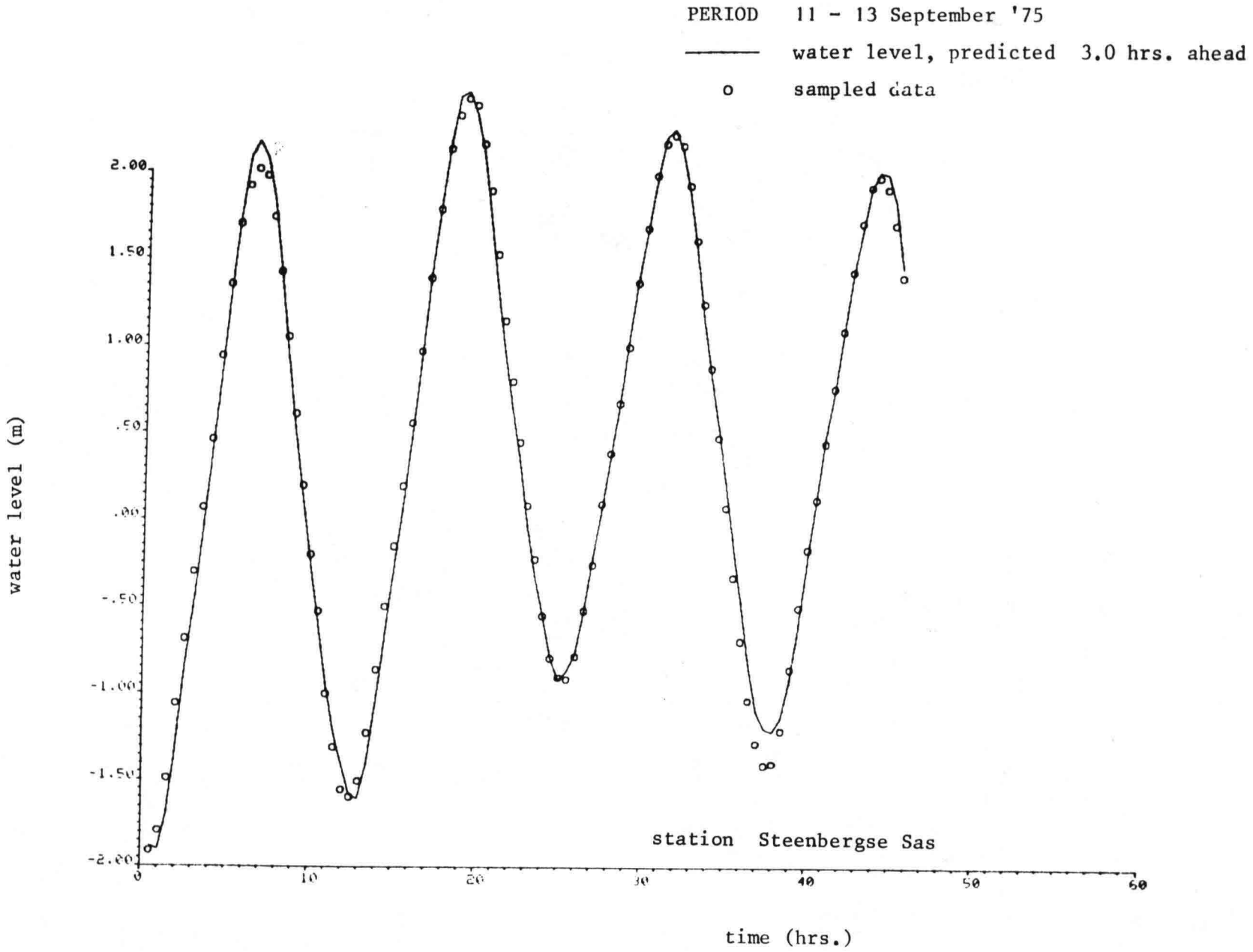


Fig. 4.23b

PERIOD 11 - 13 September '75

— water level, predicted 1.5 hrs. ahead

o sampled data

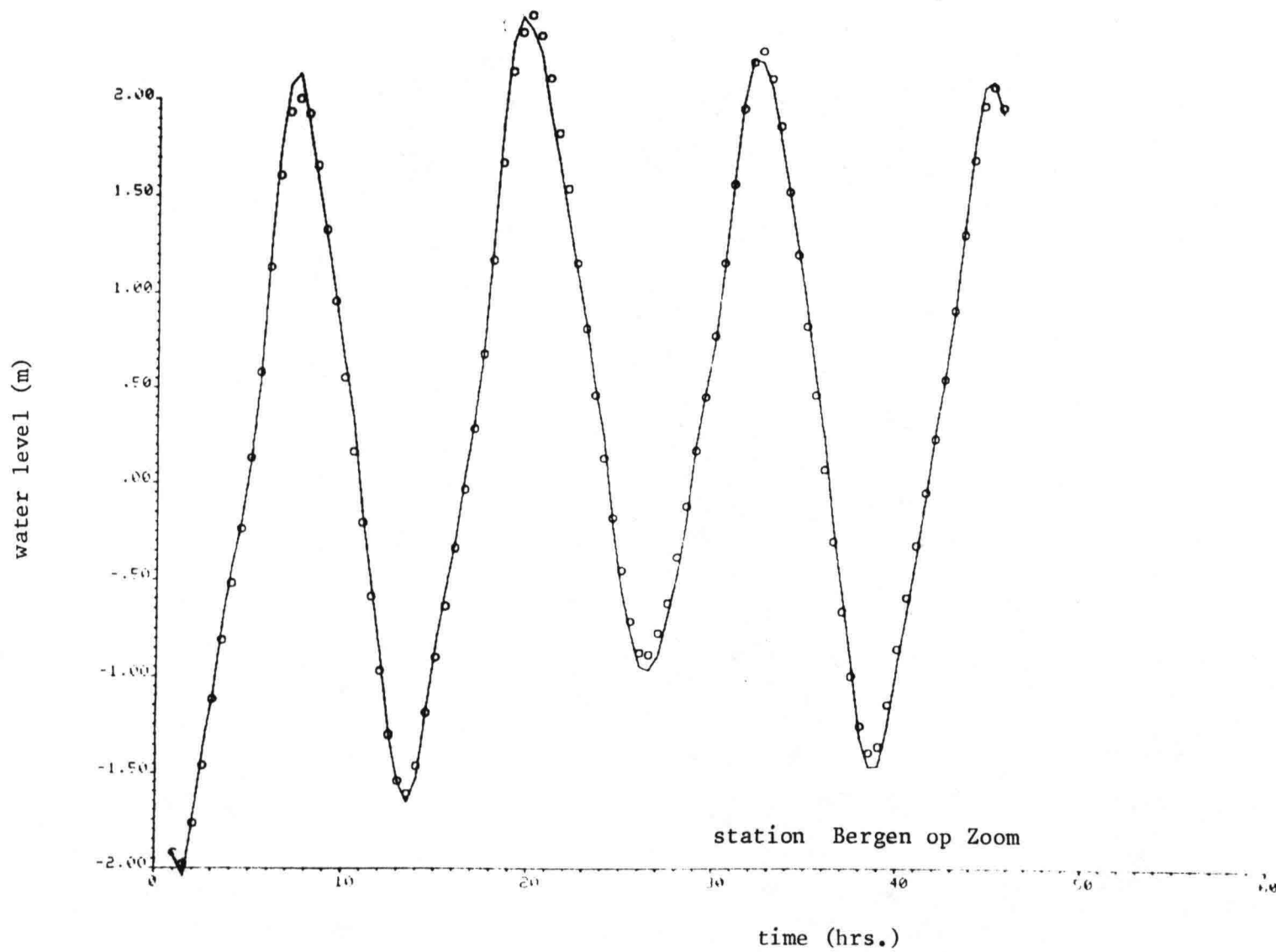


Fig. 4.24a

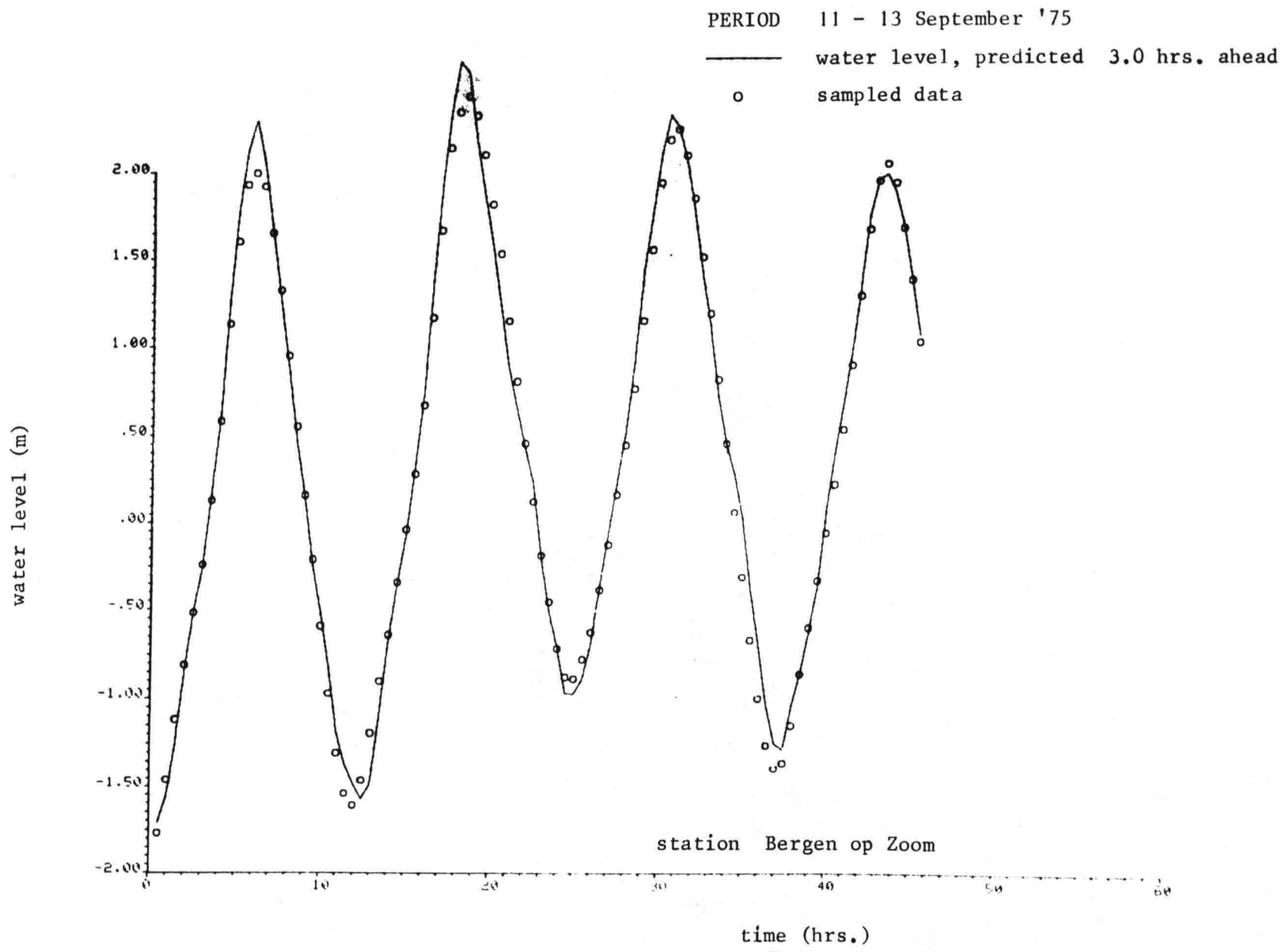


Fig. 4.24b

PERIOD 18 - 20 January '83

— water level, predicted 1.0 hrs. ahead

- - o - - sampled data

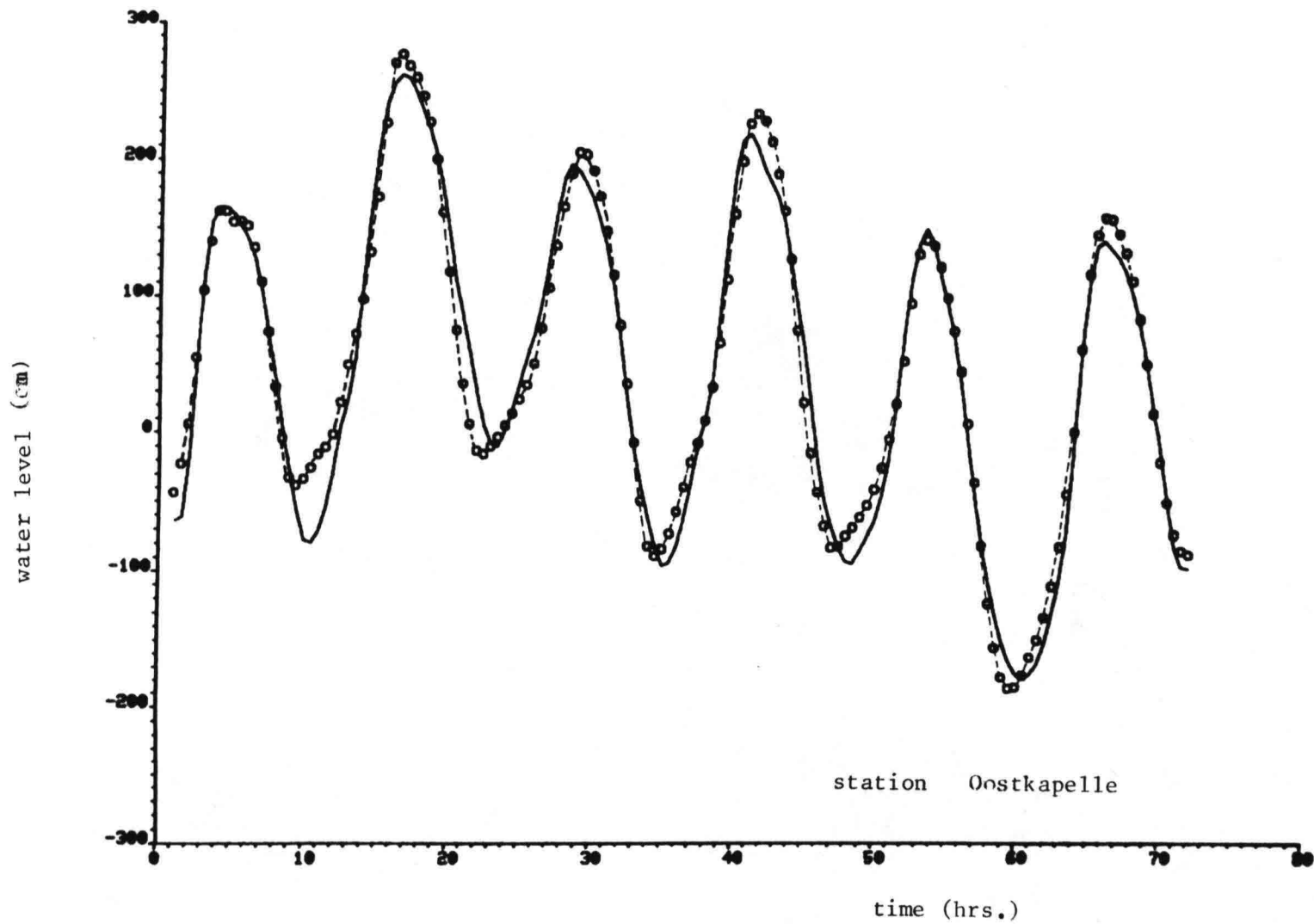


Fig. 4.25a

PERIOD 18 - 20 January '83

— water level, predicted 1.5 hrs. ahead

---o--- sampled data

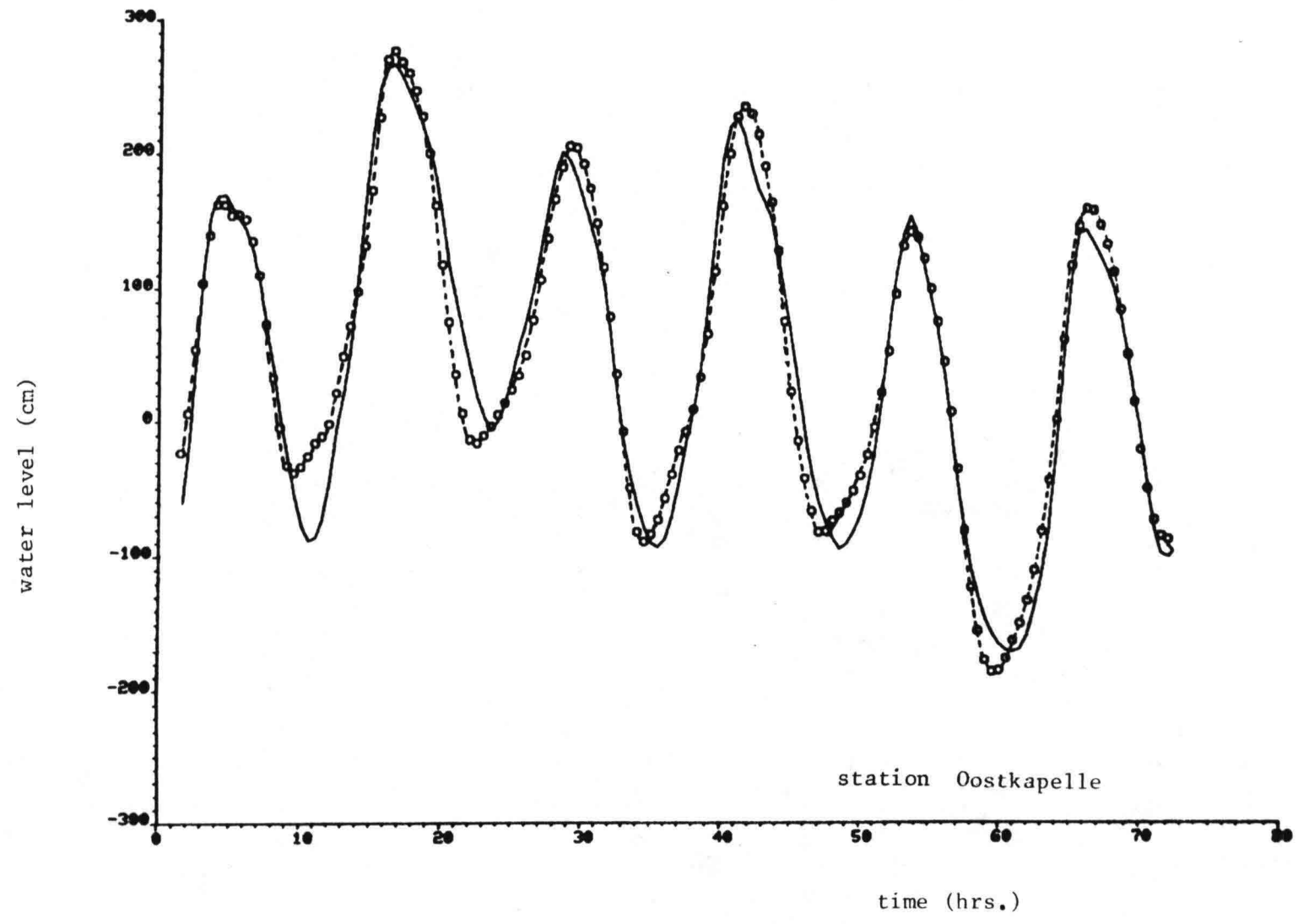


Fig. 4.25b

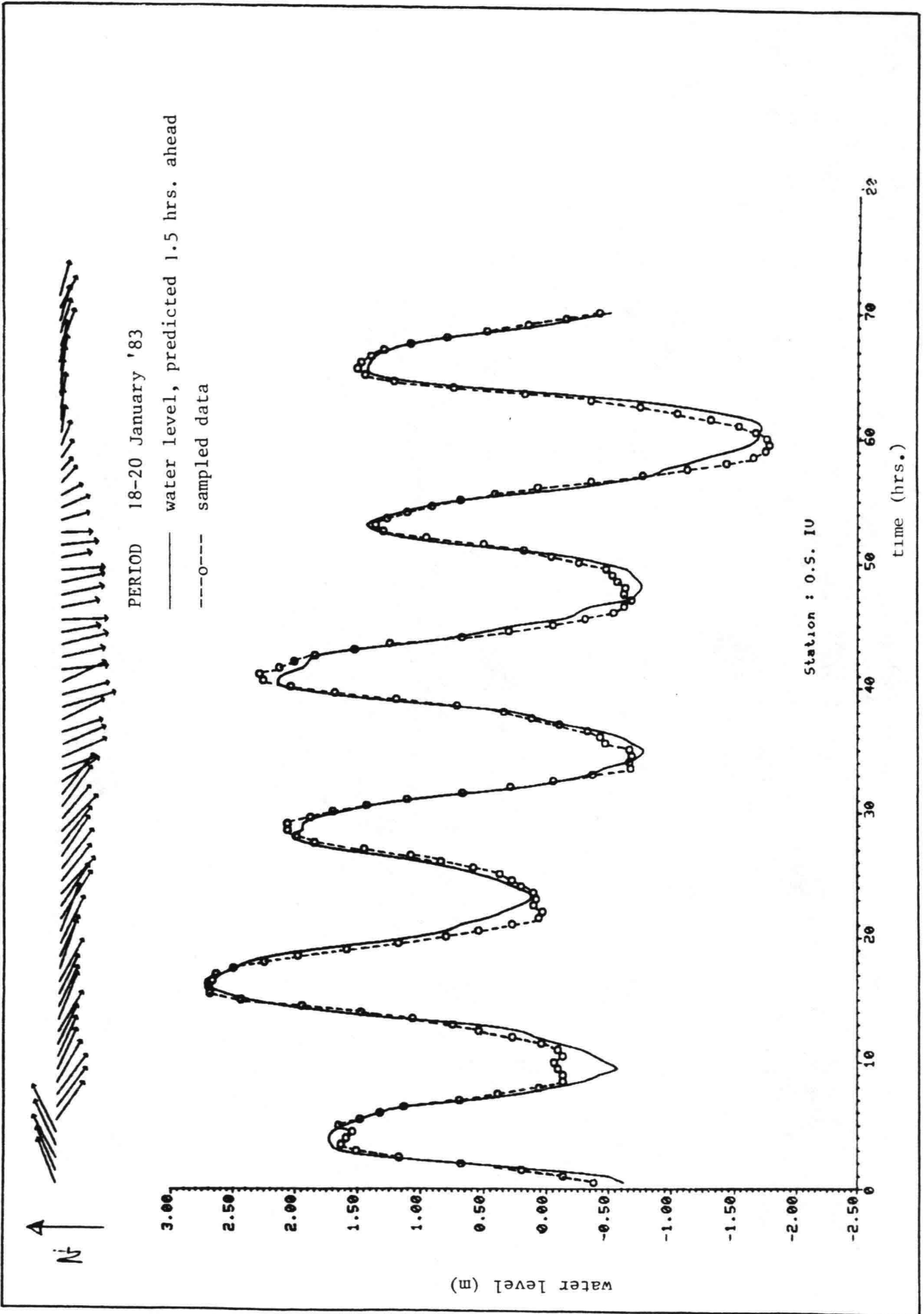


Fig. 4.26a

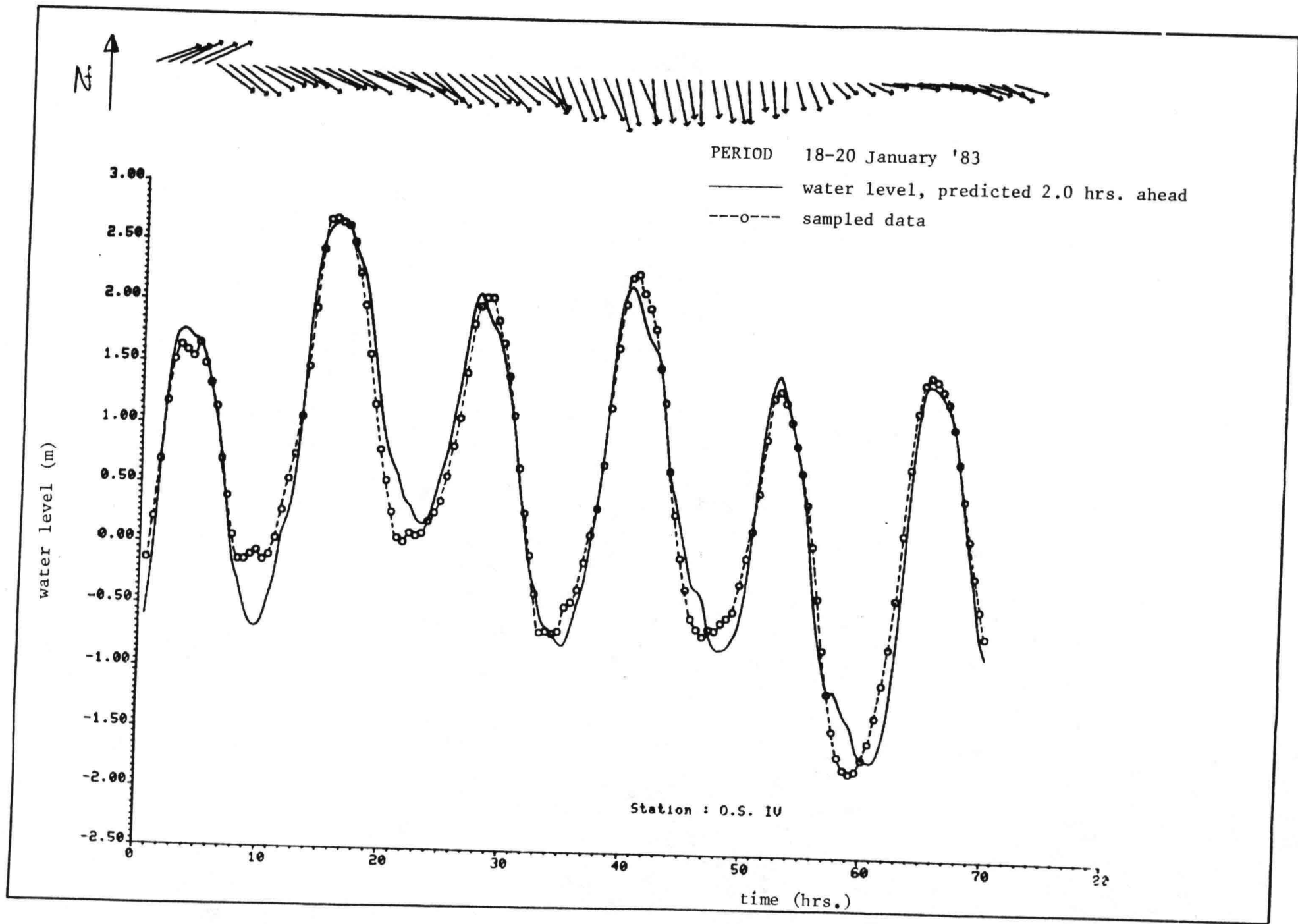


Fig. 4.26b

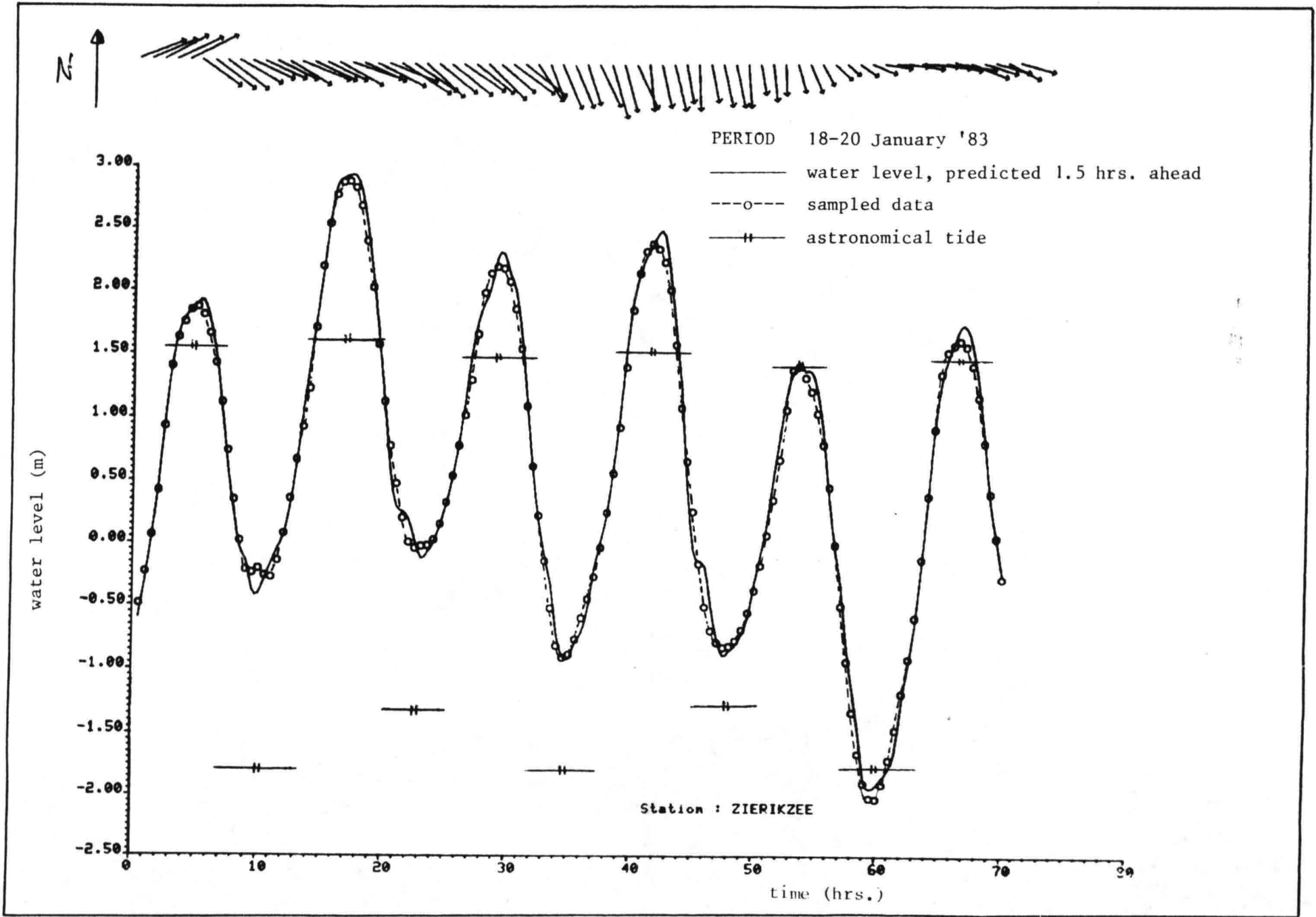


Fig. 4.27a

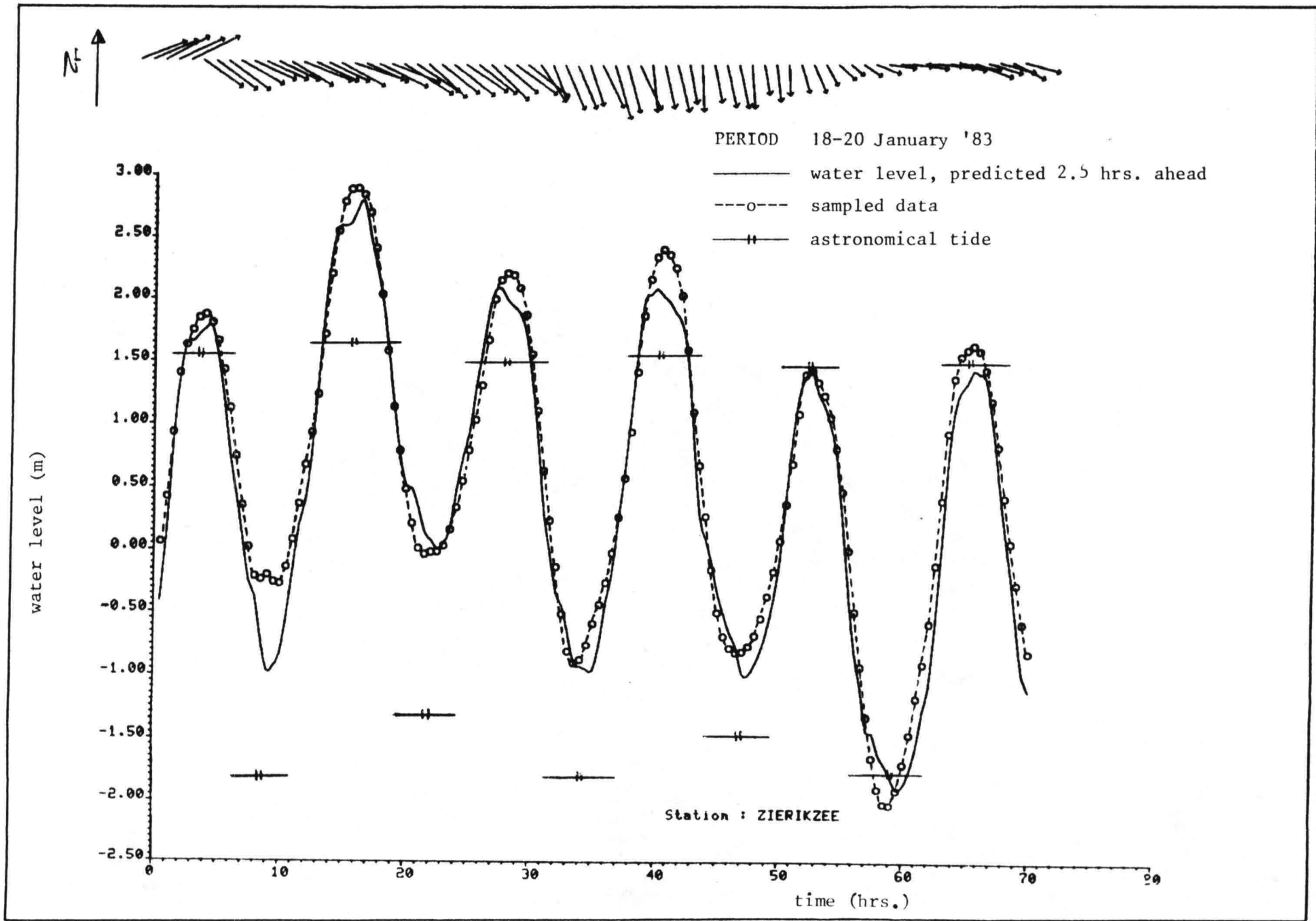


Fig. 4.27b

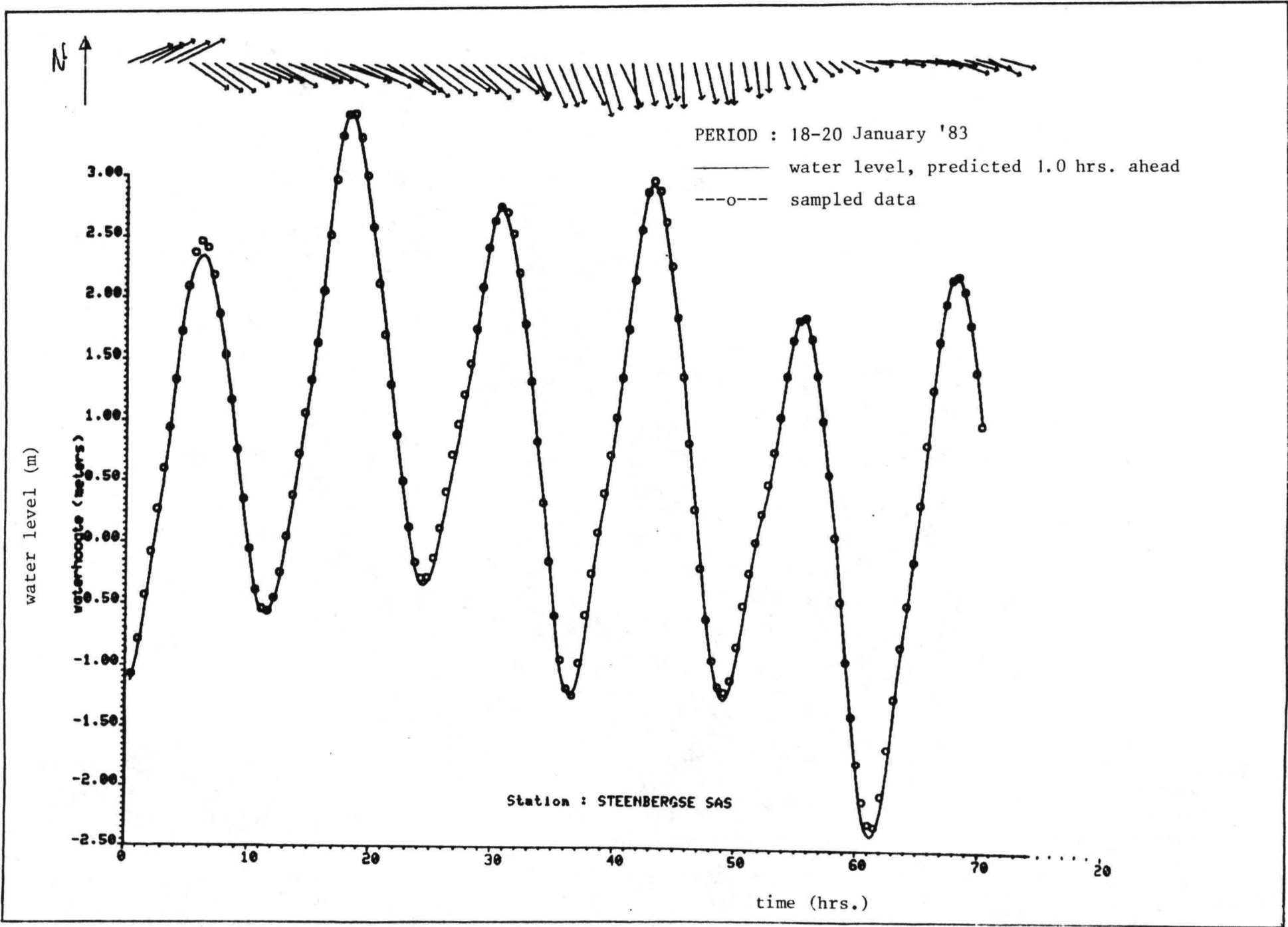


Fig. 4.28a

PERIOD : 18-20 January '83

— water level, predicted 1.5 hrs. ahead
-o- sampled data

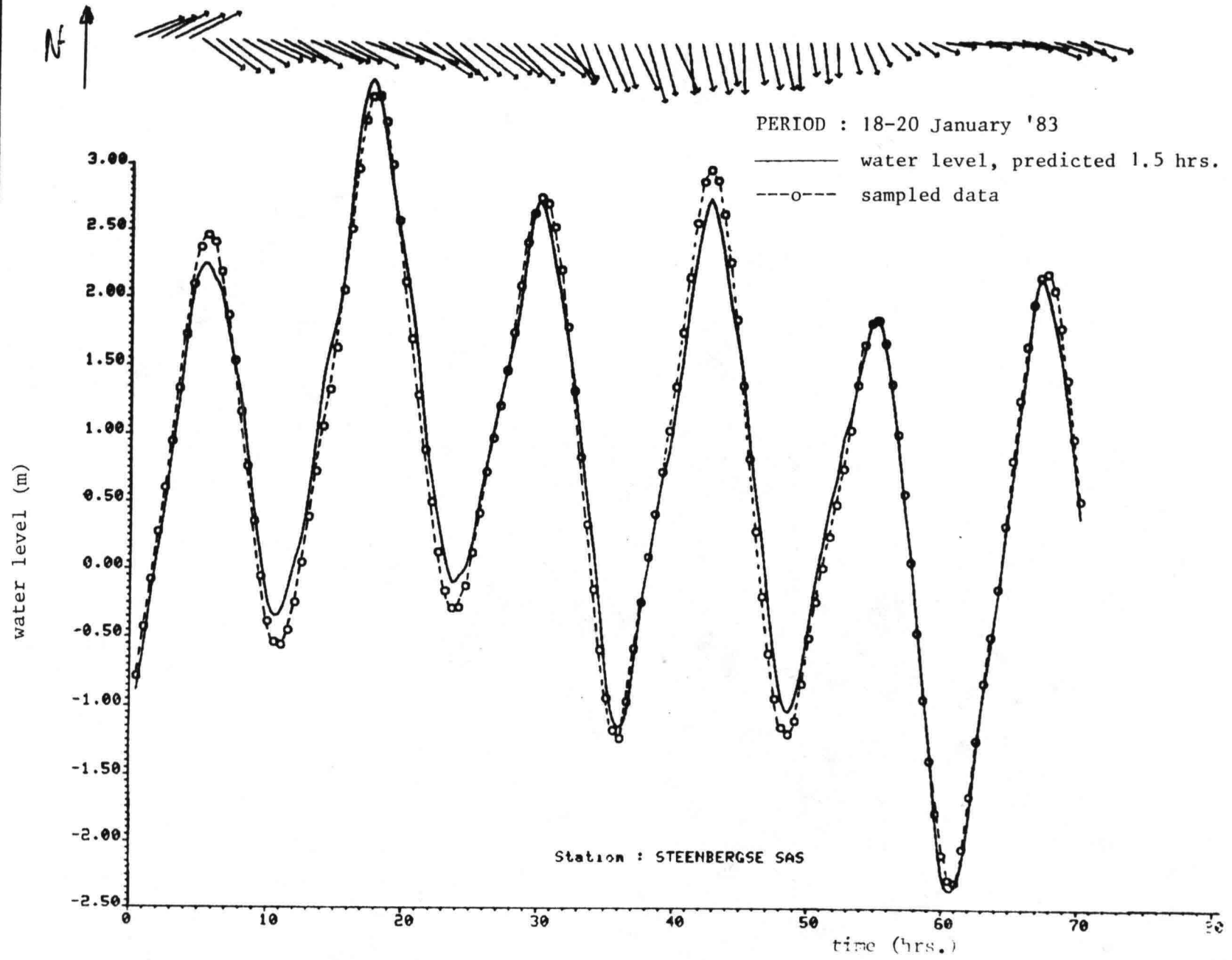


Fig. 4.28b

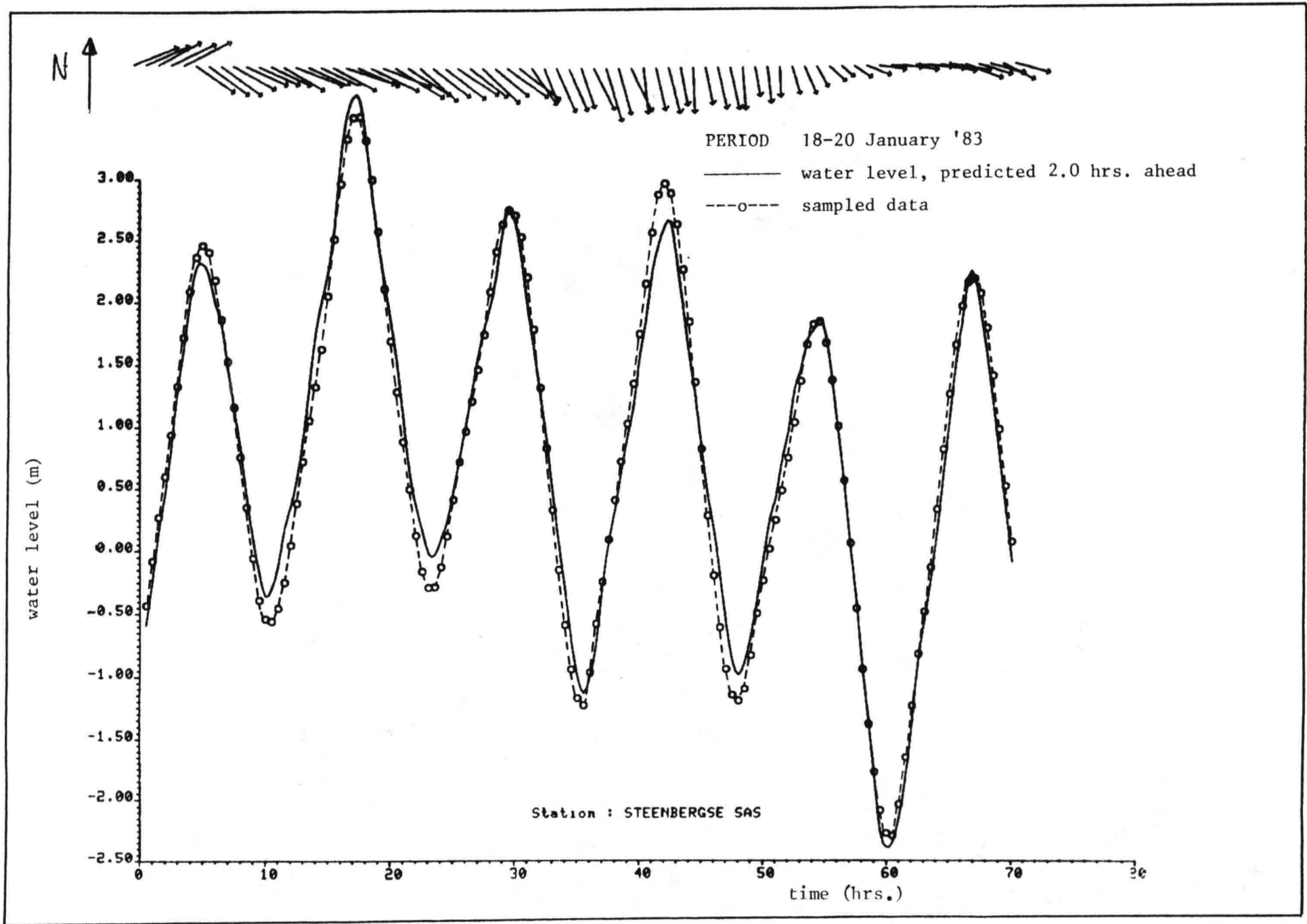


Fig. 4.28c

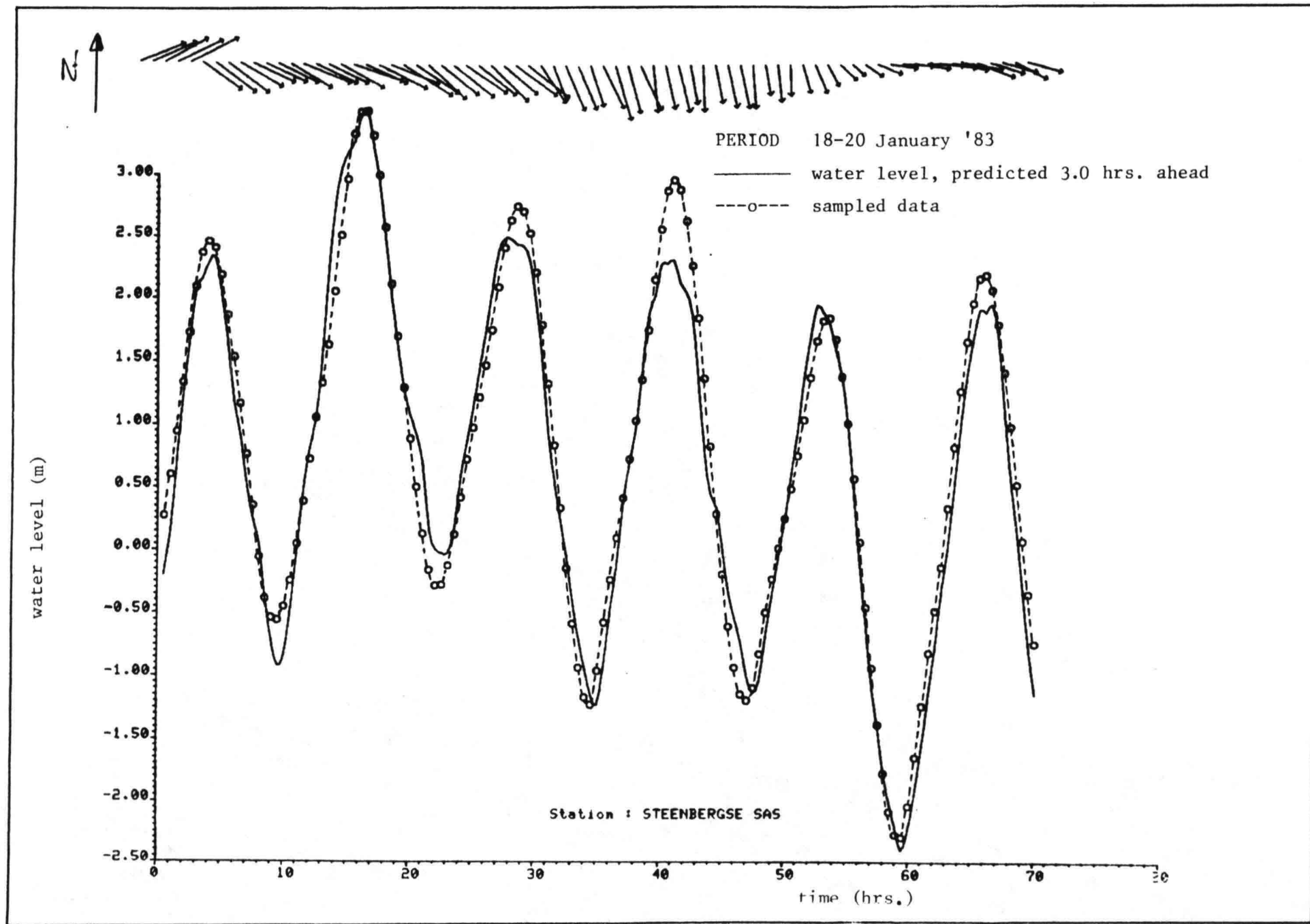


Fig. 4.28d

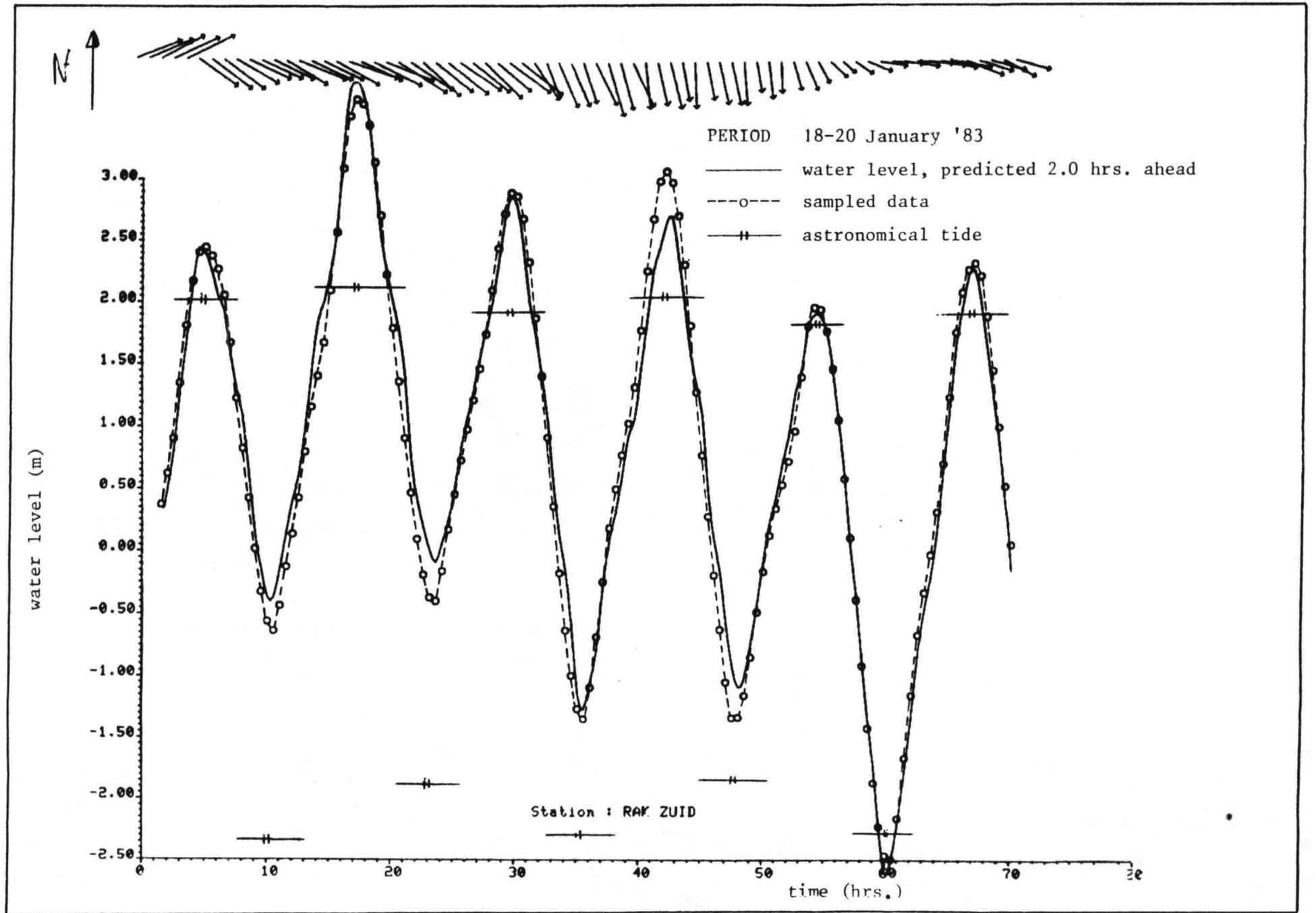


Fig. 4.29

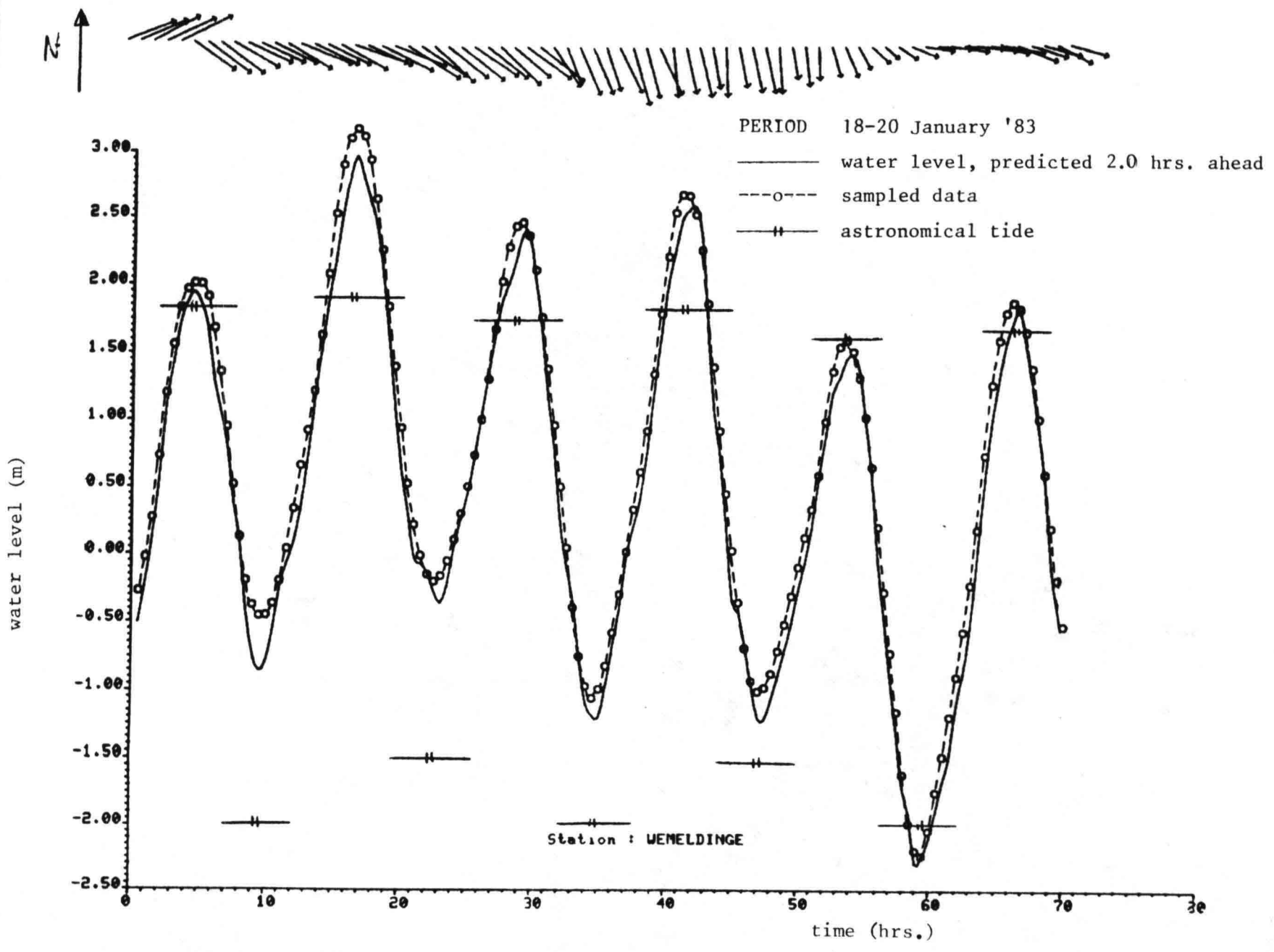


Fig. 4.30a

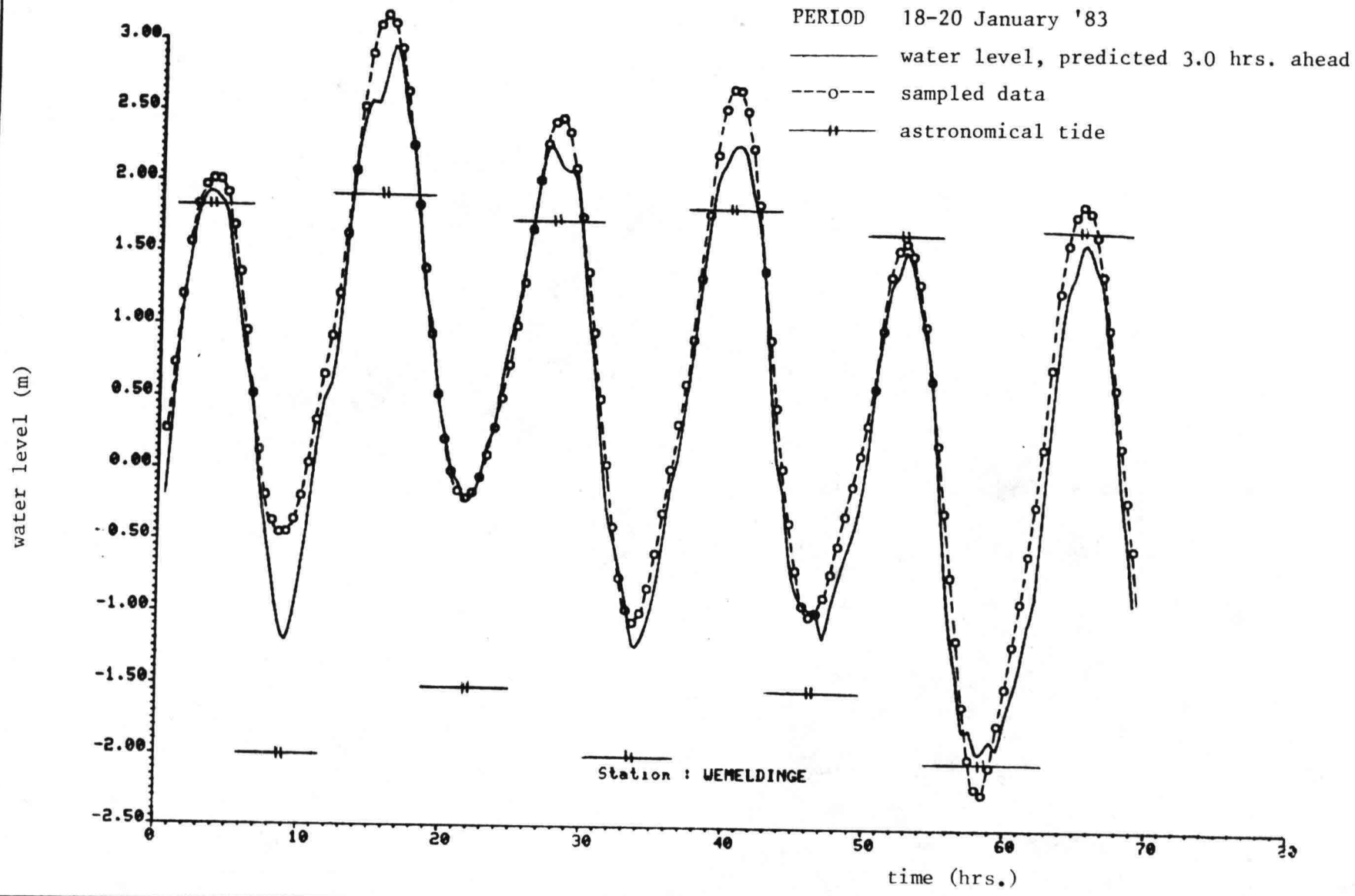


Fig. 4.30b

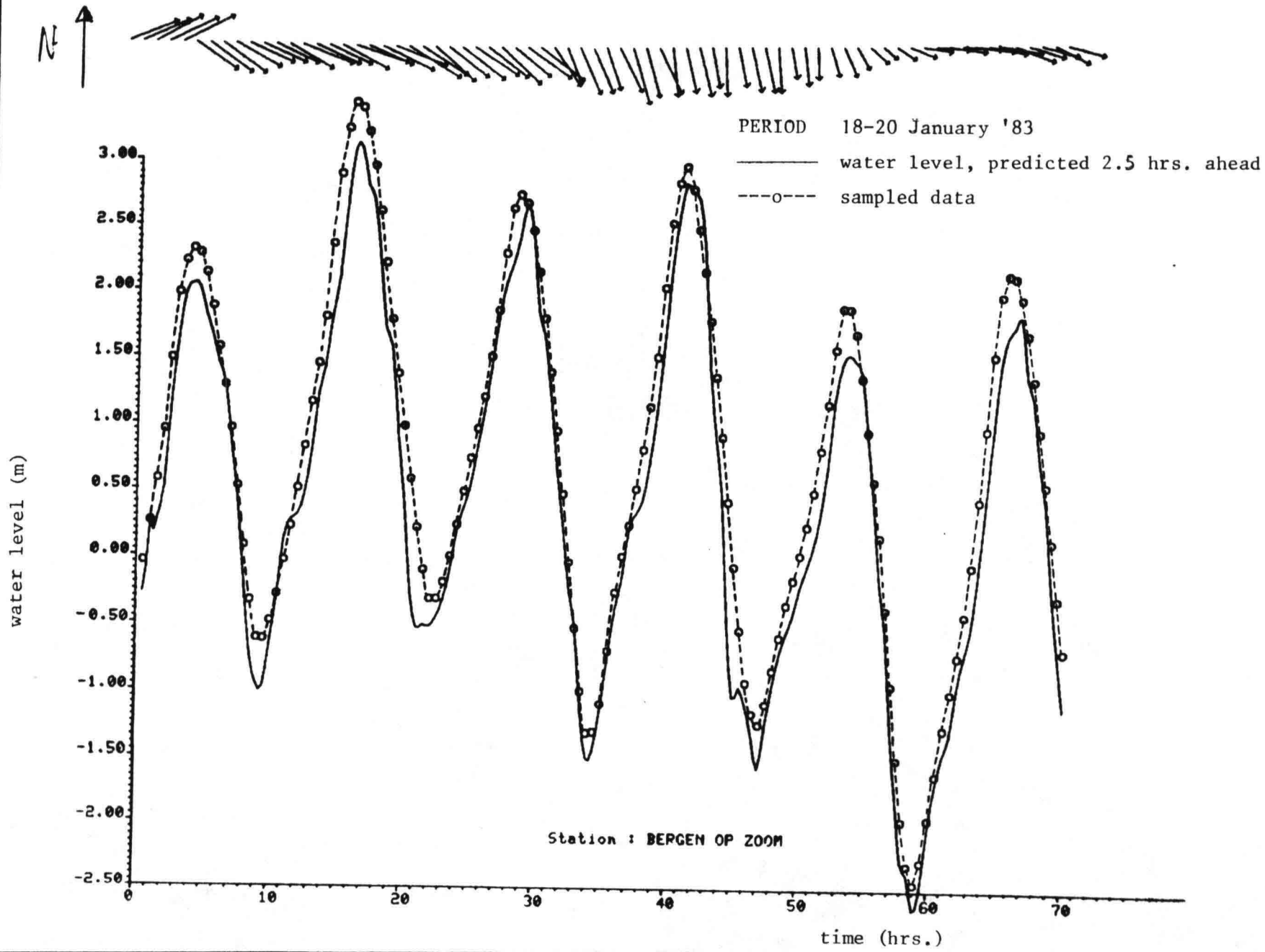


Fig. 4.31a

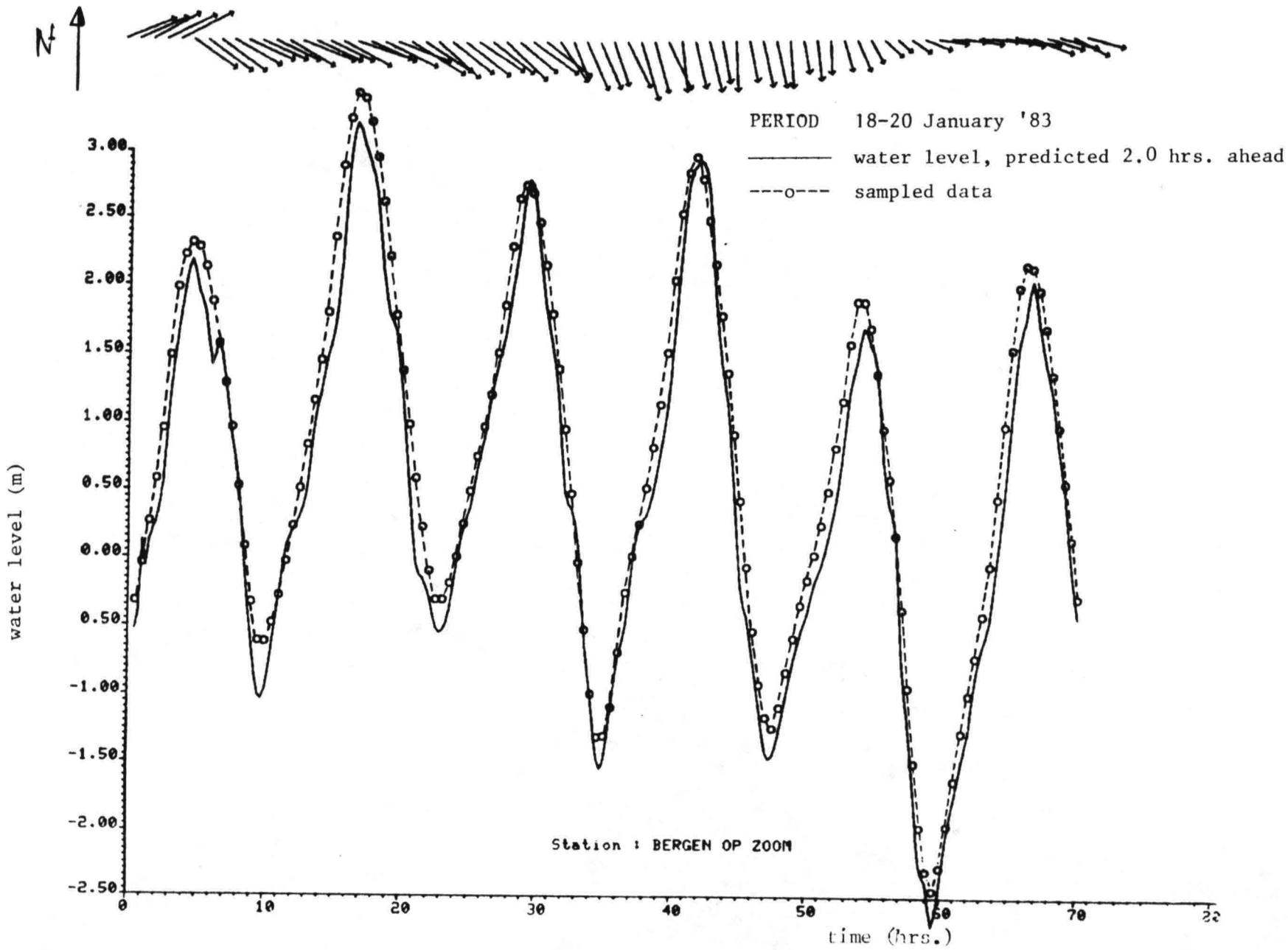


Fig. 4.31b

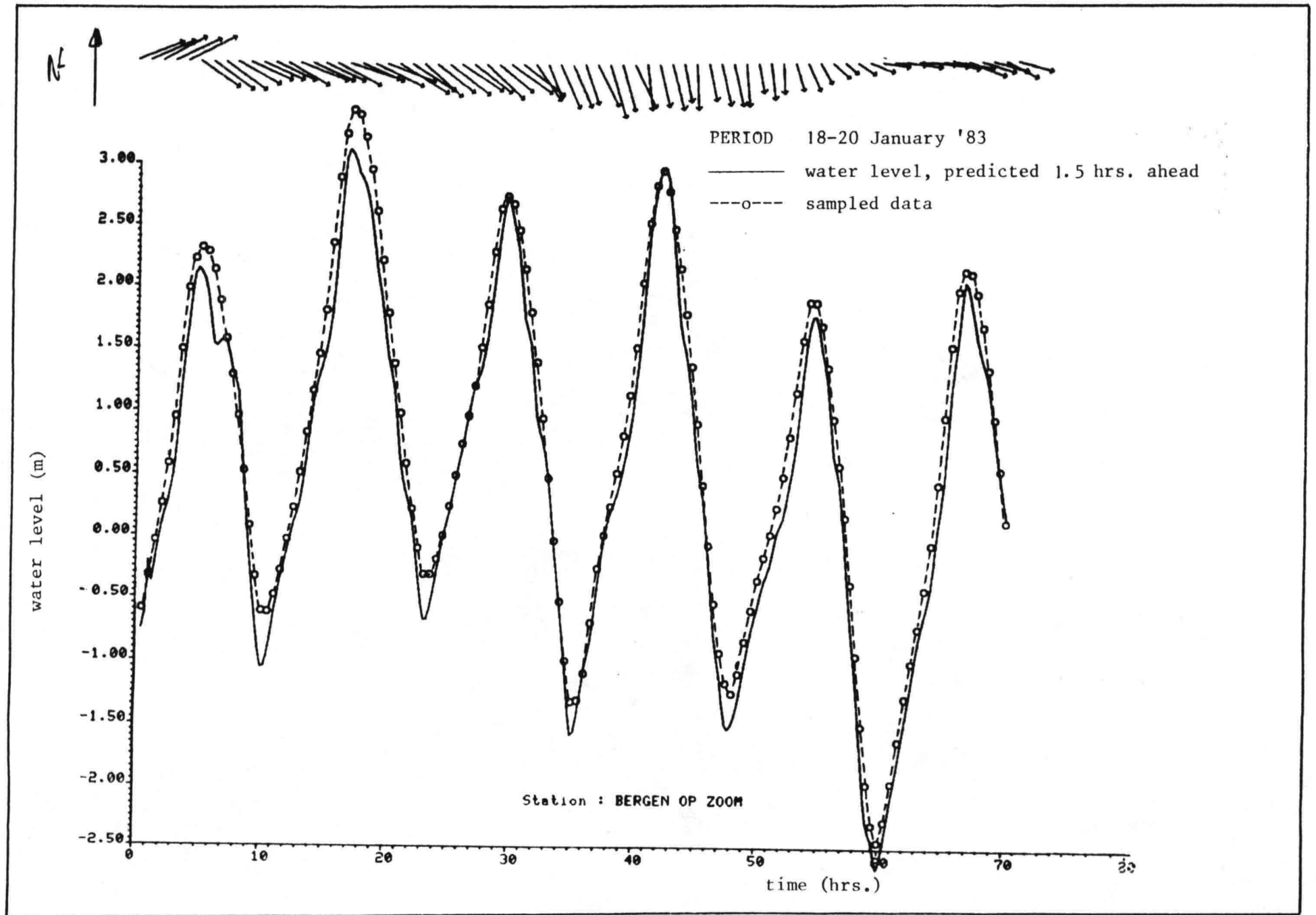


Fig. 4.31c

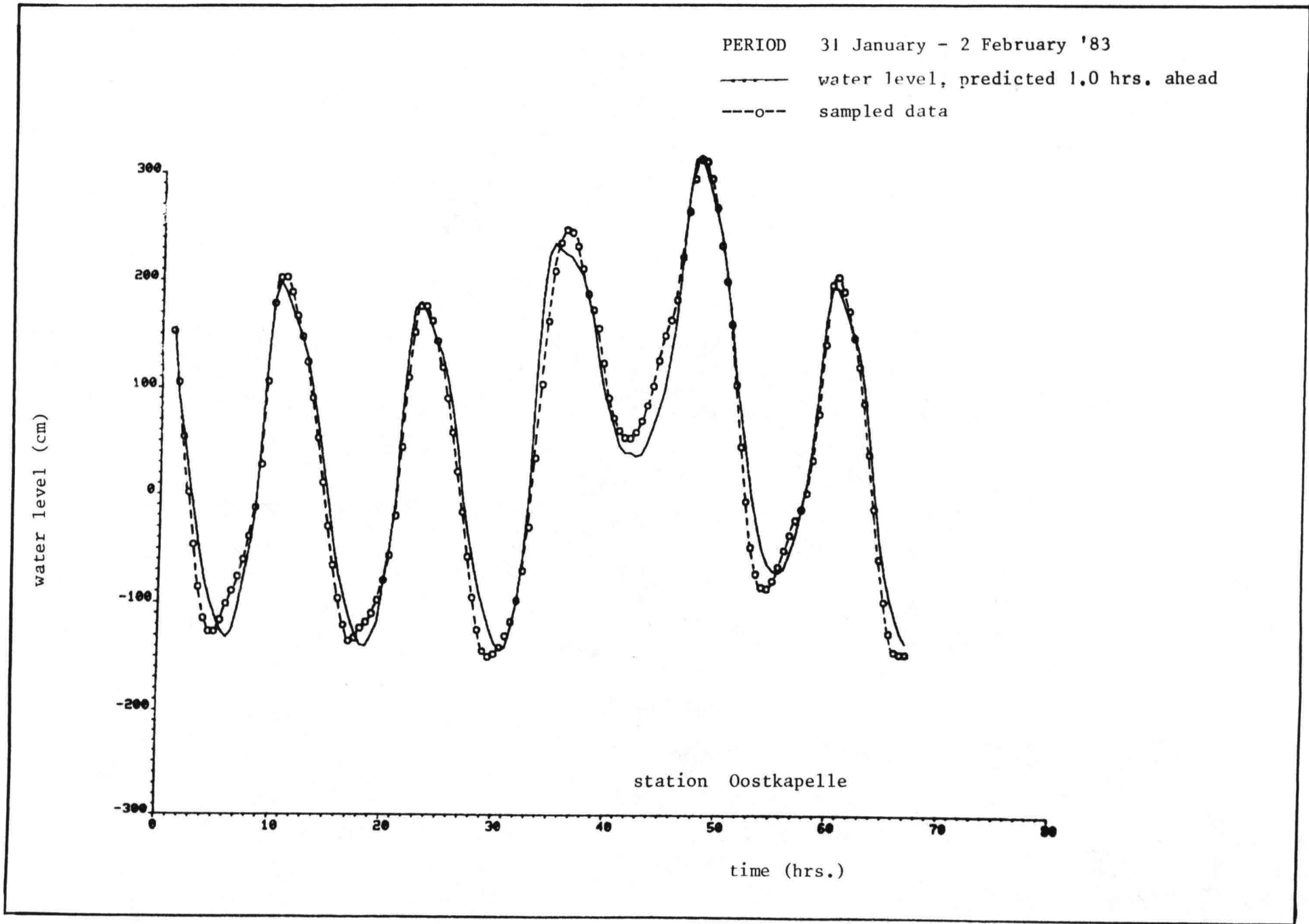


Fig. 4.32a

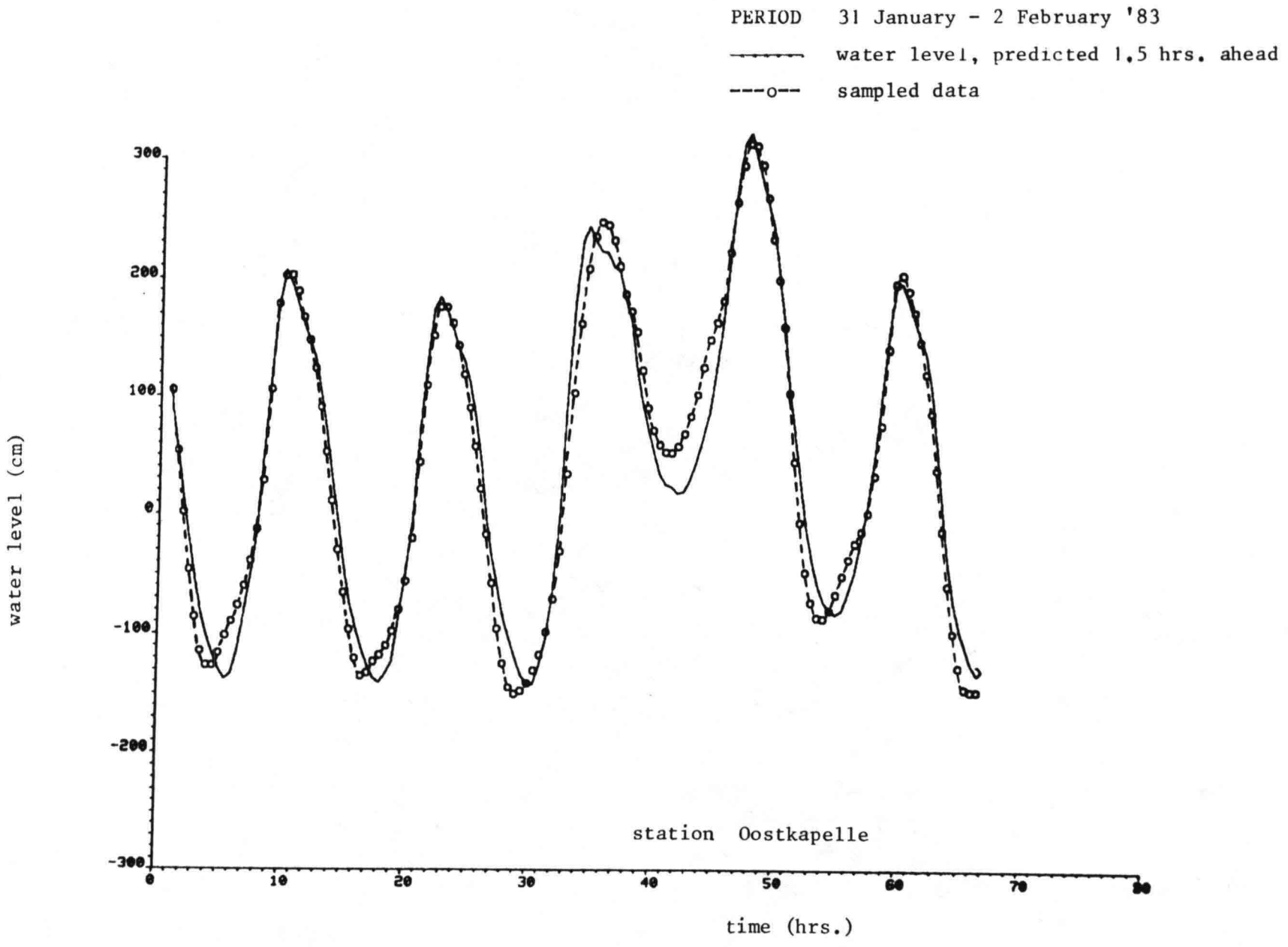


Fig. 4.32b

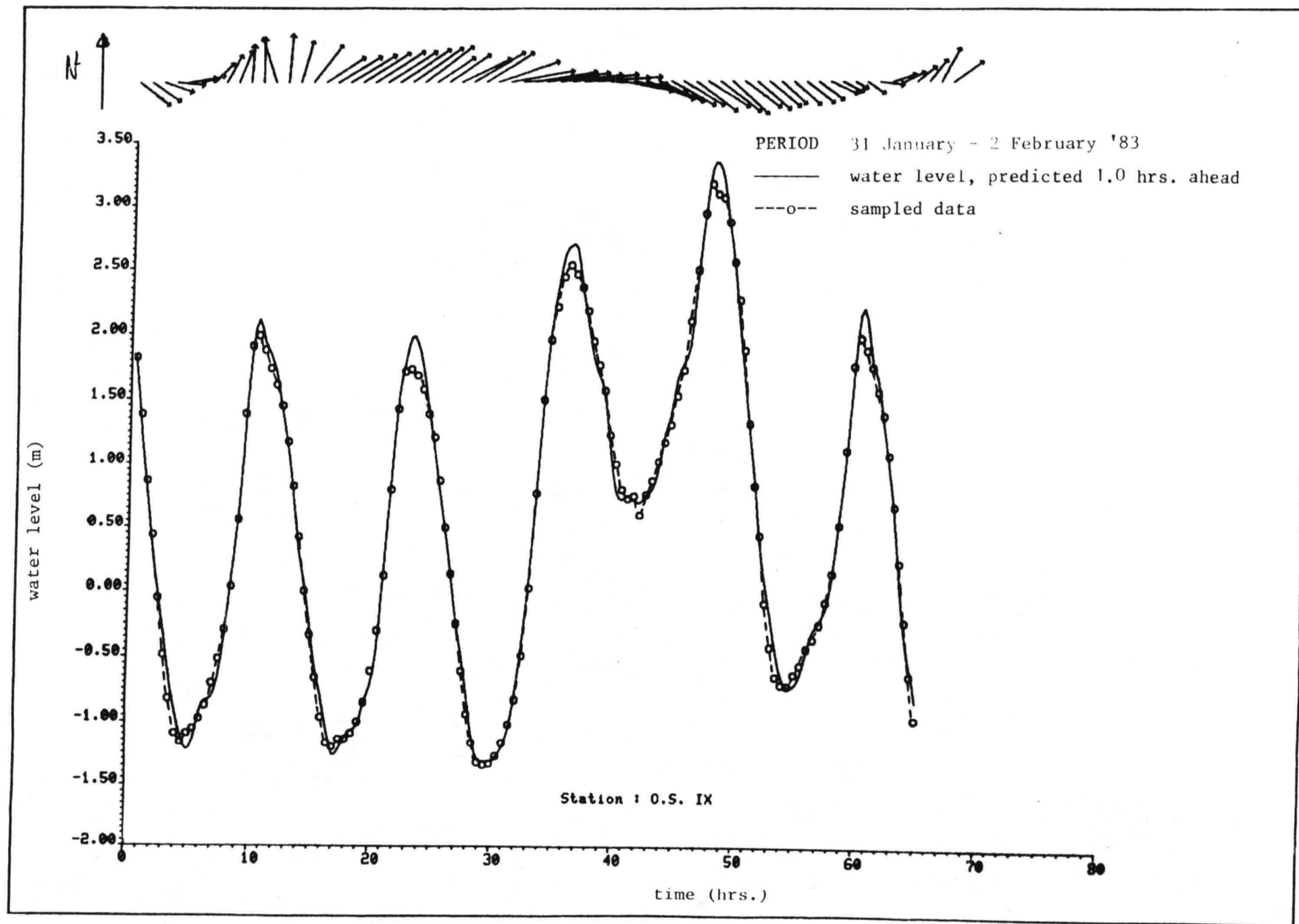


Fig. 4.33a

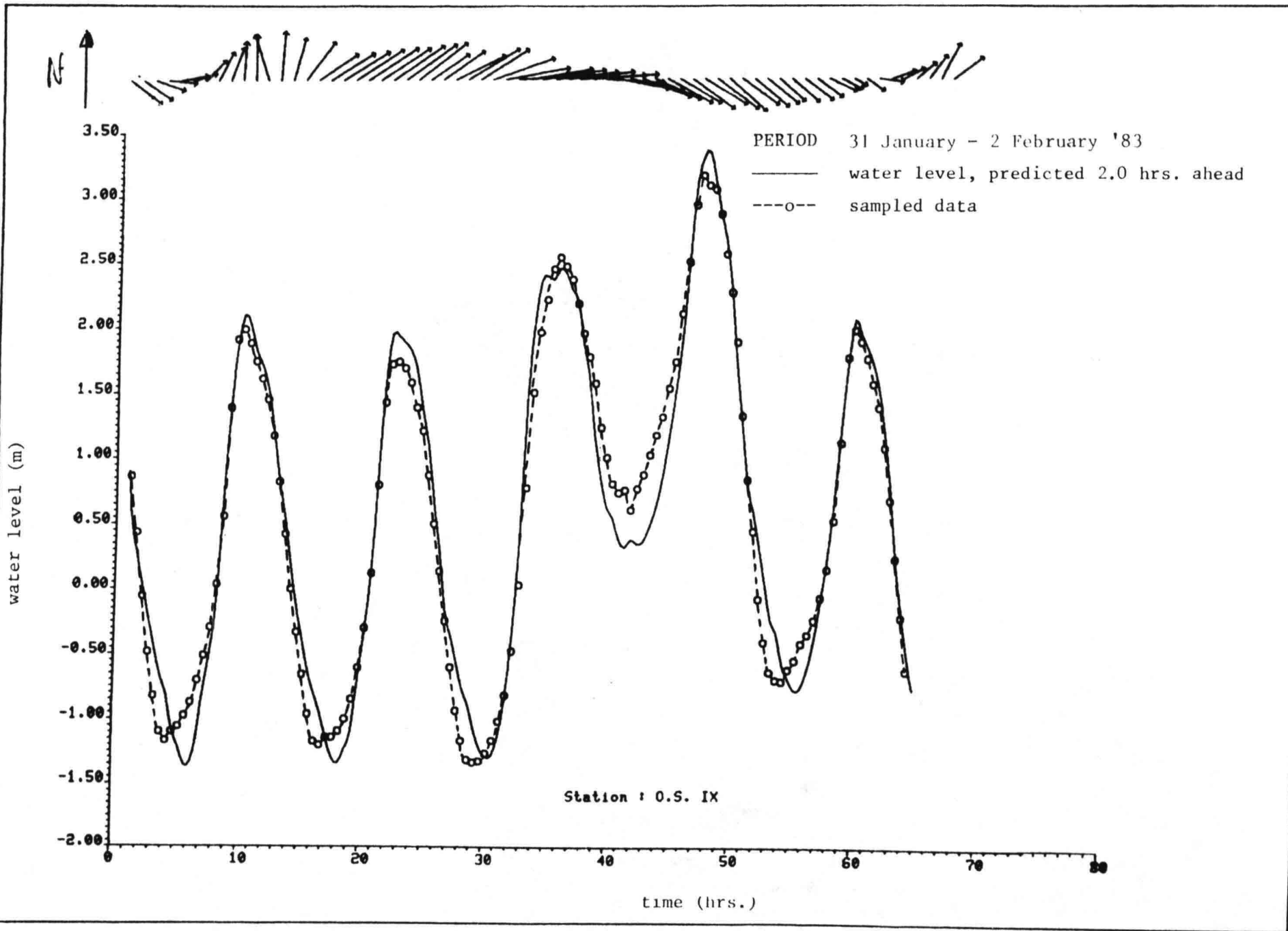


Fig. 4.33b

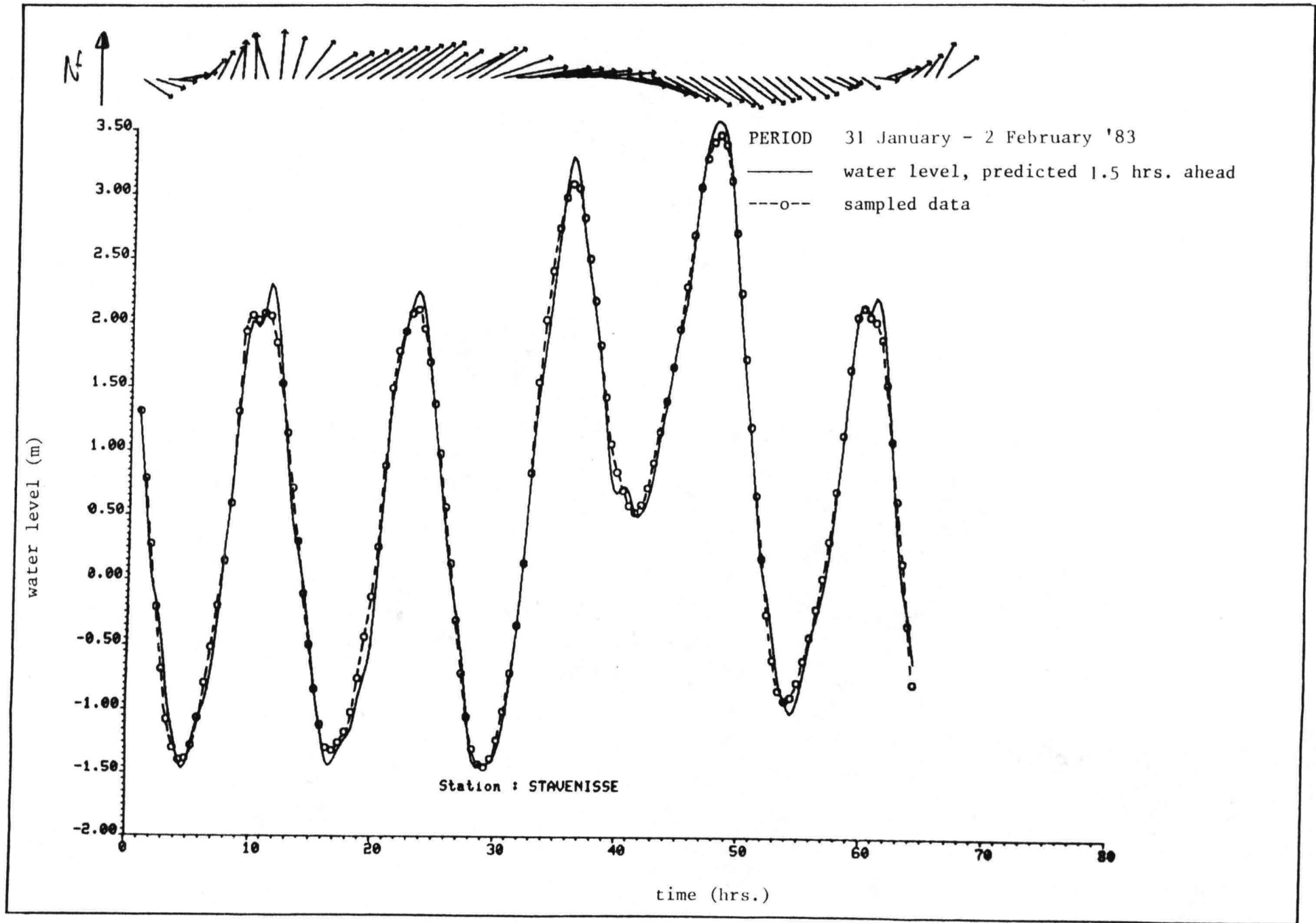


Fig. 4.34a

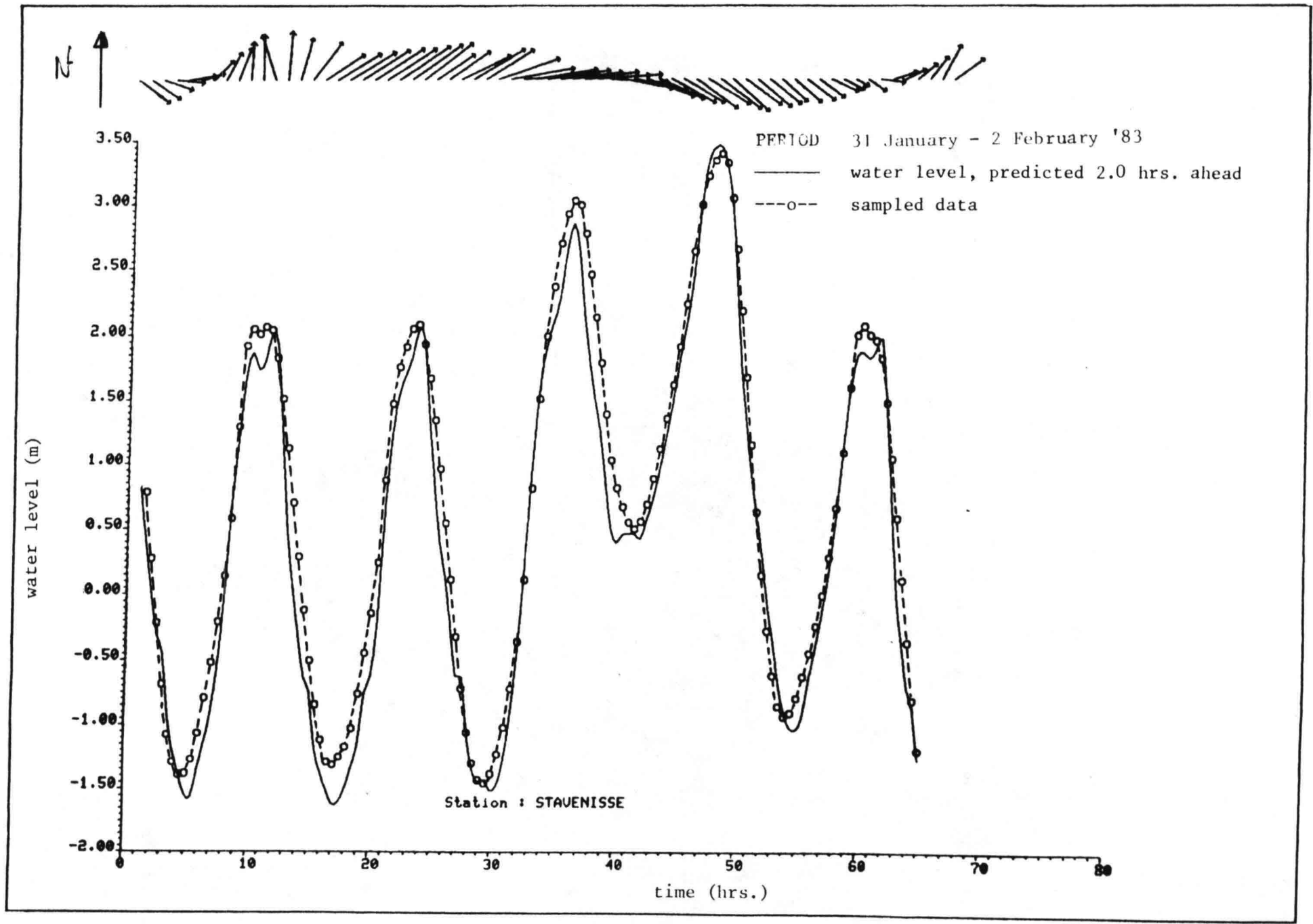


Fig. 4.34b

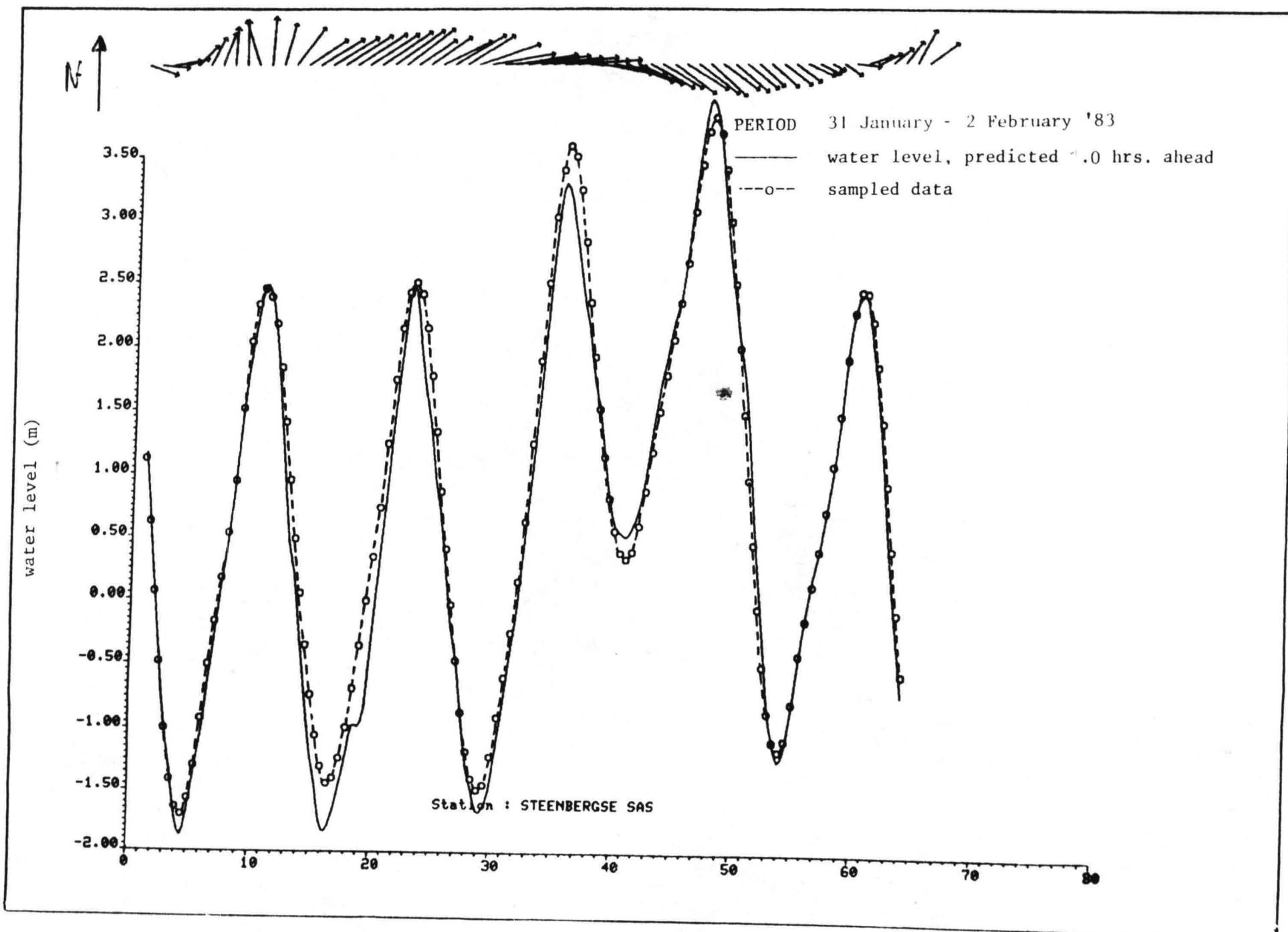


Fig. 4.35a

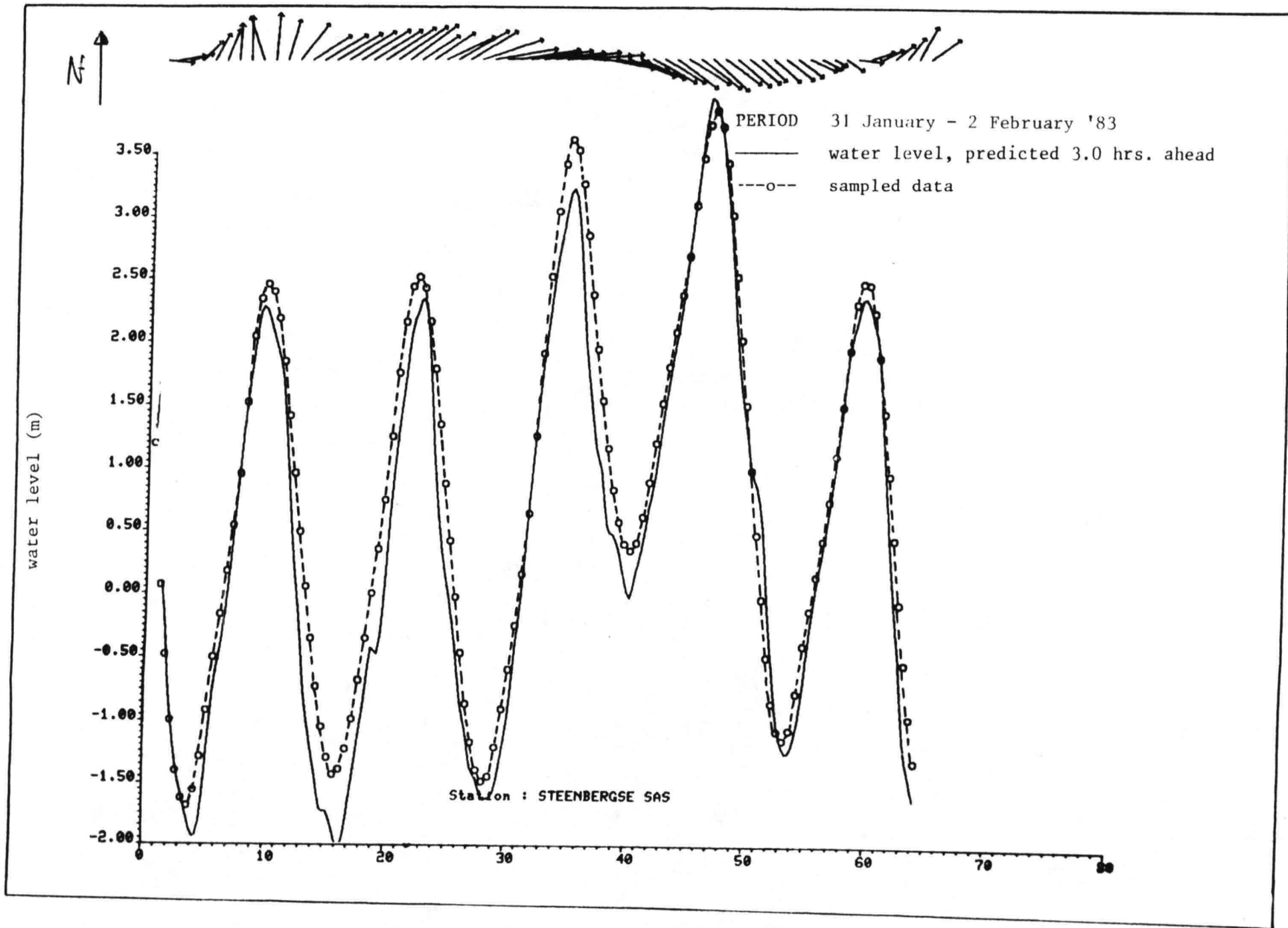


Fig. 4.35b

Fig. 4.36a

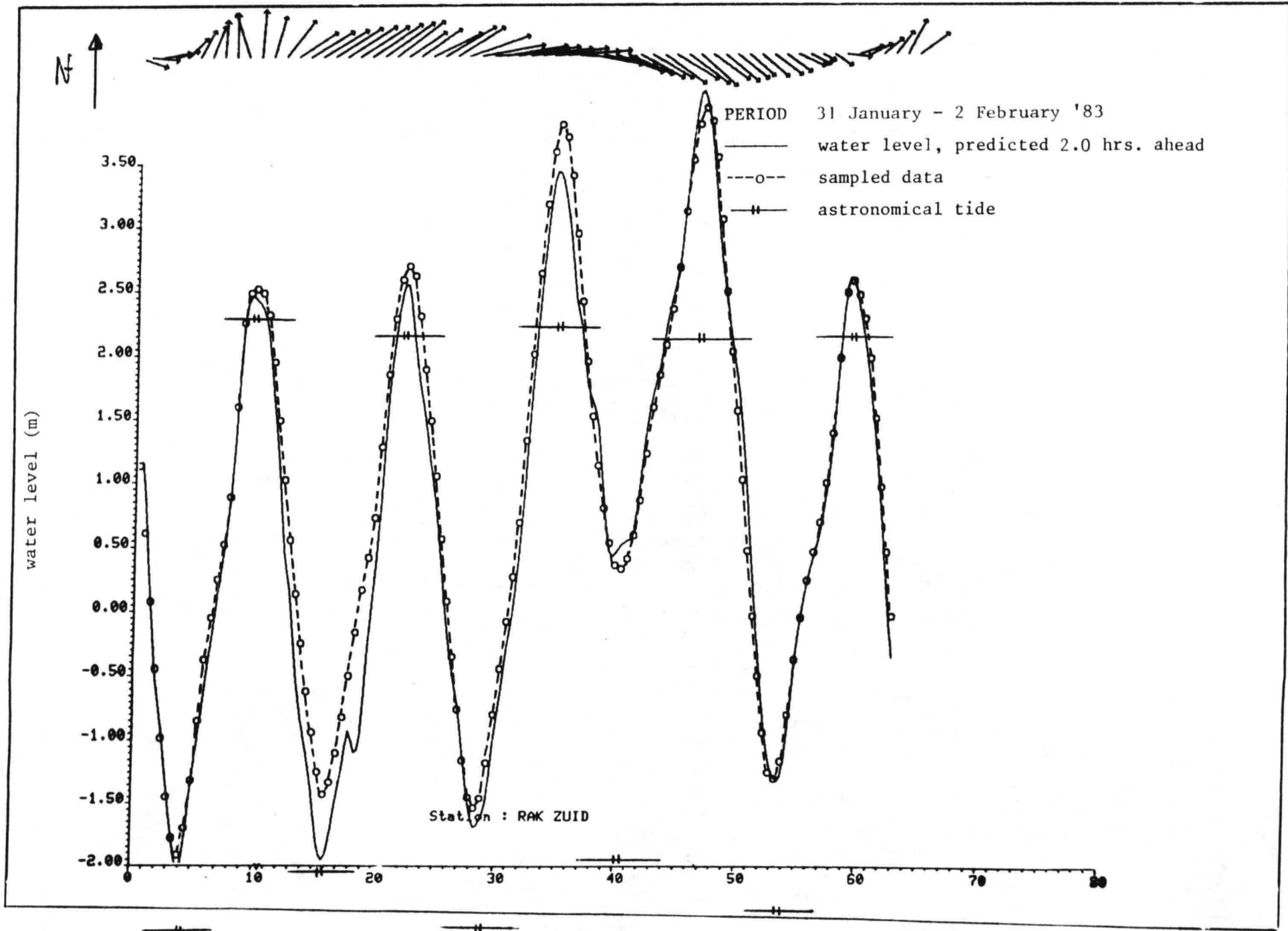
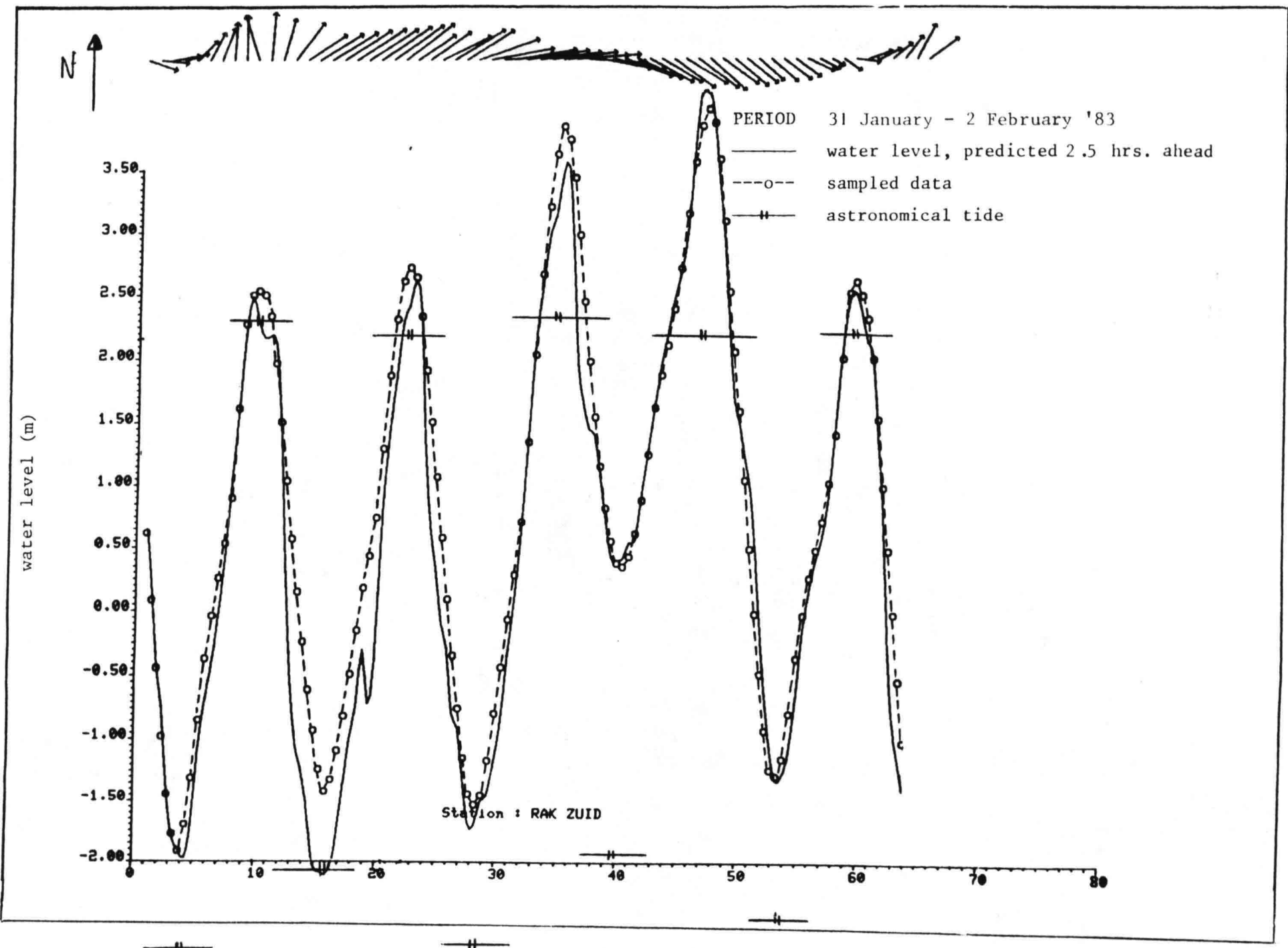


Fig. 4.36b



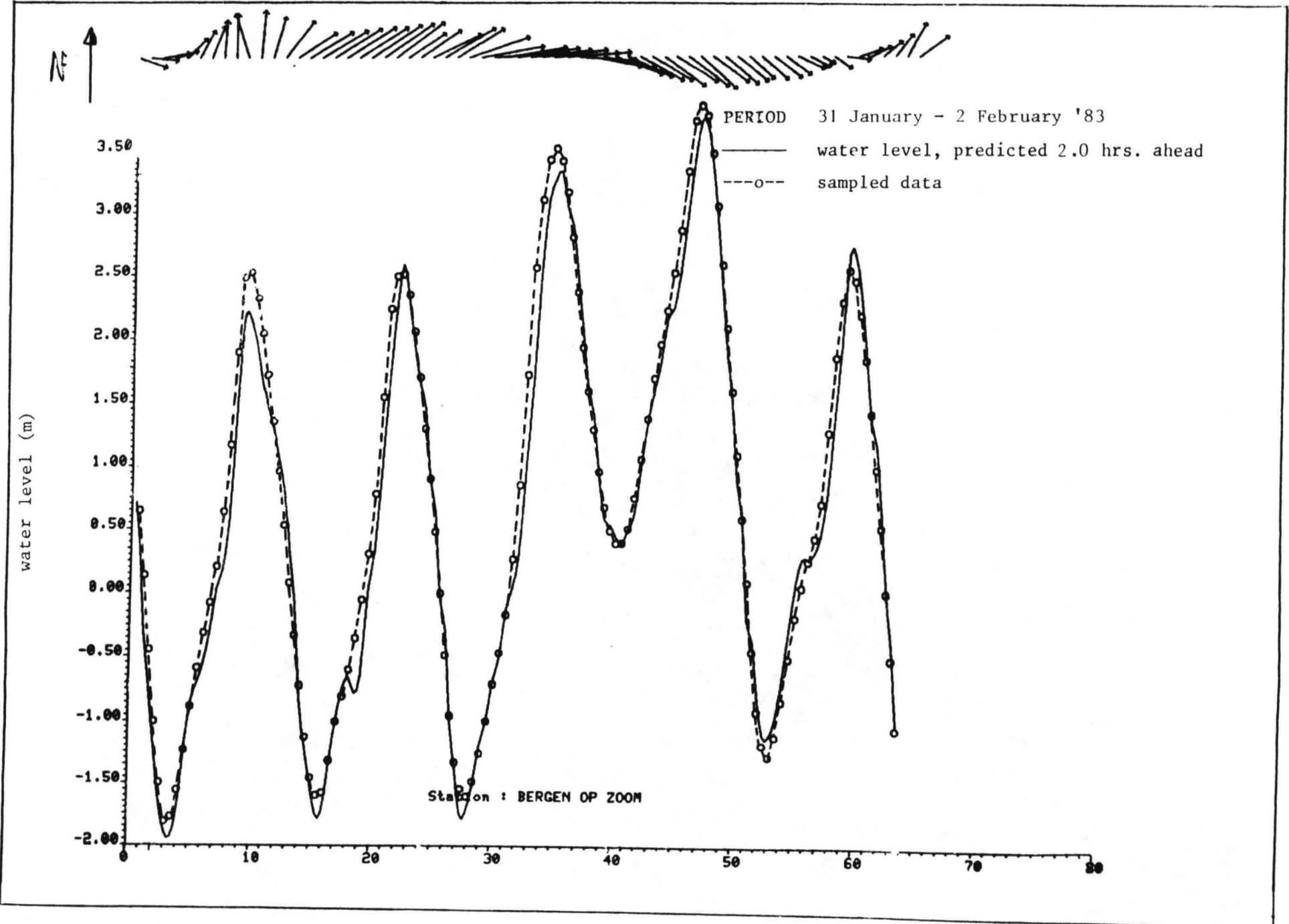


Fig. 4.37a

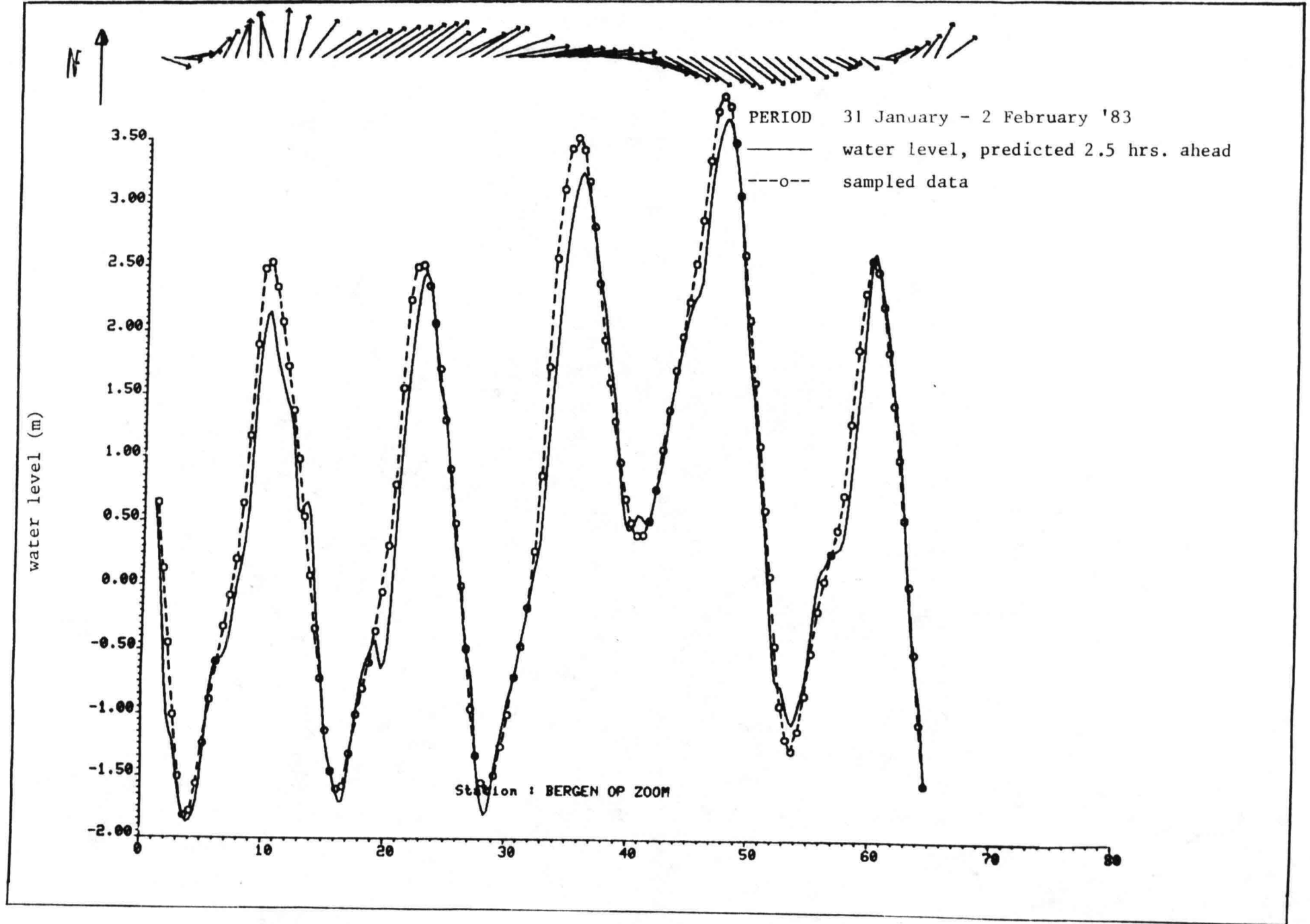


Fig. 4.37b

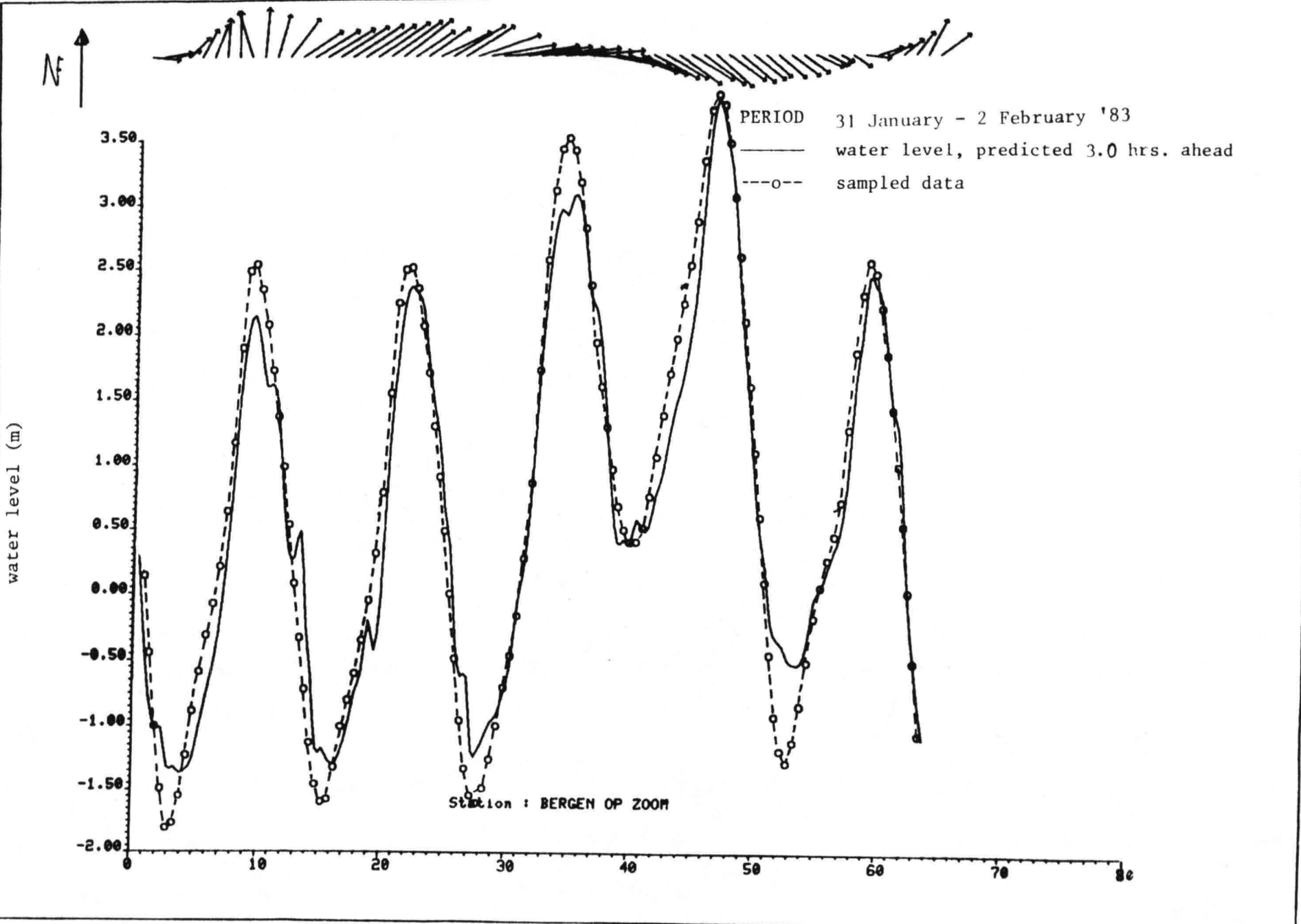


Fig. 4.37c

CHAPTER 5

CONCLUSIONS

From the results, presented in chapter 4, we will summarize the essential points:

- The filter, based on a 1-D deterministic model and a discretization on a crude grid proves to be effective in describing and predicting the tidal motion in the Dutch coastal area.
- The various applications that have been shown can all be performed with the same model, the specific use requires only another interpretation of the results, see the optimization of sampling networks.
- The tuning of the filter is relatively time-invariant which implies that the (sub)-optimality is preserved under different meteorological circumstances. This feature and the fact that the filter algorithm is recursive makes it very suited to use on-line, for obtaining short term predictions.
- One of the arguments to start this MARTHA-II research project was to improve the predictions in the mouth of the Eastern Scheldt [Heemink, 1981]. The table below shows the r.m.s. errors of the predicted water levels at O.S.4,

	r.m.s. error pred. 0.5 hrs. ahead	r.m.s. error pred. 1.0 hrs. ahead	r.m.s. error pred. 1.5 hrs. ahead
MARTHA-I 11-13 Sept. '75	9 (cm)	13 (cm)	16 (cm)
MARTHA-II 11-13 Sept. '75	5.1	7.4	9.3

TABLE IV: The r.m.s. errors, found at O.S.4.

We may conclude that the connection with the Eastern Scheldt model reduces the r.m.s. errors in the mouth of the estuary significantly.

- By means of a tuned filter it is possible to detect measurement errors: the residuals must match their computed mean and variance σ^2 . A measurement is said to be in error of the actual value if the residual exceeds the 2σ -bound.
- Model - and input errors can be deduced from the estimates, but definitive and quantitative conclusions must be postponed since these are disturbed by the simplicity of the model. For example, the global geometry does not distinguish the storage width from the live width which again influences the estimates of the friction coefficients μ . On the other hand the relation between the wind stress coefficient C_d and the wind velocity $V \cos \psi_a$ that is derived, see fig. 4.15 permits more definitive conclusions with respect to the real values of C_d and the input errors of the wind velocity and - angle, see section 2.
However the simultaneous parameter estimation is a very favourable property of the filter since it can provide useful information with respect to the value (or behaviour) of certain parameters and also indicates a way to improve the model: despite the simplicity of the model it is possible to translate various adaptations in the parameter estimation into physical effects.
- The tuning of the filter requires some experience to assign the correct intensities to the noise variables but it is not more time-consuming than the tuning of a deterministic model which is mainly due to the relatively time-invariance of the noise specification.
- The extended Kalman filter is based on a local linearization of the dynamical equations. This is acceptable since the effect of the second order terms is (relatively) small, and their neglect does not imply a severe violation of the dynamics of our model. The small contribution of the second order terms is caused by the smoothness of the restricted geometrical schematization to limit the system dimension.
- The shortcomings of our model, mentioned above, make it hard to draw definitive conclusions at all points and influence the prediction capability of the filter. For example, it would be desirable to treat the meteorological circumstances as an integrated (over the coastal area) input quantity instead of a registration of a local wind field which is taken to be valid for the entire area. The short term

predictions in storm periods are illustrating the necessity of this adaptation, see section 5.

Therefore it is perhaps useful to develop a model on a finer grid where the geometrical configuration can easily be changed and which has a greater resolution capacity with respect to the various sources of error.

REFERENCES

Abbott, M.B. [1970], An Introduction to the Method of Characteristics, American Elsevier, New York.

Budgell, P. and Unny, T.E. [1980], "A Stochastic Model for Predicting Tides in Branched Estuaries", Proceedings of the 3'th International Symposium on Stochastic Hydraulics, Tokyo.

Bierman, G.J. [1977], Factorization Methods for Discrete Sequential Estimation, Academic Press, New York.

Bretschneider, C.L. [1966], "Engineering Aspects of Hurricane Surge", in Ippen, A.T. (ed.), Estuary and Coastline Hydrodynamics, Mc Gray-Hill, New York.

Bretschneider, C.L. [1967], in Ven Te Chow (ed.) Advances in Hydroscience, Academic Press, New York.

ten Brummelhuis, P.G.J., de Jong, B. and Heemink, A.W. [1984], "On-line Prediction of Water Levels in an Estuary Using Kalman Filters", Proceedings of the 4'th International Symposium an Stochastic Hydraulics, Urbana-Champaign (to appear)

Chiu, C.L. and Iso, E.O. [1978], "Kalman Filters in Open Channel Flow Estimation", Journal of the Hydraulic Division, ASCE, 104 (HY8)

Cunge, J.A., Holly, F.M. and Verwey, A. [1980], Practical Aspects of Computational River Hydraulics, Boston (Mass.)

Dronkers, J.J. [1964], Tidal Computations in Rivers and Coastal Waters, North Holland Publishing Company, Amsterdam

Dronkers, J.J. [1975], "Tidal Theory and Computation" in Advances in Hydrosciences, Vol 10, Ven Te Chow (ed.) Academic Press, New York

Godin, G. [1972], Analysis of Tide, University of Toronto Press, Toronto

Goodson, R.E. and Klein, R.E. [1970], " Definition and Some Results for Distributed System Observability". IEEE Trans. Automatic Control, vol AC15

Heemink, A.W. [1981], Een Kalman Filter voor het Voorspellen van de Waterhoogte in de Mond van de Oosterschelde, DIV-Report RX-1981-1632

Heemink, A.W. and de Jong, B. [1982], "The Use of Kalman-Bucy Filters in Forecasting the Water Levels in the Dutch Coastal Area", Finite Elements in Water Resources, Proceedings of the 4'th International Conference, Springer Verlag, Berlin

Jazwinski, A.H. [1970], Stochastic Processes and Filtering Theory, Academic Press, New York.

Kalman, R.E. [1960], " A New Approach to Linear Filtering and Prediction Problems", Trans. ASME, Ser. D, J. Basic Eng. 82

Kalman, R.E. and Bucy, R.S. [1961], "New Results in Linear Filtering and Prediction Theory", Trans. ASME, Ser. D, J. Basic Eng. 83

Lainiotis, D.G. [1978], Partitioned Filters. An Application of Kalman Filters ot Hydrology Hydraulics and Water Resources, Chiu, C.L. (ed.) Pittsburgh

Langerak, A. [1984], private communication.

Maybeck, P.S. [1979-1982], Stochastic Models, Estimation and Control, vol I, II, III, Academic Press, New York

Morf, M. Sidhu, S.S. and Kailath, T. [1974], "Some New Algorithms for Recursive Estimation in Constant, Linear, Discrete Time systems", IEEE Trans. Automatic Control, vol 19.

Poullisse, H.N.J. [1984], "Prediction of Swell Energy on the North Sea", 9'th Conference on the Mathematics of Operations Research and System Theory (abstract), Lunteren.

Schalkwijk, W.F. [1947], A contribution to the Study of Storm Surges on the Dutch Coast, Ph.D-thesis

Timmerman, H. [1975], "On the Importance of Atmospheric Pressure Gradients for Generation of External Surges in the North Sea", Deutsches Hydrographisches Zeitschrift, vol. 28

Verboom, G.K., Stelling, G.S. and Officier, M.J. [1982], "Boundary Conditions for the Shallow Water Equations" in Abbott, M.B. and Cunge, J.A. (eds.), Engineering Applications of Computational Hydraulics vol. I, Pitman Advanced Publishing Program, Boston

Voogt, L. [1984], Getijmodel van de Noordzee gebaseerd op de JONSDAP 1976 meting. Nota WWKZ-84G 006.

